UNIVERSITY OF WARWICK

DOCTORAL THESIS

Development of Synthetic Biology Tools Driven by Membrane Potential

---

Author:

Marco DELISE

Supervisor:

Dr Munehiro ASALLY

Prof Nicholas DALE

A thesis submitted in fulfillment of the requirements

for the degree of Doctor of Philosophy

in the

Asally Group

School of Life Sciences

April 29, 2020

Declaration of Authorship

I, Marco DELISE, declare that this thesis titled, "Development of Synthetic Biology Tools Driven by Membrane Potential" and the work presented in it are my own. I confirm that:

- This work was done wholly or mainly while in candidature for a research degree at this University.
- Where any part of this thesis has previously been submitted for a degree or any other qualification at this University or any other institution, this has been clearly stated.
- Where I have consulted the published work of others, this is always clearly attributed.
- Where I have quoted from the work of others, the source is always given. With the exception of such quotations, this thesis is entirely my own work.
- I have acknowledged all main sources of help.
- Where the thesis is based on work done by myself jointly with others, I have made clear exactly what was done by others and what I have contributed myself.

Signed:

_____

Date:

_____

UNIVERSITY OF WARWICK

Abstract

Doctoral Training Centre in Synthetic Biology

School of Life Sciences

Doctor of Philosophy

Development of Synthetic Biology Tools Driven by Membrane Potential

by Marco DELISE

Every cell, from prokaryotic to mammalian cells, has a membrane sustaining an electrical potential difference, called membrane potential, which can provide an interface between external environment and cellular processes.

Following the discovery of an eukaryotic voltage-sensitive-domain (VSD) that changes conformation upon membrane potential shifts and that is independent from other attached domains, membrane potential reporters for mammalian cells have been obtained by coupling the VSD with fluorescent proteins.

In this work, I described the efforts of using such a VSD to develop a membrane potential sensor for prokaryotes and a voltage-sensitive protease for mammalian cells.

First, as recent discoveries in *Bacillus subtilis* showed the tight involvement of membrane potential in biological processes such as cell-cell communication, biofilm formation and sporulation, a tool to better study prokaryotic membrane potential was needed. The Prokaryotic ASAP1-based Potential Sensor (PAPS) constructs were obtained by codon-optimizing the eukaryotic VSD for *B.subtilis*, by coupling it with cpYFP in different topological positions and by linking the VSD to the membrane-targeting domain t216. PAPS-Gt was the PAPS variant with the largest fluorescence change upon cell depolarization (-6.3% in the microscope, -13% in the flow cytometer), even if it did not show clear membrane specificity. PAPS-Gt(D342Y) mutant showed a lower fluorescence change (-5.3% in the flow cytometer), suggesting an important role for D342 in the VSD conformational changes.

Second, the ability of controlling cellular processes with external stimuli is gaining interest with the recent development of optogenetics, magnetogenetics and sonogenetics, but electrical control has lagged behind. An electro-biological interface to complement and enhance bioelectronic systems is proposed with a novel class of proteins named Membrane potential-Activated Targeting Enzymes (MATEs). The first developed MATE is LOTEV, a voltage sensitive TEV protease which cleaves the specific ENLYFQ/S peptide upon externally-induced cell depolarization. The novel protein was obtained by flanking the eukaryotic VSD with the two halves of a split TEV protease (nTEVp and cTEVp). LOTEV showed to increase its proteolytic

activity by +8.6% in *HeLa* cells, when the cell membrane was stimulated with a +60 mV electric stimulus.

Acknowledgements

First of all I want to thank my supervisor Munehiro, for being not only a PhD supervisor but a real mentor for life and a friend. I thank him immensely for leading me during the scientific research but also for encouraging me to follow my passions and my career goals.

I thank Nick Dale for the insights on my project and for initiating me into the exciting technique of patch clamp. I extend my gratitude to Sarbjit Nijjar for the help in Nick's lab.

I thank my friends Magda, Jesus, Iago, Randa, Maria, Conor and Jonatan to help me spend three incredible years during my PhD (especially outside the lab).

I thank Arthur for having helped me carry out parts of my PhD project as part of his Master Project.

I thank the Doctoral Training Centre in Synthetic Biology for giving me the opportunity to become part of the exciting field of SynBio and I thank the University of Oxford for the training provided during the first year. I thank BBSRC and EPSRC for the funding provided.

Most importantly, I want to thank my parents, without whom I would not be who and where I am right now.

Contents

List of Figures

List of Tables

List of Abbreviations

CCCP	**C**arbonyl **C**yanide m-**C**hloro**P**henyl hydrazone
Ci-VSD	**C**iona **i**ntestinalis **V**oltage **S**ensitive **D**omain
FP	**F**luorescent **P**rotein
GEVI	**G**enetically **E**ncoded **V**oltage **I**ndicator
GFP	**G**reen **F**luorescent **P**rotein
Gg-VSD	**G**allus **g**allus **V**oltage **S**ensitive **D**omain
MATE	**M**embrane potential **A**ctivated **T**argeting **E**nzyme
MCR	**M**embrane (to) **C**ytoplasm **R**atio
MP	**M**embrane **P**otential
MPS	**M**ammalian **P**hysiological **S**olution
NCR	**N**ucleus (to) **C**ytoplasm **R**atio
NMR	**N**ucleus (to) **M**embrane **R**atio
PAPS	**P**rokaryotic **A**SAP1-based **P**otential **S**ensor
PCR	**P**olymerase **C**hain **R**eaction
RCF	**R**elative **C**entrifuge **F**orce
RFU	**R**elative **F**luorescence **U**nit
RMP	**R**esting**M**embrane **P**otential
SD	**S**tandard **D**eviation
SNR	**S**ignal (to) **N**oise **R**atio
TEVp	**T**obacco **E**tch **V**irus **p**rotease
ThT	**Th**ioflavin **T**
TMRM	**T**etra**M**ethyl**R**hodamine, **M**ethyl ester
VGIC	**V**oltage **G**ated **I**on **C**hannel

VSD **V**oltage **S**ensitive **D**omain

VSP **V**oltage **S**ensitive **P**hosphatase

YFP **Y**ellow **F**luorescent **P**rotein

To my parents, that I don't see enough

1 Introduction: Novel uses of a Voltage Sensitive Domain

Every cell, from prokaryotic to human cell, has a membrane to separate the internal cellular processes from the extracellular environment. Among the substances that the lipid bilayer blocks, ion accumulation on the two sides of the membrane form an electrochemical gradient. The electric potential that is generated by the ion concentration difference between the cytoplasm and the extracellular environment is called membrane potential (MP) and is maintained by the membrane's differential permeability to ions. Its magnitude can be estimated by the Goldman equation (Goldman, 1943):

$$E_m = \frac{RT}{F} \ln \left(\frac{\sum_i^n P_{M_i^+} [M_i^+]_{out} + \sum_j^m P_{A_j^-} [A_j^-]_{in}}{\sum_i^n P_{M_i^+} [M_i^+]_{in} + \sum_j^m P_{A_j^-} [A_j^-]_{out}} \right)$$

where E_m is the membrane potential, R the universal gas constant R = 8.312 joules per kelvin per mole, T the absolute temperature in kelvins, F the Faraday constant F = 96.485 coulombs per mole, P_i the partial permeability to ion i, M a monovalent positive ionic specie, A a monovalent negative ionic specie, $[i]_{out}$ the extracellular concentration of ion i and $[i]_{in}$ the intracellular concentration of ion i.

When a cell is in a quiescent state, its membrane potential is relatively stable and takes the name of resting membrane potential (RMP). Depending on the cell type, RMP typically ranges between -40 mV and -70 mV, with exceptions going up to -8 mV in chondrocytes (Lewis et al., 2011) and down to -95 mV in muscle cells

(Hodgkin and Horowicz, 1960).

Ion channels can open and close in response to intracellular or environmental stimuli. For instance, voltage-gated ion channels open when the MP surpasses a threshold; ligand-gated ion channels open when a specific ligand presents at the membrane; mechano-sensitive channels and acid-sensing ion channels open upon mechanical stretch and decrease of extracellular pH, respectively. When a channel opens, specific ions can cross the cell membrane following the electrochemical gradient, causing the membrane potential to change. Membrane potential shifts can vary in duration and magnitude, depending on the ion channels involved. Such changes are called graded potentials and, in normal conditions, the counteraction of different ion channels can rapidly restore the RMP.

Among the effects that MP shifts have on the cell, the more immediate one is the induction of conformational changes in transmembrane domains called "voltage-sensitive-domains" (VSDs). Such domains are at the core of voltage-gated ion channels where they have the capability of controlling the opening and closing of pore domains (Bezanilla, 2008). VSDs have for long been associated uniquely with ion channels; however, recently, a novel type of VSD was discovered as part of the eukaryotic voltage-sensitive phosphatases (VSPs). In VSP, the VSD regulates the activity of the attached phosphatase in a way which is dependent on the membrane potential (Sakata and Okamura, 2014). While in voltage-gated ion channels the separation of the VSD from the pore domain leads to the loss of voltage-sensitivity, it was shown that the conformational changes of the VSD from the VSP are independent from the phosphatase domain (Villalba-Galea, 2012). This capability makes such a domain ideal for the construction of voltage-sensitive fusion proteins.

So far, coupling VSP's VSD with fluorescent proteins has led to the creation of membrane potential reporters called Genetically Encoded Voltage Indicators (GEVIs). These reporters are used to study neuronal action potentials and variants with high accuracy, large dynamic range, fast-kinetics and low cytotoxicity have been created.

In this chapter I propose two ideas on how to use the modular VSD for the creation of novel membrane-potential driven proteins. In particular:

- a membrane potential reporter for prokaryotic cells, following inspiration from eukaryotic GEVIs;
- a voltage-sensitive-enzyme for mammalian cells, with the purpose of controlling a defined cellular process with an external electrical stimulus.

1.1 A modular Voltage-Sensitive Domain (VSD)

The first voltage-sensitive phosphatase was discovered when a gene homologous to both an ion channel and a phosphatase was identified in *C.intestinalis* (Murata et al., 2005). It was the first time that a protein was found with both an enzymatic and a voltage sensitive domain, thus, it was further characterized.
C.intestinalis VSP (Ci-VSP) is constituted by a voltage sensitive domain (Ci-VSD), made of four transmembrane helices (S1-S4), that is linked at the C-terminus to a cytoplasmic domain with high sequence similarity to a phosphatase and tensin homolog (PTEN) (Fig.1.1).

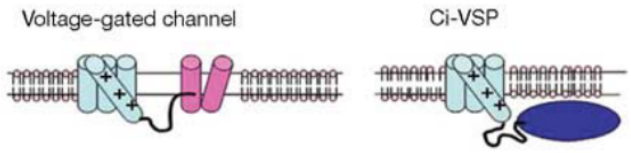

FIGURE 1.1: Comparison of domain topology in a voltage-gated ion channel (VGIC, on the left) and *C.intestinalis* voltage-sensitive phosphatase (Ci-VSP, on the right). While in VGICs the VSD (light blue cylinders) is linked to a transmembrane pore domain (pink cylinders), in Ci-VSP the VSD is linked to a cytoplasmic phosphatase (dark blue ellipse). In both cases, the second domain is attached to the transmembrane helix undergoing conformational changes upon charge displacement (cylinder with positive charges). Figure adapted from (Murata et al., 2005)

.

When the cell membrane depolarizes, charge displacement on the S4 helix causes an upwards movement of the helix, pulling the attached phosphatase domain closer

to the cytoplasmic face of the membrane. The phosphatase acquired vicinity to the membrane triggers the dephosphorylation of membrane phosphoinositides. It is still uncertain the final consequence of such dephosphorylation and whether it triggers a signalling cascade.

What makes Ci-VSP particularly different from voltage gated ion channels (VGICs) is its monomeric nature. Voltage gated sodium channels (VGSCs), in fact, form tetramers and the tetramerization of four VSDs is required for the correct functionality of the protein. If a single VSD is isolated from a VGSC, it shows loss of voltage-sensitivity. On the contrary, the monomeric nature of Ci-VSP translates in the modular characteristic of its VSD.

Given its uniqueness, Ci-VSP VSD (Ci-VSD) has been well characterized.

1.1.1 VSD Dynamics

In Ci-VSP, the enzymatic activity increases gradually over a wide range of membrane potentials. In particular, the upwards movement of S4 upon cell depolarization occurs in multiple steps, each step determining a different activity level of the phosphatase (Li et al., 2014).

A structural analysis of VSD movements found that S4 helix sits in a 'groove' between S1 and S3, kept in place by ionic attractions between its positively-charged residues and the opposite S1/S3 negatively charged residues. In particular, four positively-charged arginines on S4 and an hydrophobic phenylanine at the C-terminus of the helix play a major role.

When the membrane depolarizes and the cytoplasm becomes more positive, outwards movement of negative charges attracts the positively-charged arginines of S4 to the outer membrane, initiating the VSD conformational change. In total, a 5Å-upwards shift of the S4 helix across the membrane is induced, together with a rotation of 60° (Fig.1.2A) (Li et al., 2014).

The importance of the arginine residues in the VSD dynamics is shown by the effects of their substitution . In fact, when R217 is substituted with a basic residue (R217Q), the charge-voltage (Q-V) curve shifts to the left by 50 mV. Substitution with an acidic residue (R217E) shifts the Q-V curve by 100 mV to the left, letting the conformational changes happen at the more physiological MPs between -100 mV and 0 mV (Fig.1.2B) (Li et al., 2014).

Another meaningful mutations is D129R which was shown to make *Xenopus* oocytes' VSD insensitive to voltage changes (Tsutsui et al., 2013)

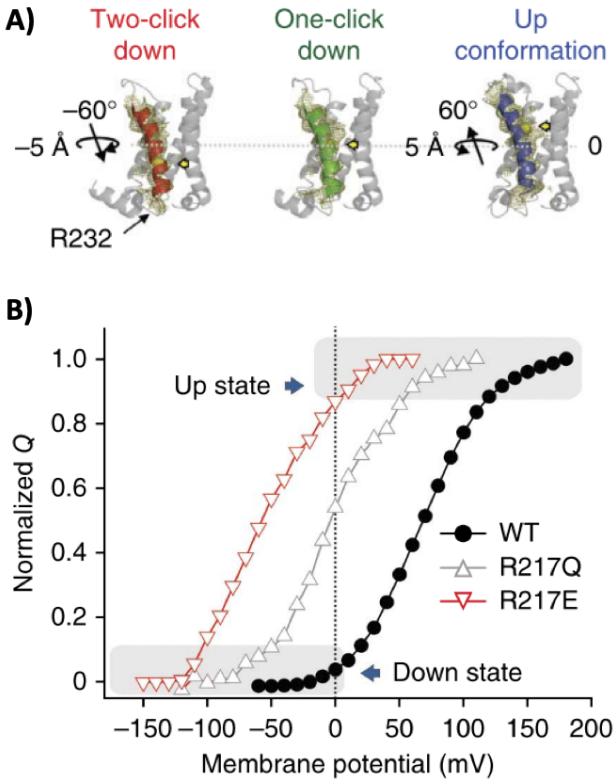

FIGURE 1.2: A) Three conformation models from VSD electron density map: 6-residue downward movement (left), 3-residue downward movement (centre), up conformation (right). B) Q-V curve for VSD WT compared to R217Q and R217E variants.

.

1.2 Explored uses of VSD for fusion proteins: Genetically Encoded Voltage Indicators (GEVIs) for Mammalian Cells

VSPs were found in different organisms - mainly *Ciona intestinalis* and *Gallus gallus* - and so far their VSD have been used only to develop membrane potential reporters, by coupling the VSD to a fluorescent protein (FP). Given the VSD conformational changes described in Sec.1.1.1, an appropriate combination of FP's structure with VSD movements makes the emitted fluorescence dependent on the MP.

The idea to develop membrane potential reporters by fusing a fluorescent protein to a VSD had already been explored by using VSDs from VGIC, producing proteins such as FlaSh (Siegel and Isacoff, 1997) and VSFP1 (Sakai et al., 2001). However, VGIC-based GEVIs showed low voltage sensitivity ($< 5\% \Delta F/F$ per 100 mV), slow kinetics (10-200 ms activation) and often poor membrane trafficking (Baker et al., 2007).

When Ci-VSD modular properties were discovered, a new generation of GEVIs based on this VSD started to be developed, leading to better results.

In "cpmKate" (Gautam et al., 2009), a circularly permuted Green Fluorescent Protein (cpGFP) was divided in two halves (N-cpGFP and C-cpGFP) and coupled to the Ci-VSD termini (Fig.1.3a). When the VSD movement pulls the thwo halves closer, the fluorescence increases. cpmKate showed <1% fluorescence change between -140 mV and +60 mV. The poor performance was associated to an improper protein folding of the cpGFP halves.

In 2012, two Ci-VSD based GEVIs were developed. In "ElectricPk" the C-terminus of the Ci-VSD was attached to a circularly permuted Enhanced GFP (cpEGFP), resulting in a fluorescence decrease of 1.2% when the cell was electrically stimulated

with +100 mV from the holding potential of -70 mV (Barnett et al., 2012); in "ArcLight" the same Ci-VSD terminus was linked to a pHluorin2 and resulted in a fluorescence decrease of 35% upon +100 mV stimulus (Jin et al., 2012). ArcLight proved to be able to track neuronal action potentials up to 100 Hz. The polarity was later inverted to 31% fluorescence increase upon +100 mV simulation by several round of site-directed mutagenesis (ArcLight A389 A390 V442) (Platisa et al., 2017). Nonetheless, ArcLight use has been limited due to its sensitivity to pH changes unrelated to membrane potential.

The "Accelerated Sensor of Action Potential" (ASAP1) (St-Pierre et al., 2014) was developed by combining the VSD from *G.gallus* VSP (Gg-VSD) with a circularly permuted super-folder GFP-OPT (cpsfGFP-OPT) (Cabantous, Terwilliger, and Waldo, 2005)). In contrast with the other GEVI proteins, the cpFP was placed in the extracellular loop between S3 and S4 helixes of VSD, to better exploit the S3-S4 loop conformational changes upon membrane depolarization (Fig.1.3b). The R153Q mutation was introduced to shift the voltage sensitivity towards a more physiological range of potentials, as already mentioned (Dimitrov et al., 2007). ASAP1 showed a fluorescence change of -17.5% upon 70 mV depolarization and +23.4% upon 50 mV hyperpolarization. The fluorescence specificity to membrane potential changes and the quick dynamics - able to track single action potentials up to 200 Hz - made ASAP1 a promising GEVI.

Lastly, in 2017, the "Luminescent Optical Tool for Universal Sensing of Voltage" (LOTUS-V) (Inagaki et al., 2017) was developed. In this fusion protein, the luciferase "NLuc" (Hall et al., 2012) was attached to the N-terminus of the Ci-VSD, while the YFP "Venus" was attached to the C-terminus (Fig.1.3c). When the VSD undergoes conformational changes after cell depolarization, the distance between the luciferase and the YFP decreases, increasing YFP fluorescence by Förster Resonance Energy Transfer (FRET) effect (Clegg, 1992). It was shown that LOTUS-V had a fluorescence increase of 22.6% upon +100 mV stimulation.

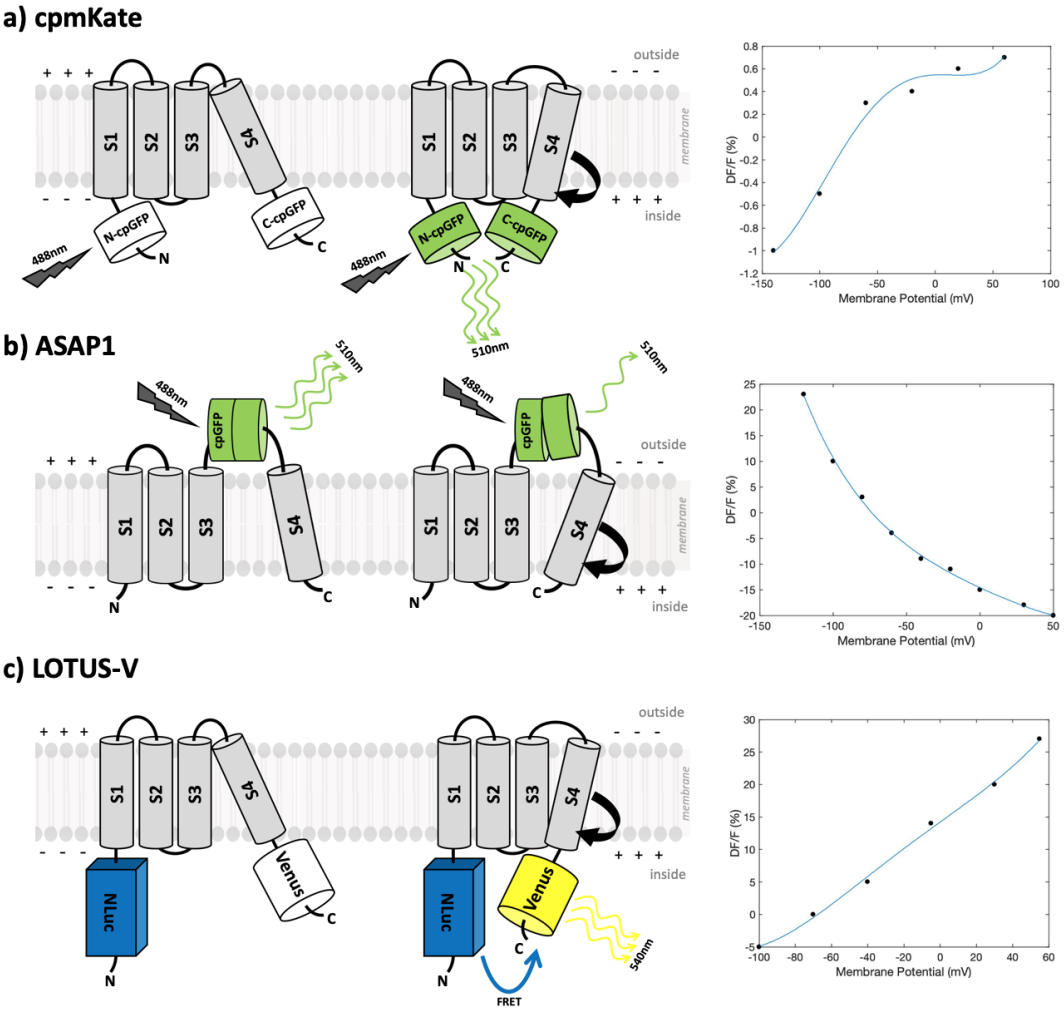

FIGURE 1.3: Examples of GEVIs developed for mammalian cells. While cpmKate showed only <2% increase upon +200 mV stimulus (A) and ASAP1 41% decrease upon +170 mV (B), LOTUS-V reached 23% increase upon +100 mV (C) but was not affected by photoxicity thanks to natural bioluminescence stimulating the FP

.

1.3 Unexplored uses of VSD for fusion proteins

Ci-VSD has the capability of turning proteins voltage-sensitive with appropriate coupling. However, so far, they have been fused only with fluorescent proteins and have been expressed only in mammalian cells. More applications are foreseen:

- membrane potential has an important role not only in eukaryotic but also in prokaryotic electrophysiology. Since current solutions to measure prokaryotic MP showed toxic effects, the development of a functional GEVI for bacteria would ideally bring the same benefits that were brought by GEVIs to

mammalian electrophysiology studies.

- External control of cellular processes with artificial inputs has been explored in recent years with the development of technologies such as optogenetics, magnetogenetics and sonogenetics. An electrogenetic option would bring several advantages, especially in the field of bioelectronics, but no eletrically-controlled protein has yet been developed. The development of an enzyme made voltage-dependent by addition of Ci-VSD would open new possibilities for electrogenetic cell control.

1.4 VSD for a novel Prokaryotic GEVIs

1.4.1 Membrane Potential Role in Prokaryotes

Different cellular processes are linked to membrane potential in prokaryotes, from cell proliferation and viability (Stratford et al., 2019) to flagellar motor rotation (Lo et al., 2012), mitotic site (Strahl and Hamoen, 2010) and cell signalling.

In *Bacillus subtilis* biofilms, membrane potential shifts are used as a signal to communicate. When the biofilm increases in size, the cells in the inner part can reach less nutrients from the environment and they consequently hyperpolarize to slow down their metabolism. The hyperpolarization is transmitted to the surrounding cells and reduces cell proliferation, with the result that the biofilm growth stops temporarily to allow more nutrients to reach the inner cells (Prindle et al., 2015). Further research found out that after hyperpolarization, the cells at the boundaries of the biofilm release potassium ions into the surrounding, attracting motile bacteria towards the biofilm (Humphries et al., 2017). Such mechanism is not well understood, but causes the formation of mix-species biofilms, raising the threat of thick biofilms with antibiotic resistant bacteria such as *Pseudomonas aeruginosa* (Baron, 1996). Moreover, it was shown how bacteria communication does not restrict to single biofilms, but is also used by different biofilms to communicate and time-share

common nutrients (Liu et al., 2017).

Another bacterial process linked to MP is sporulation. It was recently found that, when sporulating, an endospore inside a mother cell undergoes a "quality control" of the spore. In particular, the charge of the spore will determine whether the sporulation will be successful or will germinate (Sirec et al., 2019).

1.4.2 The importance of measuring membrane potential

As showed in section 1.4.1 membrane potential is involved in a variety of cellular process which understanding can have important consequences for human purposes.

For instance, mixed-biofilms containing *P.aeruginosa* are responsible for a large proportion of hospital-related infections (Baron, 1996). Knowing how bacterial biofilms survive via membrane potential communication can help disrupt biofilm infections and prevent the formation of biofilms in unwanted places such as medical devices. Formation of unwanted spores in sterile environment could be prevented by disrupting the mechanism leading to successfull sporulation.

The more it is studied, the more membrane potential shows its involvement in different cellular processes. To be able to analyse MP role extensively, it is important to have MP reporters with high accuracy, large dynamic range, fast-response and low toxicity. Mainly, the potentiometric reporters used by researchers for prokaryotes fall in the category of inorganic fluorescent substances, while only one GEVI-like protein has been developed.

1.4.3 Prokaryotic electrophysiological probes

Inorganic fluorescent substances

Chemicals such as tetramethylrhodamine (TMRM) (Scaduto and Grotyohann, 1999) and Rhodamine 123 (Chen, 1988) are used to visualise membrane potential changes within bacteria. TMRM is a fluorescent lipophilic cation, which is attracted to the

internal negative charge of the cell at resting potential and leaves the cell upon depolarization. Such a behaviour establishes a relationship between cell depolarization and a decrease of TMRM fluorescence in the cell.

More recently, the positively-charged fluorophore Thioflavin T (ThT) was established as membrane potential dye (Prindle et al., 2015). Its charged status let it diffuse down electrochemical gradients and in particular accumulate inside hyperpolarized cells where the more negatively charged cytoplasm attract it. The advantage of ThT over TMRM is the reactivity of such a potentiometric dye to fast voltage changes.

However, the downsides of potentiometric dyes stand in their phototoxicity and photo-bleaching effect (Cundall, 1981), which restrict prolonged imaging of MP. Moreover, the mode of action of potentiometric dyes does not provide spatial resolution of membrane potential in bacteria.

The only GEVI in Prokaryotes

The only GEVI protein developed for prokaryotic cells is based on bacterial rhodopsins. The Proteorhodopsin Optical Proton Sensor (PROPS) (Kralj et al., 2011) was developed by using a green-absorbing proteorhodopsin and introducing a D97N mutation to reduce its light-sensitivity and make it sensitive to pH. Used as a membrane potential reporter it showed a $\Delta F/F = +150\%$ upon +100 mV stimulus. Nonetheless, as mentioned, this reporter depended on pH changes rather than directly on MP. Such low MP-specificity could present issues of reporting not accurate MP-changes.

1.4.4 The need of a novel GEVI for Prokaryotes

It can be seen from Sec.1.2 that a large variety of GEVI proteins have been developed for mammalian cells, while similar electrophysiological probes have not been given the same consideration for prokaryotic usage.

Nonetheless, a further understanding of MP involvement in microbial processes is

critical, not only for the sake of basic science but also to prevent dangerous infections. On the basic science side, bacteria electrophysiology can shed light on how cells developed from single-cell communities to multicellular organisms (Newell, 1978), and maybe clarify the relationship between genetic programs and physiological state. On the applied science side, its development could be used to prevent infections. For example, formation of biofilms can constitute a threat for patients during medical treatments, with species such as *Staphylococci* forming stable and infectious structures on medical devices (Mack et al., 2006) and co-coltures of *P. aeruginosa* and *B.subtilis* being responsible for hospital-related infections resistant to antibiotics (Lister, Wolter, and Hanson, 2009; Baron, 1996). Sporulation allows bacteria to defy sterilization, causing potential infection threat in environments where complete sterilization is needed.

A further understanding of prokaryotes' membrane potential dynamics would increase the basic knowledge on prokaryotic electrophysiology for potential uses in Synthetic Biology, in relation also to sporulation and biofilm formation.

As shown, the possibilities to study bacteria electrophysiology have been limited due to dye toxicity and low MP-specificity in the current GEVIs. Given the success of VSD-based GEVI systems in mammalian cells (Sec.1.2), it is proposed to develop a similar system for prokaryotes. A VSD-based protein would be less toxic, would show higher MP-specificity than current solutions and would propagate from generation to generation, solving the lower accessibility issue of potentiometric dyes.

To find a suitable VSD-based GEVI system for prokaryotes, the VSD-based GEVIs developed for mammalian cells were considered. In particular, given the large fluorescence dynamic range and the fast kinetics, ASAP1 was selected as a valid candidate and chosen to be heterologously expressed in *B.subtilis* and optimised for the novel host. Membrane composition is different in mammalian and prokaryotic

cells, constituting a possible problem for a correct membrane-targeting of ASAP1's eukaryotic VSD. However, the similarity in resting membrane potential between *B.subtilis* (-80 mV (Hosoi, Mochizuki, and Kasai, 1980)) and neurons (-70 mV (Watson, 2015)) suggested it could be worth testing a mammalian GEVI into bacteria, after appropriate modifications for host optimisation. The novel prokaryotic GEVI derived from ASAP1 was called "Prokaryotic ASAP1-based Potentiometric Sensor" (PAPS).

1.5 VSD for an Electric Control of Mammalian Cells

1.5.1 External control of cell processes in mammalian cells

Engineering mammalian cells that autonomously react to environmental stimuli and do not require external intervention is sufficient for most synthetic biology applications that do not require external supervision. Nonetheless, the ability to externally tune a biological activity with accurate spatio-temporal precision is necessary for the development of safer and more customizable technologies. So far, such exogenous control on synthetic processes in mammalian cells has been achieved with different external stimuli:

- biochemical molecules;
- light;
- magnetic fields;
- temperature and ultrasounds;
- electrical fields.

Together with the nature of the stimulus, it is also important whether the stimulus is affecting the cell processes at the transcriptional, translational or post-translational level. In fact, while the nature of the stimulus determines the limits of the signal reaching the cell, the process that is targeted determines the reactiveness of the

desired biological response to the stimulus. For example, if the desired controlled outcome is the presence of an active protein in the cytoplasm, transcriptional control would produce a slower system reaction compared to a direct, post-translational activation of the protein in the cytoplasm.

Chemogenetics

The simplest and most used method to regulate transgene expression for scientific research and industrial biomass production (Donovan, Robinson, and Click, 1996) is the use of biochemical substances. To deliver the inducers into the cell, they need to be added to the cell proximate environment so they are transported inside the plasma membrane and are able to act at the transcriptional or post-translational level.

Biochemical control of transgene expression can be obtained by appropriate selection and engineering of the promoter region. Examples of the most used biochemical inducers/repressors are isopropyl b-D-1-thiogalactopyranoside (IPTG), arabinose (ara) and tetracycline (tet). When the corresponding promoter (Plac, PBAD and Ptet, respectively) is placed upstream of the gene of interest, gene expression becomes proportionally induced or repressed depending on the presence of the inducer/repressor (Marbach and Bettenbrock, 2012).

Examples of chemical-induced gene expression can be found extensively in literature, with inducers ranging from methanol (Selvamani et al., 2017) and aminoacids (Ravikumar et al., 2015) to caffeine (Bojar et al., 2018) and menthol (Bai et al., 2019).

Chemogenetics is the most used approach to regulate gene expression with an external stimulus, requiring only the addition of the inducer to the cell environment. Nonetheless, the need to access the cell environment and the difficulties in removing the inducer from the media limit its uses to a controlled environment and where a tight on-off control is not needed. Moreover, the risk that the inducer presents toxicity makes this solution poorly suited for *in vivo* applications.

Optogenetics

Optical conformational changes are not unusual in nature and they have been exploited in the last decades to develop novel tools to control biology with light. In 2005, the use of the light-activated cation-channel channorhodopsin-2 in neurons by Boyden et al. (Boyden et al., 2005) gave birth to the field of optogenetics. With optogenetics, neurons action potentials can be triggered by light stimulus with accurate spatio-temporal precision. While already in 2002 Shimizu-Sato et al had developed a transcription system triggered by far-red light dimerization of Gal4 (Shimizu-Sato et al., 2002), the birth of optogenetics fostered novel light-biology interfaces. In particular, light-sensitive proteins such as LOV2 and cryptochrome-2 (CRY2) were fused with other proteins to make them photosensitive. LOV2 domains were fused with peptides (Lungu et al., 2012) or with PDZ protein (Strickland et al., 2012) to form respectively photoactivable gene transcription system and photoactivable dimerization tags called TULIPs. CRY2 was fused with transcription factor (Idevall-Hagren et al., 2012) and with TALE (Konermann et al., 2009) to control phosphoinositide metabolism and create transcription system called LITE. Photoactivable enzymes were also developed by fusing proteases with a conformation-changing fluorescent protein Dronpa (Zhou et al., 2012) or with a LOV domain (Smart et al., 2017). More recently, a photoactivated Cas9-sgRNA system has also been designed to control targeted gene-editing upon stimulus with near-infrared light (Pan et al., 2019). Regardless the progress and success of optogenetics, it still presents issues. In particular, light presents low tissue penetration, with red light having the wavelength penetrating the most with 5 mm (Clement, Daniel, and Trelles, 2005). This limit is a problem for reaching cells of interest that are in deep tissue *in vivo* and it is added to light scattering issues, which already cause poor spatial precision *in vivo*. For these reasons, therapeutic applications of optogenetics still require invasive surgery and the insertion of a light source in the body, constituting distress for the patient and complication of the procedure. On the other

hand, light scattering also hinders the possibility of creating sophisticated electro-biological hybrid devices, since each component would require optical insulation.

Magnetogenetics

While light stimulus presents problems of tissue penetration, a natural entity that reaches deeper tissue without showing the same attenuation is represented by magnetism. Huang's et al. fused the thermo-sensitive channel TRPV1 with superparamagnetic ferrite nanoparticles to give birth to the field of magnetogenetics (Huang et al., 2010). In their work, the scientists stimulated the engineered neurons with a radio-frequency magnetic field and showed how the heating of the nanoparticles opened the thermo-sensitive ion channel. The result was the induction of action potentials in neurons. In a successive work, the fusion of the cation channel TRPV4 with the paramagnetic protein ferritin generated the novel protein Magneto (Wheeler et al., 2016), proving it is feasible to achieve magnetic control of action potentials in neurons without heating the cell. Coupling the mechanosensitive protein Notch with magnetoplasmonic nanoparticles proved it it could also be possible to initiate downstream signalling and trigger gene expression (Seo et al., 2016).
Magnetogenetics generated a lot of interest given the potential to substitute optogenetics by solving the burden of light low tissue penetration. Moreover, the use of magnetoliposomes is seen as a promising approach to deliver drugs to the brain (Thomsen, Thomsen, and Moos, 2015) and the heart (Namdari et al., 2017). Together with the excitement that this field has gained, it has also been debated that the paramagnetic nature of proteins can limit the potentials of this field (Anikeeva and Jasanoff, 2016).

Sonogenetics

Affecting gene expression with thermal changes has been carried out for decades by using heat-shock promoters (Villaverde et al., 1993; Piraner et al., 2016), followed

then by RNA thermometers (RNAT) (Klinkert et al., 2012) which can regulate translation by blocking ribosomes binding sites at low temperatures. Nonetheless, in industrial settings, changing the temperature to induce gene expression in big vessels is expensive and ineffective (Palomares, Estrada-Mondaca, and Ramirez, 1987). Moreover, temperature induction presents small dynamic range and low spatiotemporal resolution, which are essential requirements for effective remote cellular drive. While temperature input alone does not represent a viable option to control biology, coupling the thermosensitive promoters with ultrasound stimuli unveils the most exciting applications. In fact, the mechanic nature of ultrasounds (US) make them ideal to induce specific local hyperthermia in cells *in vivo*, triggering the activation of thermo-sensitive promoters. The possibility to initiate gene expression *in vivo* with ultrasounds had been discussed since 1998 (Madio et al., 1998), but it is the advent of cell therapy that motivated the use of high-intensity focused ultrasound (HIFU) to control gene expression with high spatiotemporal resolution. This technique has been initially used to express fluorescence (Guilhon et al., 2003) and luminescence (Deckers et al., 2009) in tumours and later to express pro-inflammatory factors to permeabilize the Blood-Brain-Barrier (BBB) for drug delivery in mice brain (Xiong et al., 2015).

Apart from thermosensitive channels and promoters, also mechanosensitive channels can be used as transducers for the ultrasound-biology interface. An example of this alternative approach is represented by the use of mechanosensitive ion channel TRP-1 in *C.elegans* to translate focused ultrasounds into action potential and drive worm behaviour (Ibsen et al., 2015). In another work, mechanosensitive Ca^{2+}-channel Piezo1 was stimulated by high frequency ultrasounds (HFU) to tune the intake of Ca^{2+}, activate calcineurin and initiate specific gene expression in T-cells for therapeutic applications (Pan et al., 2018).

Sonogenetics represent a promising field that is expected to follow – or even surpass – the rise optogenetics. Its potential applications range from external control

of blood sugar levels to substitution of invasive pacemakers with external US stimulation.

Electrogenetics

Activating biological processes with electric stimuli has not been as popular as optogenetics, sonogenetics or magnetogenetics. Even if research has given attention to the cell-electronics interface, more often it has been on the translation of cellular processes into electrical signals (Collier and Mrksich, 2006; Moreau et al., 2008) rather than the opposite. Systems to control biological behaviour electrically were developed by creating transistor-like devices to control glucose intake in yeast (Song, Wang, and Yau, 2014) or by using redox molecules to tune an enzymatic pathway on a chip (Tschirhart et al., 2016).
Weber et al. gave birth to the field of electrogenetics by engineering a system to trigger specific gene transcription in mammalian cells after superimposition of an electric field (Weber et al., 2009). When turned on, the electrical field caused the oxidation of the ethanol present in the extracellular media, the produced acetaldehyde was transported inside the cell and activated the acetaldehyde-dependent transactivator AlcR inducing gene transcription (Fig.1.4A). Tschirhart developed a similar system in prokaryotes, this time exploiting the electrochemical conversion of ferrocyanide into ferricyanide in the extracellular media (Tschirhart et al., 2017). Then, through cellular respiration, ferricyanide perfused inside the cell and could oxidise the reduced pyocyanin. Oxidised pyocyanin bound to the sensitive PsoxS promoter and initiated gene expression. When activating the promoter, pyocyanin got reduced closing the cycle (Fig.1.4B).

Electrogenetics is still a rather unexplored field and lacks a connection between stimulus and cellular response that is independent from redox biomediators. The

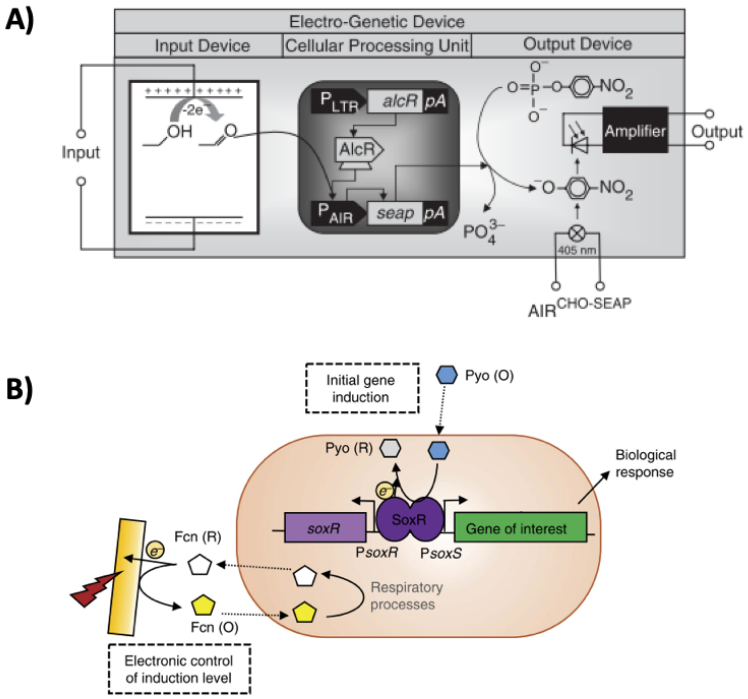

FIGURE 1.4: A) Electrogenetic system in mammalian cell. The electrical field oxidises ethanol into acetaldehyde (left), the acetaldehyde-dependent transactivator AlcR binds to its cognate promoter P_{AIR} and triggers the transcription of SEAP (centre), SEAP catalyses the production of coloured p-nitrophenolate which is detected by a photodiode and reconverted in electrical signal. AlcR, acetaldehyde-inducible transactivator; pA, polyadenylation signal; P_{AIR}, AlcR-responsive promoter; P_{LTR}, murine stem cell virus 50 long terminal repeat-derived promoter (Weber et al., 2009). B) Electrogenetic system in prokaryotes. Oxidised pyocyanin Pyo (O) initiates gene induction of the gene coding for the SoxR protein and a gene of interest through the divergent overlapping PsoxR/PsoxS promoters. Electrochemical conversion of ferrocyanide Fcn(R) into ferricyanide Fcn (O), through respiratory machinery, allows electronic control of induction level. Fcn (R/O), ferro/ferricyanide; Pyo, pyocyanin (Tschirhart et al., 2017).

stimulation delivery promises higher tissue penetration than light - after electropermeabilization (Pavšelj and Miklavčič, 2008) - but lower than ultrasounds and magnetic fields. It has high temporal control, while spatial control is lower than light and ultrasound. Still, complex electric field patterns can be formed by appropriate placement of charges on a surface, that would be reflected in complex gene expression spatial pattern in a tissue. The biggest value of electrogenetics stands in the opportunity that its establishment would have to link electronic devices with biological tissues. Such a connection would be especially useful in the field of

wearable devices and prosthetic.

Comparison

To summarize, a comparison of the different technologies to externally trigger a specific cell responses is shown in Tab.1.1.

As it can be seen from the last two columns in Tab.1.1, the approach that shows the highest capabilities in remotely controlling cell processes is sonogenetics. The high tissue penetration and high spatio-temporal control provided by US stimuli coupled with minimal – if any – side effect represents the most promising results. Nonetheless, it is also apparent that the field of electrogenetics has not been explored thoroughly, given its potentiality of providing interfaces with both electronic devices and naturally excitable cells such as neurons and cardiomyocytes. In particular, the only attempts of harnessing cell biology with electrical fields have been carried out by using redox biomediators to induce gene expression, not considering electrosensitive ion channels. For every other field considered, except electrogenetic, cellular response could be triggered by the external stimulus through conformational changes of sensitive ion channels:

- Rhodopsin proteins in optogenetics;
- Thermosensitive and mechanosensitive ion channel in sonogenetics;
- Mechanosensitive ion channels linked to magnetic nanoparticles or paramagnetic proteins in magnetogenetics.

On the other side, every cell expresses a variety of voltage-sensitive membrane proteins that change conformation when membrane potential shifts. Since membrane potential can be shifted with an external electrical field (Marszalek, Liu, and Tsong, 1990), the exploitation of such a protein for electrogenetics would liberate from the burden of redox biomediators limits. Moreover, the electric activation of a protein at the post-translational level would result in immediate biological response to

External Control of Biology						
	Delivery	Action Potential	Promoter	Conformational Changes	Drawbacks	Advantages
Chemogenetics	Inoculation (chemical substance)	Y	Chemosensitive	X	Accessibility *in vivo*, toxicity, low spatio-temporal precision	Facility of use in controlled environment
Optogenetics	Remote (light)	Y	X	Rhodopsins	Low tissue penetration, Light Scattering	High spatiotemporal precision
Sonogenetics	Remote (ultrasound)	Y	Thermosensitive	Thermosensitive, Mechanosensitive	Overheating	High spatiotemporal precision; high tissue penetration
Magnetogenetics	Remote (magnetic field)	Y	Y	Mechanosensitive (nanoparticles)	Interference with protein (paramagnetism)	High spatiotemporal precision (with appropriate pattern structure), High tissue penetration
Electogenetics	Remote (electric field)	Y	Redox-sensitive	X	Accessibility *in vivo* (addition of biomediators for transcriptional change), potential interference with cell biology	High spatiotemporal precision (with appropriate pattern structure), direct interface with electronic devices, interface with excitable cells

TABLE 1.1: Comparison of stimuli of different nature, able to control cellular processes. For each stimulus type, it is stated the delivery method, whether it has the capability (natural or synthetic) to trigger action potential in neurons, whether exist promoters that are sensitive to the stimulus, whether exist proteins that undergo conformational changes, the drawbacks and advantages of the system ("Y"= yes; "X" = no).

the external stimulus, solving the waiting time involved in gene expression. Such a protein-based electrogenetic system would provide a tight electro-biological interface, particularly needed to form a stable two-way cross-talk system between bioelectronic devices and engineered cells.

1.5.2 Bioelectronics

Bioelectronics is a field at the convergence between biology, electronics and biomaterials. It includes biosensors and devices that are wearable, ingestible or implantable. The broad definition embraces a variety of novel technologies, here discussed.

Stretchable bioresorbable electronic devices

Stretchable, skin-bioresorbable electronic devices have been recently developed, which incorporate sensors to monitor parameters such as temperature, strain, electrophysiological parameters, light and also photodiodes and modules for radio-frequency communication (Kim et al., 2011). They proved these devices can integrate seamlessly with skin and any human body part and can interface with cells in two-way communication. For instance, they developed: a silicon-based device that can sense intracranial pressure and temperature and can disappear in the brain by hydrolysis and metabolic action after the use (Kang et al., 2016); an electrically-wired membrane that folds around the heart, monitors myocardial cells and is able to produce a stimulus in abnormal circumstances (Xu et al., 2014) (Fig,1.5A); a bioresorbable device that stimulates neurons in-situ after a traumatic injury to improve regeneration (Koo et al., 2018).

Interfaces with neurons

Interfaces with neurons dominate the applications of bioelectronics, given the common nature of electrical signals. Electrodes composition and morphology have been improved for a variety of applications. For experimental settings, novel sensor boards have been established to detect low-noise cells signals in the range of pico-amperes in glioma cells (Rocha et al., 2015). Intracellular recording with vertical nanopillars has also established a tighter interface with neurons without the invasiveness of patch clamp (Xie et al., 2012).

Brain electrodes have been functionalised with conductive hydrogel to incorporate neural cells on their surface and create an improved prosthetic implant in injured brain (Green et al., 2017; Goding et al., 2019). This device, named "living electrode", constitutes a better system of delivering electrical signals for Brain-Machine-Interfaces. In fact, sending stimuli through the incorporated neurons rather than directly from the electrode avoids negative effects on the brain tissue such as cell electroporation, undesired generation of chemicals, local pH changes, inflammatory reactions and degradation of the electrode itself.

Wearable and ingestible devices

A promising application of bioelectronics stands also in the rising field of wearable devices. These devices are expected to deliver on-body valuable functionalities from bio-sensing to bio-actuating, especially in the medical space. An example of such technologies is the tattoo-based glycemic biosensor. Such device extracts the interstitial glucose by reverse iontophoresis and quantifies it by amperometric biosensing using a glucose oxidase as a transducer (Bandodkar et al., 2015) (Fig,1.5B).

For the development of the field of wearables the elaboration of power-generating systems such as biofuel cells (BFC) has been critical. The ability of enzymatic BFC

to generate power from local and renewable biochemical species (Barton, Gallaway, and Atanassov, 2004; Cracknell, Vincent, and Armstrong, 2008; Zhou et al., 2012) or from local stretch (Jeerapan et al., 2016) allows bioelectronic devices to be self-sustained and independent from batteries.

Beyond wearables, another example of the biology-electronics alliance is represented by ingestible devices such as the one developed by Mimee in Tim Lu's lab (Mimee et al., 2018). The capsule the researchers engineered hosts bacteria and use them as gut health biosensors. Once in the gut, the bacteria in the capsule generate a signal in response to high concentration of specific biomarkers in the gut. The biological response is measured by the capsule electronic sensors and it is wirelessly communicated to an external machine that would detect eventual abnormalities (Fig,1.5C).

Cell-free technologies

Cell-free environments as well have been used for bioelectronic applications, especially in the biosensing field. After showing that lisozyme motion can be monitored and measured by tethering single enzymes to carbon nanotube transistors (Choi and Weiss, 2012) (Fig,1.5D), viruses as well were bound to conductive polymers to enhance their sensing capabilities. In particular, integrating the virus ability of biosensing analytes onto nanowire platforms, it was shown how the quantity of antibody binding to the virus could be coupled with a proportional change in electrical signal (Arter et al., 2010).

All the reported examples have in common the effort of developing a tighter integration between electrical devices and cells to find novel solutions for medical and environmental problems. Nonetheless, it is true that the approaches followed so far have mainly focused on the biological-to-electric translation, limiting the electric-to-biological control restricted only to neuron action potential stimulation (Kim et al., 2018).

The electrical nature of neuron signals represents in fact a natural access for electrical inputs in biology. However, the possibility to develop an artificial interface to control molecular processes with electricity would enhance bioelectronics capabilities by establishing a robust feedback loop at the biological-electrical interface. Given the higher complexity in delivering photo- magneto- or sono- stimuli with high spatial accuracy in the context of bioelectronic devices, the only biotechnology that promises to directly fill and standardize the electro-biological control is electrogenetics.

As I foresee a future where it can be possible to integrate electrical stimuli from bioelectronic devices with cell biology, a better understanding of the electrical-biological interface limits is needed. In particular, it is important to assess how an electrical stimulus, apart from triggering the electrogenetic system, would affect the natural cell electrophysiology and whether it could potentially cause unwanted side effects to cells and tissues.

1.5.3 Eukaryotic membrane potential and electric fields

Membrane potential role in eukaryotic cells

In excitable cells such as neurons and muscle cells, when the RMP is depolarized by a certain degree – usually from -70 mV to -50 mV in neurons – specific ion channels that are sensitive to shifts of membrane potential are triggered. When voltage-gated sodium channels open, they cause an inward flux of sodium ions that quickly increases cell depolarization. As more channels open, the membrane potential polarity is inverted for a few milliseconds (typically between 1 and 100 ms) reaching +40 mV. After this spike, sodium channels close and potassium channels open, leading to outward flow of potassium ions across the membrane and re-establishing the RMP. Such a membrane potential behaviour is usually triggered by an external stimulus in a restricted portion of the cell membrane. The local depolarization activates adjacent voltage-gated ion channels, causing novel depolarization in the adjacent

membrane portion. This repeated chain of events makes the signal travel the whole cell membrane. Such an electrochemical signal travelling along an excitable cell is called action potential and it is the mechanism that allows neurons to communicate with each other.

Membrane potential does not show action potential-like dynamics in non-excitable cells however, in every cell it undergoes significant deviations from the RMP in relation to a variety of cellular processes.

It has been known for long time the association between cell viability and membrane potential: cells in a hyperpolarized state tend to be quiescent and do not undergo mitosis, while cells in a more depolarized state tend to be in a proliferative status (Cone, 1971). It was shown more recently that the circadian rhythm itself synchronises with periodic RMP changes (Kuhlman and McMahon, 2004; Noguchi et al., 2012). The association between depolarization and proliferation is so tight that cancer cells, which are subjected to a higher proliferative status, are in fact characterized by a more positive RMP than their healthy counterparts (Cone, 1971). It was shown that a metastatic phenotype is effectively triggered by an abnormal depolarization of the RMP (Chernet and Levin, 2013), which was found to be associated with overexpression of voltage-gated sodium channels (Diss et al., 2005; Fraser et al., 2005). For this reason, depolarization itself can be used as marker for neoplasia. While a link between ionic current-induced physiological electrical field and cell motility – a behaviour called galvanotaxis - has been studied for years (Nuccitelli, 1988), more recently it has been associated particularly to metastatis (Mycielska and Djamgoz, 2004).

Membrane potential plays an important role in the development and regeneration of an organism limbs. From the early twentieth century it was suspected that endogenous ion currents were involved in cell polarization (Mathews, 2019) and therefore explaining cell galvanotaxis and galvanotropism (Nuccitelli, 1988). During development, the importance of RMP extends from neuronal differentiation (Messenger

and Warner, 2000) to determining the early asymmetry between the left and right side of the organism (Levin et al., 2002). In fact, it was shown that such asymmetry is shaped by an asymmetric distribution of membrane potentials across the embryo. Further research led to the establishment of a tight link between RMP and an organism morphology, to the extent that, in frog embyros, craniofacial structures were found to depend on the hyperpolarization pattern (Vandenberg, Morrie, and Adams, 2011).

Membrane potential has also a similar role in wound healing. When a tissue is damaged, the cells on the edge of the wound undergo depolarization. This behaviour has been shown to sustain the formation of the actin structure that is critical for wound healing (Chifflet, Hernández, and Grasso, 2005). Moreover, ion flux in the damaged area generate a significant electrical field (EF) that initiates cell migration by galvanotaxis into the wound environment, allowing tissue repair (Reid and Zhao, 2014).

Aside from the mentioned cellular processes, membrane potential dynamics have been shown to be involved in a variety of other cellular processes, from cell signalling to volume control and secretion.

Electric Field effect on eukaryotic cells

It is clear that the electrical nature of membrane potential has a key role in the electrophysiology of a cell, being tightly linked with a variety of cellular processes. For this reason, it is critical to ask whether the application of an external electrical stimulus – which is the input to a cell in an electrogenetic system - would modify the membrane potential and have dangerous consequences on the cell. External electrical signals can be converted in cellular processes such as phosphorylation of enzymes (Zhao et al., 2006), translocation of transcription factors (Yang et al., 2004), electrophoresis of molecules and activation of voltage-sensitive channels and other membrane proteins (Tsong, 1990; Levin, 2007). Nonetheless, I will review here the effects that EFs have at a more macroscopic level, from the whole cell to

the tissue and organism context.

It is known from Maxwell's theories and Schwann equation (Marszalek, 1990) that an external electrical field can enough to generate a shift in membrane potential. For a direct current (DC) field, the transmembrane potential difference ΔE_m induced on the cell membrane at a point P is proportional to the field strength EF_{DC} and it is estimated by:

$$\Delta E_m = 1.5 * a * EF_{DC} * cos(\theta)$$

where a is the cell radius and θ is the angle between the field direction and the line connecting P with the center of the cell (Fig.1.6).

Electroporation is the most famous electric effect on cells in research laboratories. The application of electrical pulses, each with a duration of $100\mu s$ and a magnitude of 1-3 kV/cm, has the effect of temporarily change the membrane potential to +0.5-1.5 V, leading to pore formation and an increase of membrane permeability (Weaver, 1993). The phenomenon is mainly used to improve the efficiency of delivering DNA, enzymes, antibodies and viruses to cells and tissues. It is very important to calibrate the magnitude of the electrical field and the duration of the stimulus because the combination of a high-enough electrical field and a long-enough stimulus can cause membrane disruption and eventual cell death (Garcia, Davalos, and Miklavcic, 2014) (Fig.1.7).

Following from the relationship between membrane potential and cell proliferation, it was found that the quiescent and mitotic status of a cell can be manipulated by artificially driving the membrane potential. Researches showed that proliferation increases as desired by appropriately stimulating the cell membrane (Cone, 1971; MacFarlane and Sontheimer, 2000). In particular, hyperpolarization of Chinese hamster ovary (CHO) cells to -70 mV leads to mitotic arrest and the process can

be reversed when cells are depolarized back to -10 mV (Cone, 1971; Blackiston, McLaughlin, and Levin, 2009).

Since the carcinogenesis and cancer cells proliferation as well have a tight relationship with membrane potential dynamics, formation of tumorous cells can be prevented by artificially inhibit cell depolarization (Chernet and Levin, 2013). Mitotic spindle formation can be disrupted in tumorous cells by using tumour treating fields: with appropriate intensity (1-3 V/cm) and frequency (100-300 kHz), an alternate EF can target specific cancer cells and induce apoptosis (Davies, Weinberg, and Palti, 2013). Superimposition of an EF can also influence galvanotaxis of metastatic cancer cells, driving them along the EF lines and towards the cathode in prostate cancer (Djamgoz et al., 2001).

EF influence can affect a whole organism during its development, when its superimposition can influence the membrane potential and hack the mechanisms underlying limb growth. Following from the discoveries on membrane involvement in embryogenesis (Levin et al., 2002), Levin's lab started to study EF influence on embryo development. The researchers showed how the depolarization of 'instructor cells' at the tip of *Xenopus* tadpoles' tail changes the behaviour of all embryo's melanocytes. In particular, cell proliferation increases and the cell shape changes to migrate similarly to metastatic behaviour. The hyperpolarization of the same cells reverted the process (Chernet and Levin, 2013). It was soon proved that spatiotemporal differences in RMP provide specific instructions for cell regulation and complex patterning during embryogenesis and regeneration. It has been known for a long time that electrical stimulation can induce bone healing and regeneration (Lavine, 1972), but Levin's group showed that it can be possible to also regenerate frog legs with electrical stimuli (Tseng et al., 2010). As a further proof of concept of the importance of membrane potential on limb generation, planarians with two heads were obtained by his group with appropriate electrical stimulation (Lobo, Beane, and Levin, 2012; Levin, 2014; Pietak et al., 2019).

Having considered how driving the membrane potential of a cell deeply affects the

fate of the cell, an electrogenetic system can be better designed. In particular, it is important that the electrical stimulus is calibrated with appropriate duration, frequency and magnitude in order to not interfere with other cellular processes.

1.5.4 A novel Electrogenetic system as a missing link for Bioelectronic Devices

As biological interface within bioelectronic devices is mostly unidirectional, from biological stimulus to electrical output, there is the need to close the loop with a system able to control biology with electrical stimulation. An electrogenetic solution would make novel bioelectronic systems more stable and reliable.

In Sec.1.5.1 it was described the current development of electrogenetics, showing that currently it relies on biomediators such as redox molecules. The needed addition of these substances in the extracellular environment, aside from the potential toxicity of the mediators *in vivo*, blocks the potential application of the system. In fact, these features would limit the system to the cases where access to the extracellular environment is of possible implementation. Moreover, the induced gene expression is associated with a lag in time between stimulus and biological effect. This lag would limit the feedback control between an electrogenetic system and a bioelectronic device, representing also a potential problem in case an immediate action on the system is required. As shown in Tab.1.1, electrogenetics is the only field of the remotely-controlled-biological systems that has not exploited the quick conformational changes of a membrane protein that is sensitive to the external stimulus. The development of a novel electrogenetic system, able to link the electrical stimulus to cellular processes through protein conformational changes, is needed.

Coupling the VSD described in Sec.1.1 with an enzyme able to target a specific cellular process would make the enzymatic activity controllable by an external electrical stimulus and therefore allow electrical control on the targeted process itself. I called such an actuator protein Membrane potential Activated Targeting Enzyme

(MATE).

1.6 Aims and Scope

The aim of this thesis was to use a modular voltage-sensitive-domain to expand the Synthetic Biology toolbox with proteins dependent on membrane potential.

In Chapter 2 I intended to use such domain to create a membrane potential reporter for prokaryotic cells. As mentioned, studying prokaryotes' electrophysiology is important to develop strategies to fight infections, but non-toxic electrophysiological probes for bacteria are still missing. Extending VSP's VSD usage to prokaryotes would bring the benefits of mammalian GEVIs to prokaryotic studies.

In Chapter 3 the goal was to develop the first-ever voltage-sensitive-protease by coupling the voltage-sensitive-domain to a TEV protease. Such novel technology would open new scenarios in the way biology is interfaced by humans. In fact, voltage-sensitive-enzymes could constitute the basis for an electrogenetic framework analogous to optogenetics and sonogenetics. The benefits of VSD-based electrogenetics will allow to close the loop between electronics and biology in the context of bioelectronic devices.

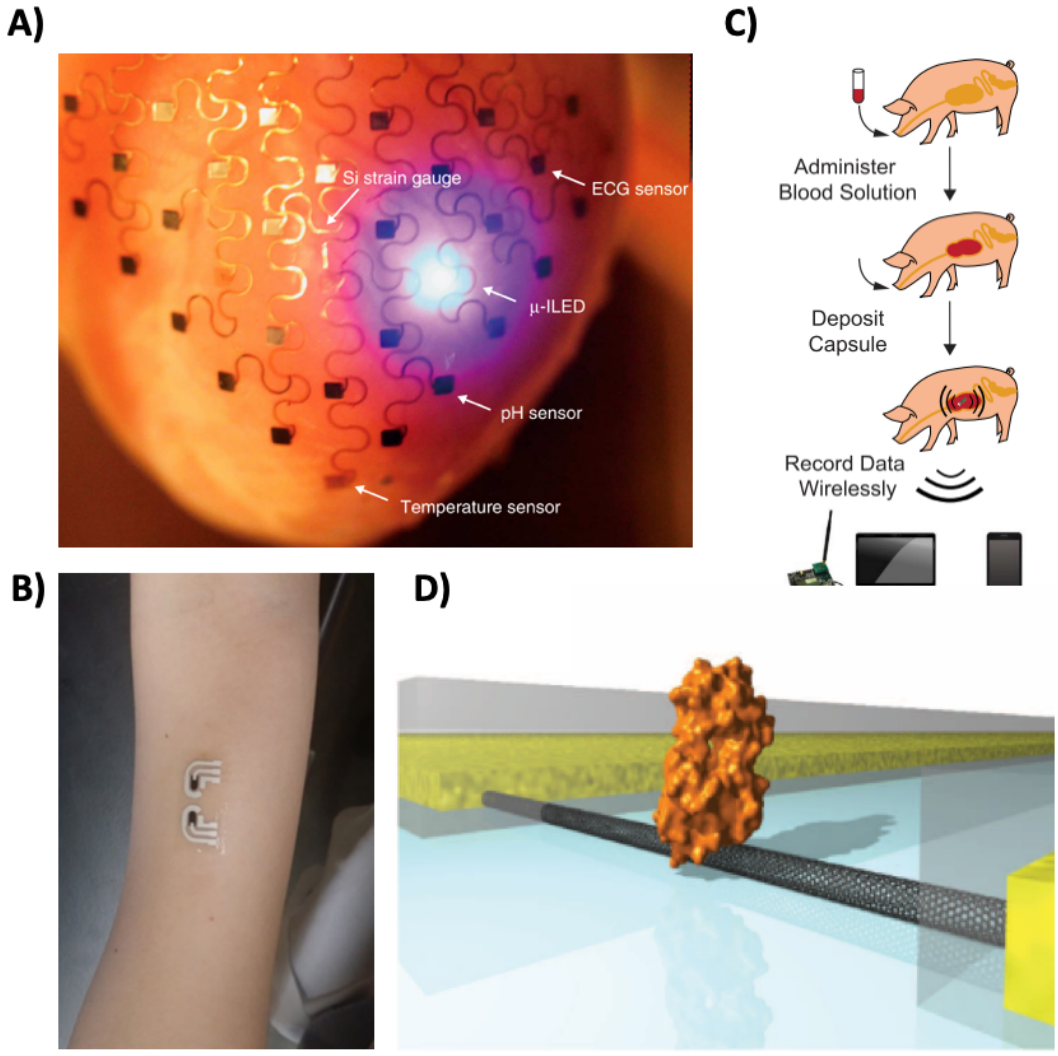

FIGURE 1.5: Examples of Bioelectronics applications. A) Elastic electronic membrane to monitor and stimulate heart cells (Xu et al., 2014). B) Tattoo-based glycemic sensor (Bandodkar et al., 2015). C) Ingestible device populated by bacterial biosensor to monitor a pig gut and send the measured parameters outside the pig body (Mimee et al., 2018). D) Cell-free interaction between a nanowire and a lysozyme for enzyme dynamics monitoring (Choi and Weiss, 2012).

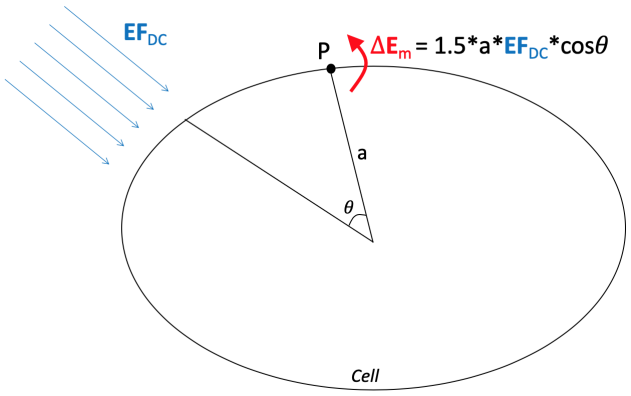

FIGURE 1.6: Representation of a cell and the effect that an external DC electrical field EF_{DC} has on the membrane potential in a point P. Following Schwann equation, the membrane potential shift ΔE_m induced by the electrical field is proportional to the electrical field by constants such as the cell radius a and the cosine of the angle θ between the field direction and the line connecting P with the center of the cell.

.

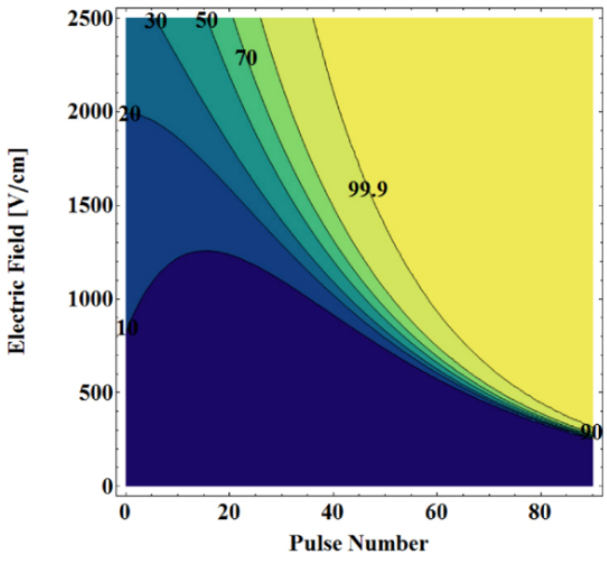

FIGURE 1.7: Simulation results of the probability of cell death (%) after electroporation. Different electrical field (EF)magnitudes and pulse number (frequency of 1 Hz) were simulated, showing cell death more probable with a combination of high EF and long duration (Figure from (Garcia, Davalos, and Miklavcic, 2014))

.

2 Development of a Membrane Potential Reporter for *Bacillus subtilis*

In the present chapter I present the effort to obtain a Genetically Encoded Voltage Indicator (GEVI) suitable for electrophysiological studies in *B.subtilis*. After expressing the eukaryotic reporter ASAP1 in prokaryotic cells, variants called PAPS were created by positioning the fluorescent protein in different locations of the voltage-sensitive domain, with the aim of increasing the fluorescence change upon membrane depolarization.

2.1 Materials and Methods

2.1.1 Cell cultures

Strains

Escherichia coli TOP10 (Invitrogen) was the chassis used for the assembly, the replication and the stock of every constructed plasmid. For the final assessment of PAPS variants, *Bacillus subtilis* PY79 cells were analysed after genomic integration of the construct in the AmyE locus.

Culturing Conditions

Both *E.coli* and *B.subtilis* cells were grown for 15 hours either on lysogeny broth (LB) agar plate (1.5% w/v agar) or in liquid LB suspension (shaking incubator at 6 RCF). Both solid and liquid media were supplemented with the appropriate antibiotic: 100 $\mu g/mL$ ampicillin for *E.coli*, 300 μ/mL spectinomycin for *B.subtilis*.

2.1.2 Construct Development

Cloning

Every construct developed during this project was inserted into a derivative of pDL30 plasmid (Kuchina et al., 2011) named JDE131 (kind gift by Gurol Suel, UC San Diego), after the IPTG-inducible promoter PHyperspank (Fig.2.1 and Fig.A.1). JDE131 plasmids were linearized by digestion with AfeI restriction enzyme while every insert cDNA was obtained by Polymerase Chain Reaction (PCR) using PrimeSTAR Master Mix (Takara) or Q5 Polymerase (New England BiolabsR Inc.(NEB)). Codon optimized sequences were obtained on GeneOptimiser (Thermo Fisher Scientific) and the synthesised DNA sequences ordered from Integrated DNA Technologies, Inc (IDT).

In order to assemble a plasmid through Gibson Assembly, the PCR primers amplifying a fragment were designed to have 20 base pairs (bp)-long overlap with the sequence of the fragments adjacent in the assembly (Gibson et al., 2009). In App.A.0.1 are listed all their DNA sequences. The length of the digested JDE131 vector and of every PCR-amplified cDNA was analysed by electrophoresis (180 V, 160 mA, 30 W for 20 minutes) in a SB buffer agarose gel (1% w/v). The bands confirming the expected weights were gel-purified (Gel Extraction Kit, NEB) and their concentration measured with NanoDropTM 2000/c Spectrophotometer (Thermo Scientific).

The vector-insert(s) assembly was obtained by Gibson Assembly with Gibson Assembly Master Mix (NEB) (Gibson et al., 2009). For every assembly, 50 ng of

backbone DNA were mixed with the inserts with a 1:3 backbone:insert molar ratio and the Gibson Master Mix was added to the total volume in a 1:1 volume ratio. The mix was incubated for 45 minutes at 50°*C*. *E.coli* Top10 cells were made chemically competent by using Mix&Go kit (ZymoGen) and the Gibson Assembly product was transformed into the competent cells by following the suppliers' instructions.

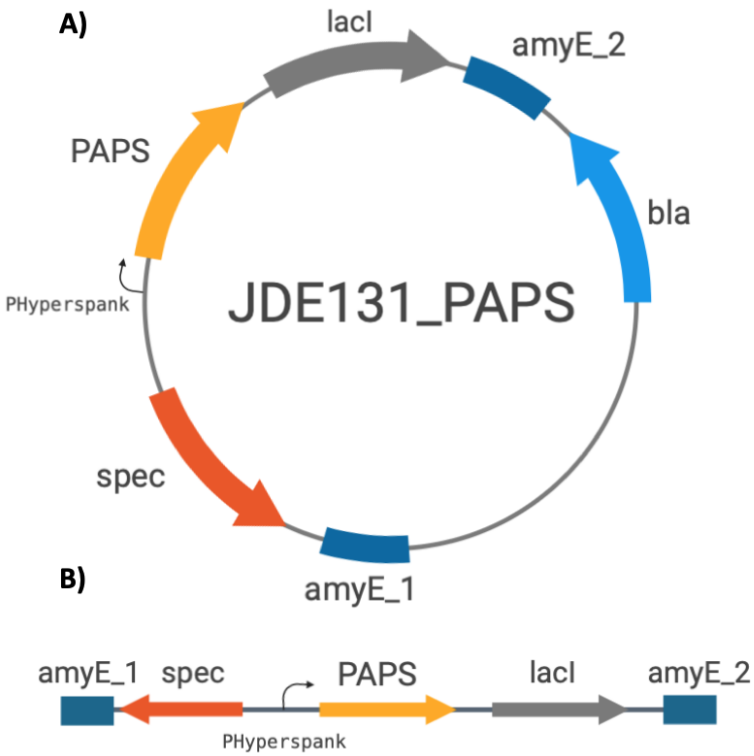

FIGURE 2.1: A) Map of the JDE131 plasmid, with "PAPS" labeling the position the gene sequence of each construct was placed. PHyperspank: IPTG-inducible promoter; PAPS: assembled construct to be analysed; lacI: *lacI* gene necessary for PHyperspank correct induction; *bla*: ampicillin restistance gene; spec: spectinomycin resistance gene; AmyE_1 and AmyE_2: two complementary sites of the AmyE locus in *B.subtilis* PY79 genome; *spec*: spectinomycin resistance gene. B) Plasmid fragment that gets integrated into *B.subtilis* genome through homologous recombination in the AmyE locus

.

The *E.coli*-assembly mix was then plated on warm LB agar plates containing 100 $\mu g/mL$ ampicillin and left to grow overnight at 37°*C*. After 15 hours, colonies (in the number of 3 or 4) were screened for positive transformation and correct insert length. This was achieved by performing colony-PCR with SapphireAmp®

Fast PCR Master Mix (Takara) and the primers AP44 and AP45 flanking the insert (Fig.A.1) and by performing electrophoresis on the amplicons as previously described.

The colonies showing DNA bands of the expected insert length were inoculated in liquid LB with 100 $\mu g/mL$ ampicillin and grown overnight (37°C, 6 RCF). Miniprep (Monarch Miniprep Kit – NEB) was performed after 15 hours and each plasmid was sent to Source Bioscience or GATC (Eurofins) together with AP44 and AP45 primers to confirm the insert sequence. Recombinant strains with correctly-assembled constructs were grown in LB cultures and stored in cryogenic tubes at $-80°C$ with 25% (v/v) glycerol.

Each plasmid to be transformed in *B.subtilis* PY79 was obtained from the *E.coli* glycerol stock by inoculating the appropriate strain into liquid LB (supplemented with 100 $\mu g/mL$ ampicillin) and performing miniprep (Monarch Miniprep Kit – NEB) after overnight growth (15 hours, 37°C, 6 RCF). The plasmid concentration was estimated with NanoDrop and $8\mu g$ of plasmid were transformed into *B.subtilis* PY79 wild type (WT) grown overnight on agar plate. To transform the plasmid in *B.subtilis*, nitrogen starvation approach was followed by growing the bacterium in a nitrogen-deprived transformation media (25 g/L $K_2HPO_4.3H_2O$, 6 g/L KH_2PO_4, 1 g/L trisodium citrate, 0.2 g/L $MgSO_4.7H_2O$, 2g/L Na_2SO_4, 50 $\mu M FeCl_3$, 2 $\mu M MnSO_4$, 0.4% w/v *Glucose*, 0.2% w/v *Glutamate*) (Jarmer et al., 2001). The final *B.subtilis*-DNA mix was plated on LB agar plates (300 $\mu g/mL$ spectinomycin) and left to grow over night at 37°C. Colonies grown on the antibiotic-supplemented plate were screened by colony-PCR for genomic integration in *B.subtilis* AmyE locus with AP44-AP45 primers. Strains previously transformed with the same plasmid in the Asally Lab were used as positive control, while WT was used as negative control. Colonies showing positive bands on the gel were sent to sequencing and, if the sequence was confirmed, the recombinant strain was stored in glycerol as previously described.

Every DNA sequence is reported in App.A.0.1.

Random mutagenesis of selected PAPS

S3 and S4 helices in PAPS-At and PAPS-Gt were amplified by mutagenic PCR by using the GeneMorph II Random Mutagenesis Kit (Agilent) together with the Agilent "Mutazyme II" error-prone DNA-polymerase. The heterogeneous mix of S3-S4 amplicons was assembled by Gibson Assembly with the rest of the plasmid, which was amplified with PrimeSTAR Master Mix (Takara) with AP586-AP592 for PAPS-At and AP586-AP590 for PAPS-Gt. After transformation in *E.coli*, all the colonies obtained on the LB plate (100 $\mu g/mL$ ampicillin) were inoculated and grown in the same liquid culture (100 $\mu g/mL$ ampicillin). Miniprep was therefore performed and the subsequent heterogeneous plasmid mix was transformed in *B.subtilis*. Again, all the colonies obtained on the LB plate (300 $\mu g/mL$ spectinomycin) were inoculated and grown in LB liquid culture (300 $\mu g/mL$ spectinomycin) and stored in glycerol as previously described. The result was a stock of *B.subtilis* with PAPS-At and PAPS-Gt constructs having S3-S4 helices with random mutations.

2.1.3 Analysis of strains and their expressed constructs

Every *B.subtilis* PY79 strain to be analysed was taken from the glycerol stock and grown over night for 15 hours in LB supplemented with 300 $\mu g/mL$ spectinomycin and then re-suspended in fresh LB (1:50 v/v ratio) supplemented with 1 mM IPTG to express the genetically-integrated construct by the IPTG-inducible Phyperspank promoter. After reaching OD = 0.8, the pseudo-rationally designed constructs were to be analysed on the fluorescence microscope. On the other hand, the heterogeneous mix of PAPS mutants obtained after S3-S4 random mutagenesis was analysed by flow cytometry.

Fluorescence Microscopy

To image the recombinant strains on the microscope, $2\mu L$ of the fresh culture were placed on squared pads (5 mm x 5mm x 3mm) prepared with fresh LB-agarose (1%

w/v) supplemented with 1 mM-IPTG. *B.subtilis* WT and *B.subtilis* YFP were used as negative control, while pads with potentiometric dyes ThT ($10\mu M$) or TMRM ($0.1\mu M$) were used as positive control of membrane potential shift. To depolarise *B.subtilis* strains, each strain was also put on pads with additional supplement of KCl (150 mM) (Friedrich et al., 2000) or CCCP ($1\mu M$). After placing the bacteria on top, the pads were flipped upside-down onto a glass-bottom dish and imaged with the inverted microscope Leica DMi8 (Leica Microsystem), inside a dark incubator at $37°C$. A 100x oil-immersion objective was used for the imaging. The microscope was interfaced from a Microsoft Windows 7 desktop computer via MetaMorph® Microscopy Automation (Molecular Devices) software.

Flow Cytometry

PAPS-At and PAPS-Gt mutants were suspended in 500 μL LB supplemented with 1 mM IPTG and sorted by Fluorescence Activated Cell Sorting (FACS) on the "FACSAria Cell Sorter" (BioRad). The FACS machine was set to select the recombinant strains showing YFP fluorescence in the 90^{th} percentile of the population. For each of the two PAPS variants, 192 mutants were distributed in two 96-well plates and grown in 50 μL LB (100 $\mu g/mL$ ampicillin) for 15 hours ($37°C$, 6 RCF). Controls with PY79_WT and PY79_cpYFP were also added to first columns of the plates. Each mutant fluorescence was then measured on the "LSR Fortessa" (BioRad) flow cytometer, before and after cells depolarization. The analysis was carried out by the flow cytometer in an automated way with the use of its robotic stage. For both PAPS-At and PAPS-Gt mutant library, the five strains showing higher $\Delta F/F$ were sent to sequencing and their YFP fluorescence re-measured in LSR Fortessa before and after cell depolarization.

Apart from the mutant library, also PY79_WT, PY79_cpYFP and the original PAPS-At and PAPS-Gt were analysed with LSR Fortessa before and after cell depolarization.

Cell depolarization was obtained with the addition of a mix of 150 mM KCl and $1\mu M$ CCCP for the original PAPS-At and PAPS-Gt constructs and with the addition of 150 mM KCl (Friedrich et al., 2000) for the mutant library.

To estimate the membrane potential change with fluorescent dyes, $10\mu M$ ThT or $0.1\mu M$ TMRM were added. Before each analysis, cell cultures were diluted until reaching 200-400 events per second rate in the Flow Cytometers.

2.1.4 Software and Data Analysis

The design of the DNA sequences of PAPS variants and control constructs, the sequence design of primers and the alignments of sequencing data were performed on Benchling (www.benchling.com).

Microscope images were visualized in Fiji Is Just ImageJ (FIJI). Signal to Noise Ratio (SNR) of cell fluorescence was computed as the average intensity of a manually-selected area (inside a cell or on the cell border when t216 was used) divided by the average intensity coming from an arbitrary background area outside the cell.

Flow cytometry data was visualized as histograms in “Flowing Software v2.5.1" and the mode of the histograms was used for comparison of different samples.

The data quantified from the microscope and the flow cytometer was processed using Matlab R2016b (MathWorks). For data from microscope images, SNR from different sample sets were compared by considering sets of 10 samples each. Mean value and standard deviation (SD) were calculated and the sets compared by performing two-tailed t-tests. For data from flow cytometer, 10000 samples were considered for each sample set and the mode was compared.

2.2 Results

2.2.1 Pseudo-rational design of PAPS

Heterologous expression of ASAP1 shows low SNR, improvable with YFP

To assess whether the eukaryotic ASAP1 construct could be used as membrane potential reporter in prokaryotic cells, it was genetically integrated in *B.subtilis* PY79 and expressed. ASAP1 showed a Signal to Noise Ratio (SNR) of 1.04 (SD_{ASAP1} = 0.004) at resting potential, compared to SNR_{WT} = 1.01 (SD_{WT} = 0.003) and SNR_{cpYFP} = 1.53 (SD_{WT} = 0.02). As a first hypothesis, it was suggested that ASAP1 fluorescent protein, cpsfGFP-OPT, was not folding correctly in the new host. Since YFP Venus was known to be a bright fluorescent protein (Shaner, Steinbach, and Tsien, 2005) and it had been used successfully in Asally's lab, sfGFP-OPT was substituted with YFP Venus. The modified version of ASAP1 bearing the circularly permuted version of YFP (cpYFP) in place of cpsfGFP-OPT was called "Prokaryotic ASAP1-based Potentiometric Sensor" ("PAPS") and it showed an SNR_{PAPS} = 1.09 (SD_{PAPS} = 0.007) (Fig.2.2).

Codon optimised PAPS show better SNR but they are not membrane-specific

It is known that codon usage bias is a cause of poor expression for heterologously expressed genes (Plotkin and Kudla, 2011). It was thus hypothesised that gene codon optimization for *B.subtilis* could improve PAPS expression. The codon-optimised version was called PAPS-G and it was obtained together with two more variants: PAPS-A and PAPS-B. Differently from PAPS-G, PAPS-A and PAPS-B were designed to have the cpYFP placed in the intracellular S2-S3 loop, between N117 and Y118, instead of the extracellular S3-S4 loop of the VSD (Fig.2.3B and C). The rational for this change was the hypothesis that an intracellular FP may ensure a better chromophore formation inside the cytoplasm and that, during VSD conformational changes, the upwards-sliding of S4 is accompanied by a

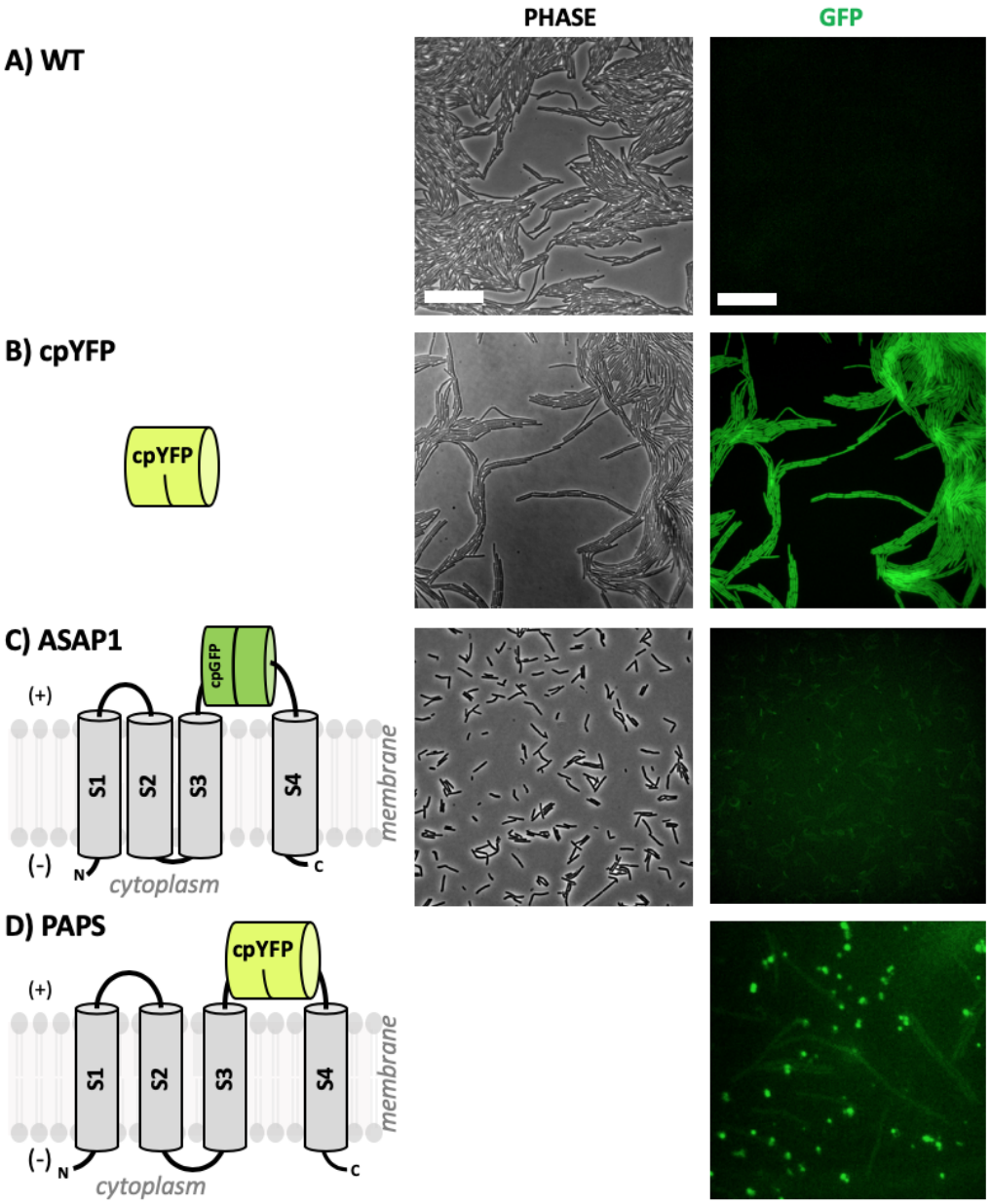

FIGURE 2.2: Cartoon (left), Phase Contrast (center) and GFP channel (right) microscope acquisition of *B.subtilis* PY79 wild type (A), PY79_cpYFP (B), PY79_ASAP1 (C) and PY79_PAPS (D). Scale: 10 μm. While ASAP1 construct showed a SNR = 1.04, the substitution of cpsfGFP-OPT with cpYFP made PAPS fluorescence increase to SNR = 1.09.

.

downwards-sliding of the S3 helix. Such a shift could be reflected in a FP fluorescence change, therefore still sustaining the reporter model. PAPS-B was designed analogously to PAPS-A, but shortening by 4 residues the linkers connecting the cpYFP with the transmembrane helices (Fig.2.3D). The new codon-optimized PAPS variants (PAPS-G, PAPS-A and PAPS-B) showed a SNR of 1.03, 1.16 and

1.21 respectively.

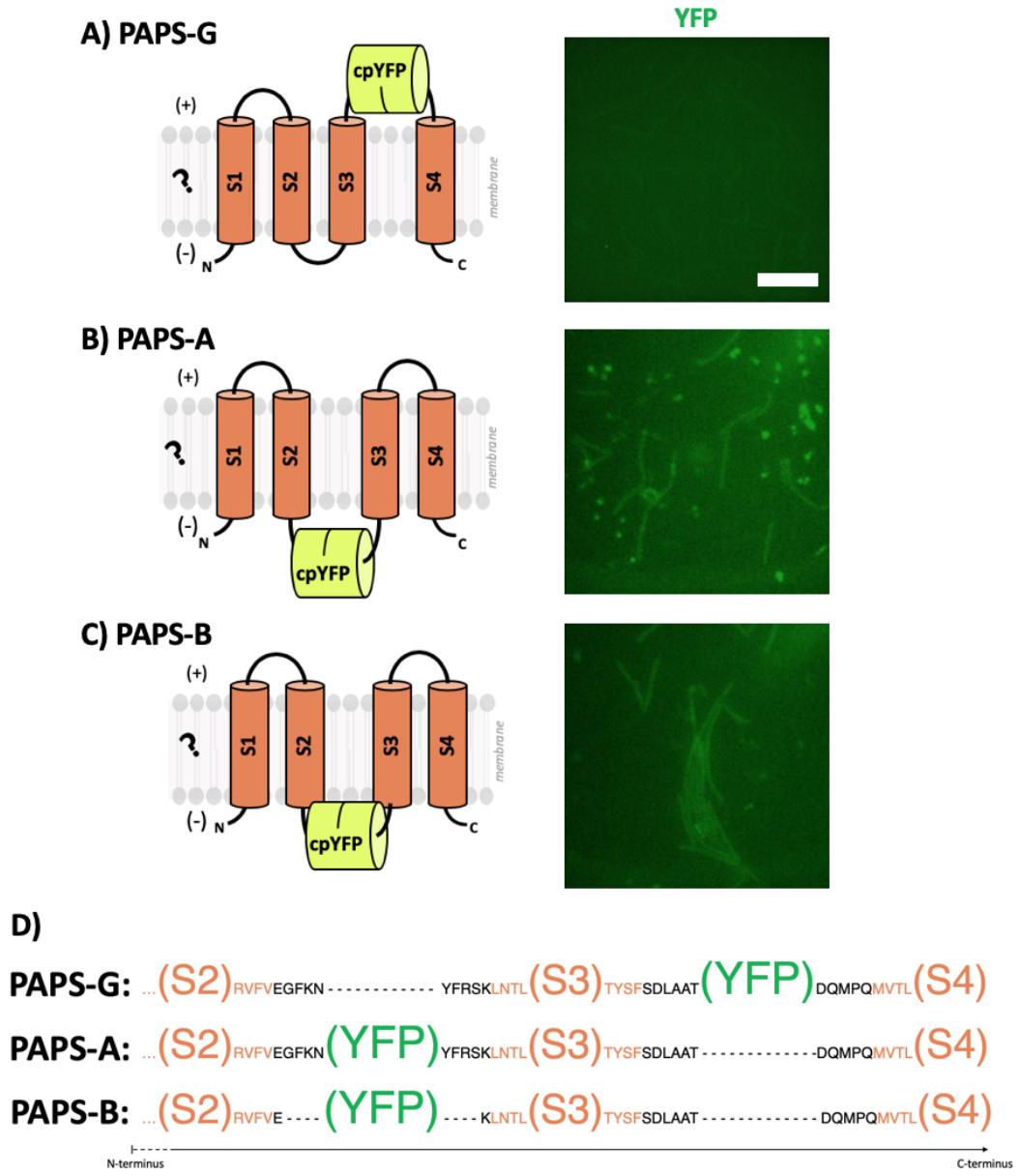

FIGURE 2.3: Cartoon (left) and GFP channel microscope acquisition (right) of *B.subtilis* PY79_PAPS-G (A), PY79_PAPS-A (B) and PY79_PAPS-B (C). The question mark on the cartoon membrane indicates the uncertainties over membrane specificity of the construct. Scale of the microscope images: 10 μm. D) Amino acid sequence of the three PAPS constructs showing the sites where the YFP was inserted and the shorter S2-S3 loop in PAPS-B. VSD helices in orange, inter-helices loops in black, YFP in green.

.

It was later found that PAPS-G plasmid had the PHyperspank promoter region disrupted, therefore the small SNR value was attributed to the protein not expressed

correctly. Even if the codon optimization increased the SNR in PAPS-A and PAPS-B, the fluorescence was cytosolic rather than membrane-specific.

Membrane targeting domain "t216" can bring proteins to the cellular membrane

In an attempt to help the VSD target the cellular membrane, it was tested the use of a domain coming from a prokaryotic transmembrane protein. It was selected a two-helices domain from *E.coli*'s methyl-accepting chemotaxis protein (MCP), which was already used in the Asally's Lab under the name of "t216". The functionality of t216 was assessed by fusing it to the N-terminus of the VSD and tagging the construct with YFP at the C-terminus. Fluorescence microscopy showed higher YFP intensity on the border of the cells compared to the cytoplasm, suggesting that the addition of the t216 transmembrane helices let the VSD target the membrane (Fig.2.4B). Substitution of t216 with a single t216 helix ("ht216") proved that one transmembrane helix was enough to bring the VSD onto the membrane (Fig.2.4C).

PAPS variants with t216 can better target the cellular membrane

Having shown that t216 could bring VSD to the cellular membrane, the two-helices domain was added to the N-terminus of PAPS-G, PAPS-A and PAPS-B to better direct the whole PAPS constructs to the membrane. The new constructs were called PAPS-Gt, PAPS-At and PAPS-Bt (Fig.2.5a-c). More variants were created by adding the single-helix ht216 to the N-terminus of the VSD. It was hypothesised that such addition would "invert" the orientation of the VSD: the VSD's N-terminus would become from cytoplasmic to extracellular, the helices flipped inside the membrane, the cytoplasmic loops become extracellular and the extracellular loops cytoplasmic. The purpose of this "inversion" was to test the functionality of the highly-moving S3-S4 loop inside the cytoplasm, where the cpYFP could have a higher fluorescence. Transmembrane helices orientation depends on the membrane-targeting signal at the N-terminus of a protein and on the charged residues in the intracellular

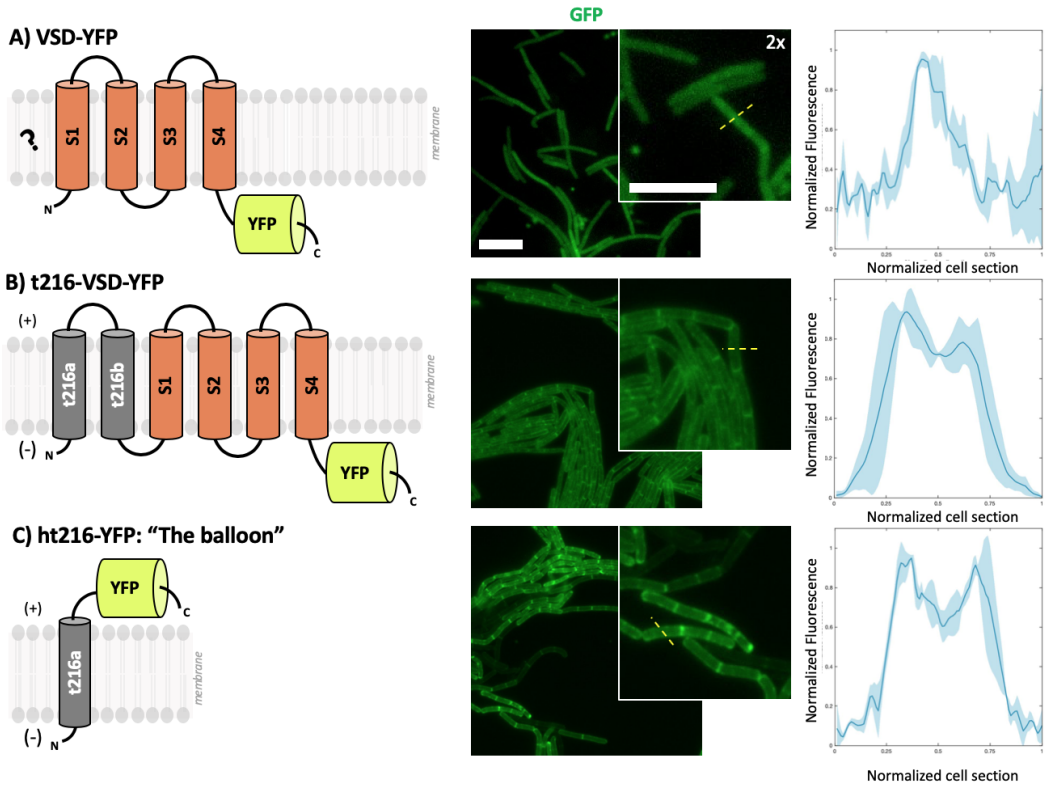

FIGURE 2.4: Cartoon (left), GFP channel microscope acquisition (center) and fluorescence intensity profile (right) of PY79_VSD-YFP (A), PY79_t216-VSD-YFP (B), PY79_ht216-YFP (C). Scale: 10 μm. A) Without t216, Ci-VSD does not show membrane specificity, localising mainly in the bacterium cytosol. The question mark indicates that the construct was supposed to target the membrane, but the microscope data do not suggest it. B) Addition of the membrane-targeting t216 domain at the VSD N-terminus makes the protein target the cellular membrane. C) One single helix of t216 is enough to target the membrane, proving it can be used as well for the creation of membrane-targeting constructs.

loops (Heijne, 2006). Since the charged residues in the intracellular loops were in the same number of the charged residues in the extracellular loops, the sole N-helix of t216 (ht216) was added to the N-terminus of PAPS-G to invert the VSD, and the new construct called PAPS-H. PAPS-Ht was derived from PAPS-H with the further addition of the second helix of t216 at the C-terminus. Finally, PAPS-J and PAPS-K were designed to be analogous to PAPS-H and PAPS-Gt, respectively, with the removal of S1 and S2 helices from the VSD. These last two constructs should not undergo conformational changes since the absence of S1 would disrupt the "groove" hosting S4 movements (as mentioned in Sec.1.1.1), but they were still designed to test such hypothesis.

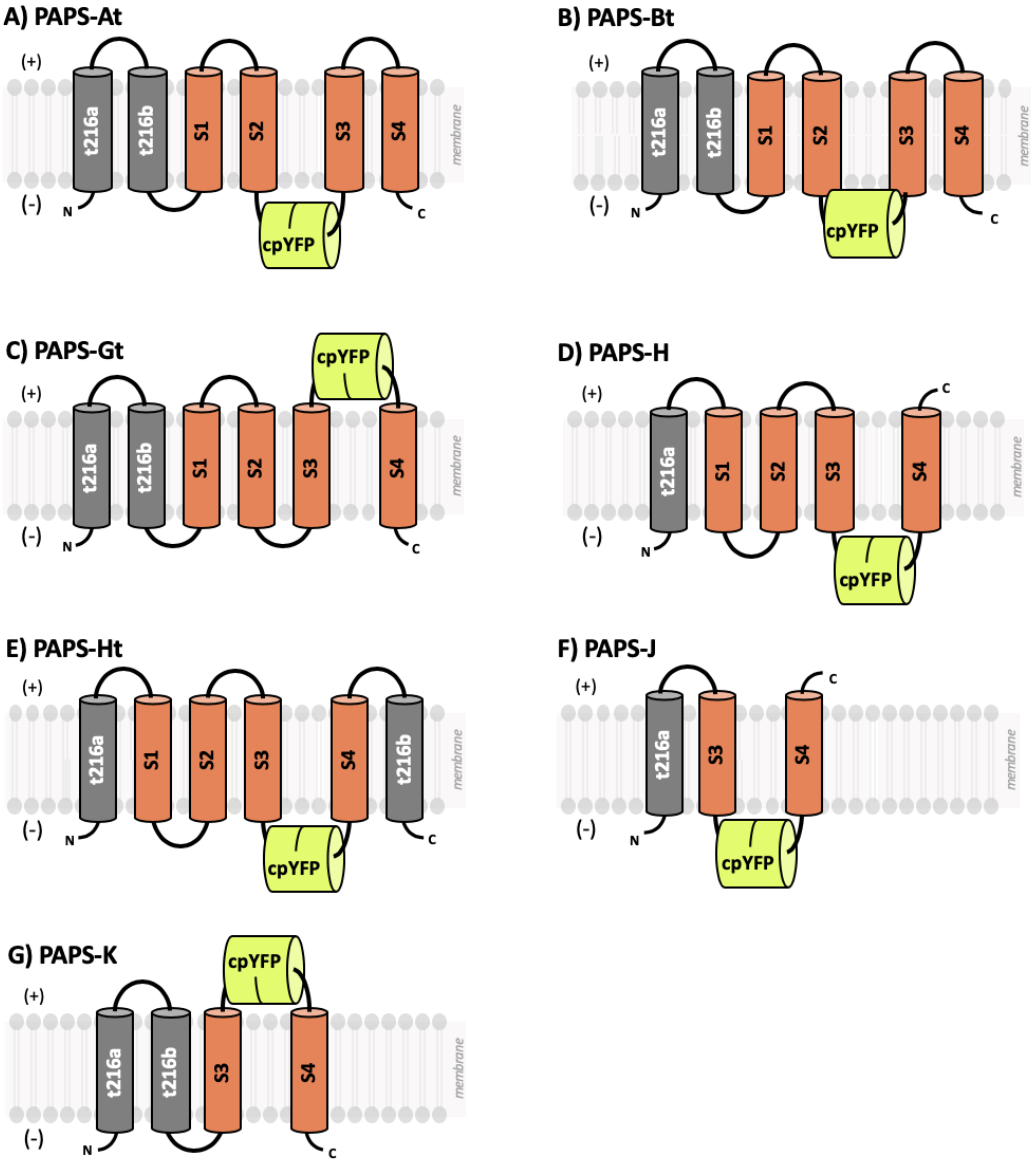

FIGURE 2.5: Cartoons of PAPS constructs with t216 or ht216 membrane-targeting domain linked to the N-terminus to direct the VSD to the cellular membrane. In particular, it is hypothesised that linking the single transmembrane helix ht216 to PAPS-G will 'invert' the VSD. PAPS-J and PAPS-K were designed to test whether the deletion of S1 and S2 helices will have the effect of depleting VSD conformational changes.

E.coli colonies did not grow after transformation with PAPS-H and PAPS-Ht Gibson Assemblies mix. The fact that no colony could grow after transformation with correctly-assembled plasmids suggested that PAPS-H and PAPS-Ht were toxic to the cells.

PAPS-Bt and PAPS-K did not show fluorescence during the microscope analysis. PAPS-Bt sequence was successively found to have a codon-shift upstream of

cpYFP, preventing the folding of the designed protein. The lack of fluorescence of PAPS-K, supported instead the hypothesis that a FP could not form a functioning chromophore in the extracellular environment.

PAPS-At, PAPS-Gt and PAPS-J were fluorescent in the microscope (2.6). PAPS-At and PAPS-J did not show a better SNR than the previous PAPS-A and PAPS-B, making it difficult to assess the localization in the cell. Nonetheless, their fluorescence was higher at the cell intersections, similarly to what was seen for t216-VSD-YFP and ht216-YFP (Fig.2.4), suggesting that they were membrane-specific. On the other hand, PAPS-Gt did not show this signal pattern, suggesting that the construct was not targeting the membrane. A comparison of the SNR of all the constructs obtained is shown in Fig.2.7.

Even if the SNR of PAPS-At and PAPS-J was lower than the SNR of PAPS-A and PAPS-B, the hypothesised membrane-specificity suggested they were fitter as membrane potential reporters. For this reason, they were tested together with PAPS-Gt under depolarization conditions.

Valinomycin and CCCP can be used to depolarize the cellular membrane

B.subtilis depolarization was tested with the potassium ionophore valinomycin and the protonophore carbonyl cyanide m-chlorophenylhydrazone (CCCP), both known to disrupt the proton motive force (PMF) (Margolin and Eisenbach, 1984; Gášková et al., 1999). Testing the effect of such chemicals on the cellular membrane potential with the potentiometric dye Thioflavin T (ThT) (Prindle et al., 2015), it was measured that ThT signal decreased from SNR=1.89 (SD=0.6) to SNR=1.29 (SD=0.2) with $20\mu M$ valinomycin and to SNR=1.14 (SD=0.1) with $1\mu M$ CCCP (Fig.2.8), constituting an intensity decrease of 32% and 40% respectively. Fluorescence intensity after addition of both valinomycin and CCCP was found to be significantly different (p=0.03 and p=0.004 respectively). Since ThT fluorescence intensity is proportional to the membrane negative polarization, it was suggested

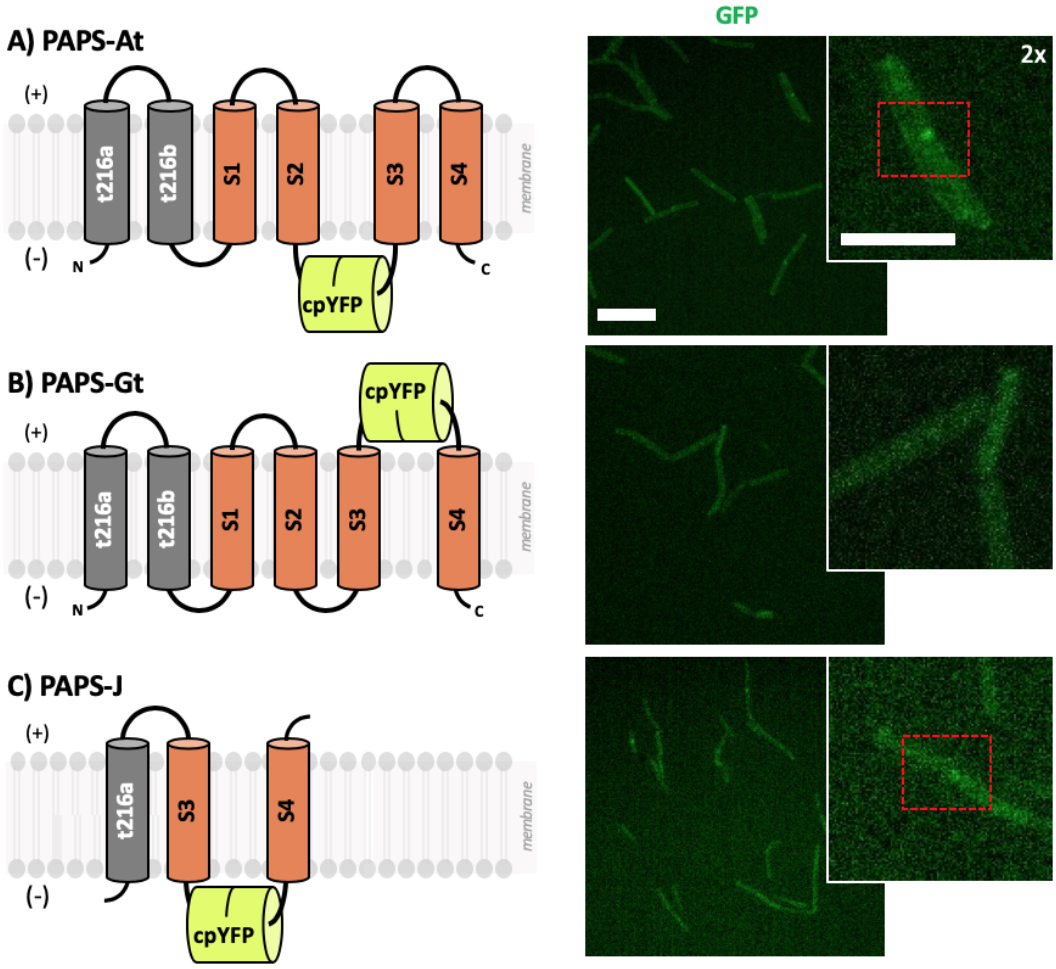

FIGURE 2.6: Cartoon (left) and GFP channel microscope acquisition (right) of PAPS-At (A), PAPS-Gt (B) and PAPS-J (C). Scale: 10 μm. It was not very clear to determine the membrane specificity of the three PAPS, but the higher fluorescence intensity at the cell contact (red squares) resembles the pattern seen in membrane-targeting proteins in Fig.2.4

that both chemical agents CCCP depolarized the cellular membrane by 32% and 40%.

PAPS constructs show different dynamics upon cell depolarization

A greater membrane depolarization was achieved in wild type *B. subtilis* by CCCP addition; therefore, the same method was used to depolarize recombinant *B.subtilis* strains with PAPS constructs. Upon cell depolarization, PAPS-At increased its fluorescence from SNR = 1.004 to SNR = 1.011 (+0.8%), PAPS-Gt decreased from SNR = 1.26 to SNR = 1.18 (-6.3%) and PAPS-J decreased from SNR = 1.05 to SNR = 1.035 (-1.4%). Fluorescence intensity increased by +0.6% in PY79 WT and

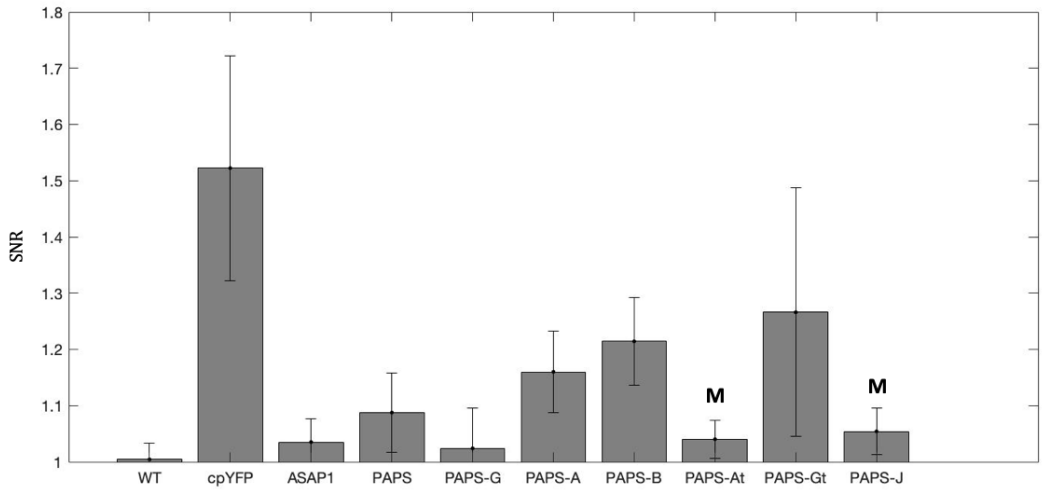

FIGURE 2.7: Comparison of the signal to noise ratio (SNR) of the GFP-channel from ASAP1 and every PAPS construct. Bars represent the mean value of the GFP signal from *B.subtilis* cells, vertical lines show the standard deviation (sample size n=10, experiments N=1). The only constructs that suggested membrane-specificity ("M" above the bar) were PAPS-At and PAPS-J, which showed the lowest SNR among all the PAPS with t216.

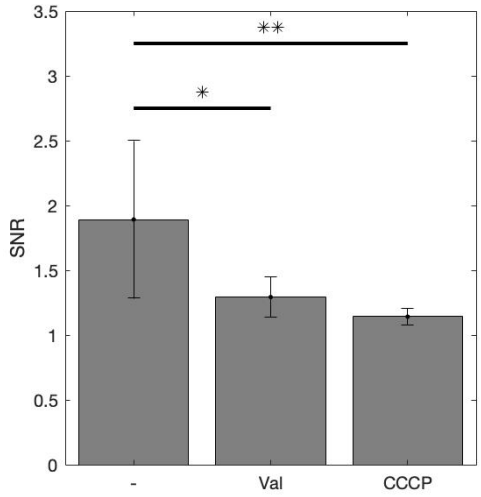

FIGURE 2.8: SNR from Thioflavin T (ThT) in *B.subtilis* PY79 at resting potential, on media supplemented by $20\mu M$ valinomycin and on media supplemented by $1\mu M$ CCCP. Bars represent the mean value of the ThT signal from *B.subtilis* cells, vertical lines show the standard deviation (n=10,N=1). Valinomycin addition made ThT intensity decrease by 32% (p=0.03) while CCCP by 40% (p=0.004).

by +0.8% in PY79 cpYFP. To compute the relative increase, two populations were divided, generating a Cauchy distribution (with the hypothesis that the distributions were normal). As Cauchy distributions do not have a defined variance, standard deviations were not computed.

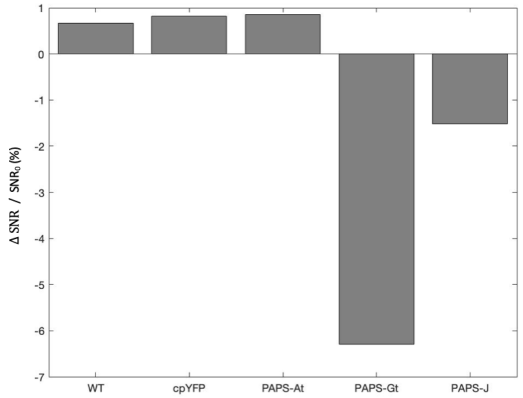

FIGURE 2.9: $\Delta F/F_0$ of the GFP signal from recombinant *B.subtilis* after depolarization with $1\mu M$ CCCP on pads in the microscope. Bars represent the mean value of the GFP signal from *B.subtilis* cells (n= 10). Standard deviation was not computed because the cells with and without the depolarizing agent were part of different populations. From a population analysis, PAPS-At show a signal increase (+0.8%) similar to the controls WT and cpYFP (+0.4% and +0.8%); PAPS-Gt showed a signal decrease of -6.3% and PAPS-J of -1.4%.

2.2.2 Random Mutagenesis

Novel PAPS-At and PAPS-Gt variants with random mutations in VSD's S3 and S4 helices were created to increase the S4 movement upon membrane potential shift. In fact, single residue mutations in S3 and S4 helices had already been found to reflect functional changes in the VSD dynamics in mammalian cells (Platisa et al., 2017). It was hypothesised that different mutations in PAPS' S3 and S4 helices could lead to beneficiary effects to the reporter dynamic range in prokaryotic cells too.

TMRM is better than ThT in estimating membrane potential shifts

ThT and TMRM potentiometric dyes were used to estimate membrane potential in flow cytometry settings before and after cells were depolarized with 150 mM KCl. Cells decreased in ThT peak fluorescence from 4300 Relative Fluorescence Units (RFU) to 3400 RFU after depolarisation (-21%) while TMRM peak fluorescence decreased from 2600 to 1100 RFU (-58%) (Fig.2.10).

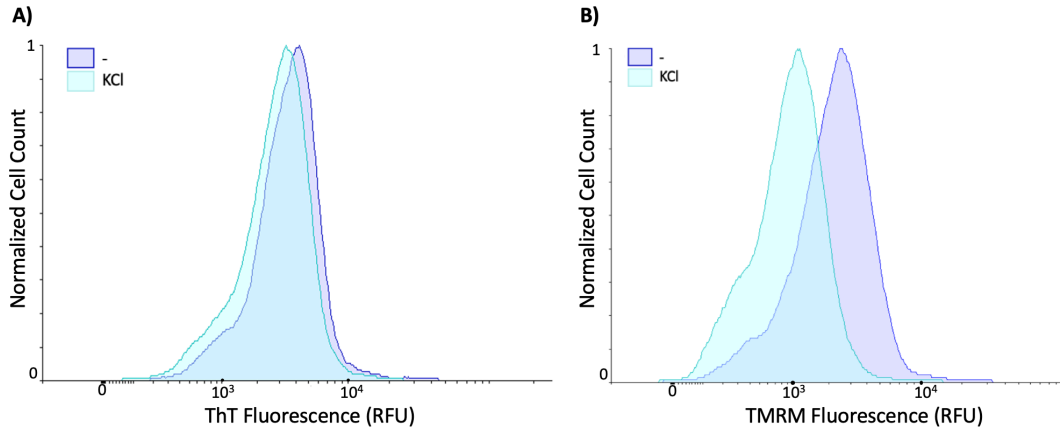

FIGURE 2.10: A) ThT intensity distribution from *B.subtilis* PY79 without (purple) and with (cyan) addition of KCl. B) TMRM intensity distribution from *B.subtilis* PY79 without (purple) and with (cyan) addition of KCl. Both ThT and TMRM intensity decrease at the population level after cell depolarization with KCl, ThT by 21%, TMRM by 58%. Figures adapted from Arthur Barker.

The depolarization analysis with TMRM was repeated also with $1\mu M$ CCCP and a combination of CCCP and KCl (Fig.2.11).

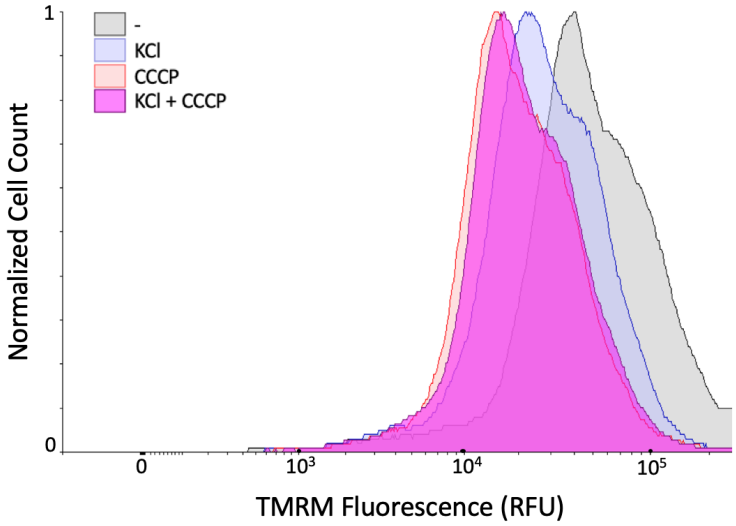

FIGURE 2.11: TMRM intensity distribution measured by flow cytometry from *B.subtilis* PY79 population at resting potential (grey) and depolarized with 150 mM KCl (blue), $1\mu M$ CCCP (orange) or a combination of CCCP and KCl (purple). Figure adapted from Arthur Barker.

TMRM peak fluorescence decreased from 39400 RFU to 22800 RFU (-42%) after KCl depolarization, to 15300 RFU (-61%) after CCCP depolarization and to 16400 RFU (-58%) after depolarization with a combination of KCl and CCCP. Since the

highest depolarization was reached with $1\mu M$-CCCP, it was decided to use CCCP to examine PAPS reporters upon larger depolarization range.

PAPS performance pre-mutations

The fluorescence from PAPS-At and PAPS-Gt mutants' population was compared in the flow cytometer before and after the depolarization induced with KCl and CCCP.

As it can be seen from Fig.2.12A-B, at resting potential, the GFP fluorescence measured by the Flow Cytometer from PAPS-Gt was lower than PY79 WT autofluorescence.

Control strains PY79_WT and PY79_cpYFP showed peak fluorescence changing from 19800 at resting potential to 20000 RFU after depolarization (+1%) and from 27500 to 28700 RFU (+4%), respectively. PY79_PAPS-At peak fluorescence changed from 20000 to 21100 RFU (+5.5%) while PY79_PAPS-Gt fluorescence changed from 17900 to 15600 RFU (-13%). As it can be seen from Fig.2.12F, PAPS-Gt fluorescence showed a change in population shape, meaning there is heterogeneity in reporter response.

PAPS fluorescence was plotted against TMRM fluorescence for cells at resting potential and after membrane depolarization (Fig.2.13).

The more linear shape of cpYFP dotplots suggested that there was a higher correlation between TMRM and YFP fluorescence at both resting and depolarized membrane potential. Apart from cpYFP, such a linear shape of TMRM/YFP fluorescence is seen for PAPS-At post-depolarization.

In every plot, a comparison of the population fluorescence before/after depolarization showed a shift on the x-axis towards more negative TMRM fluorescence values, while no (or little) translation on the y-axis (YFP fluorescence) is noticed from a visual analysis (Fig.2.13).

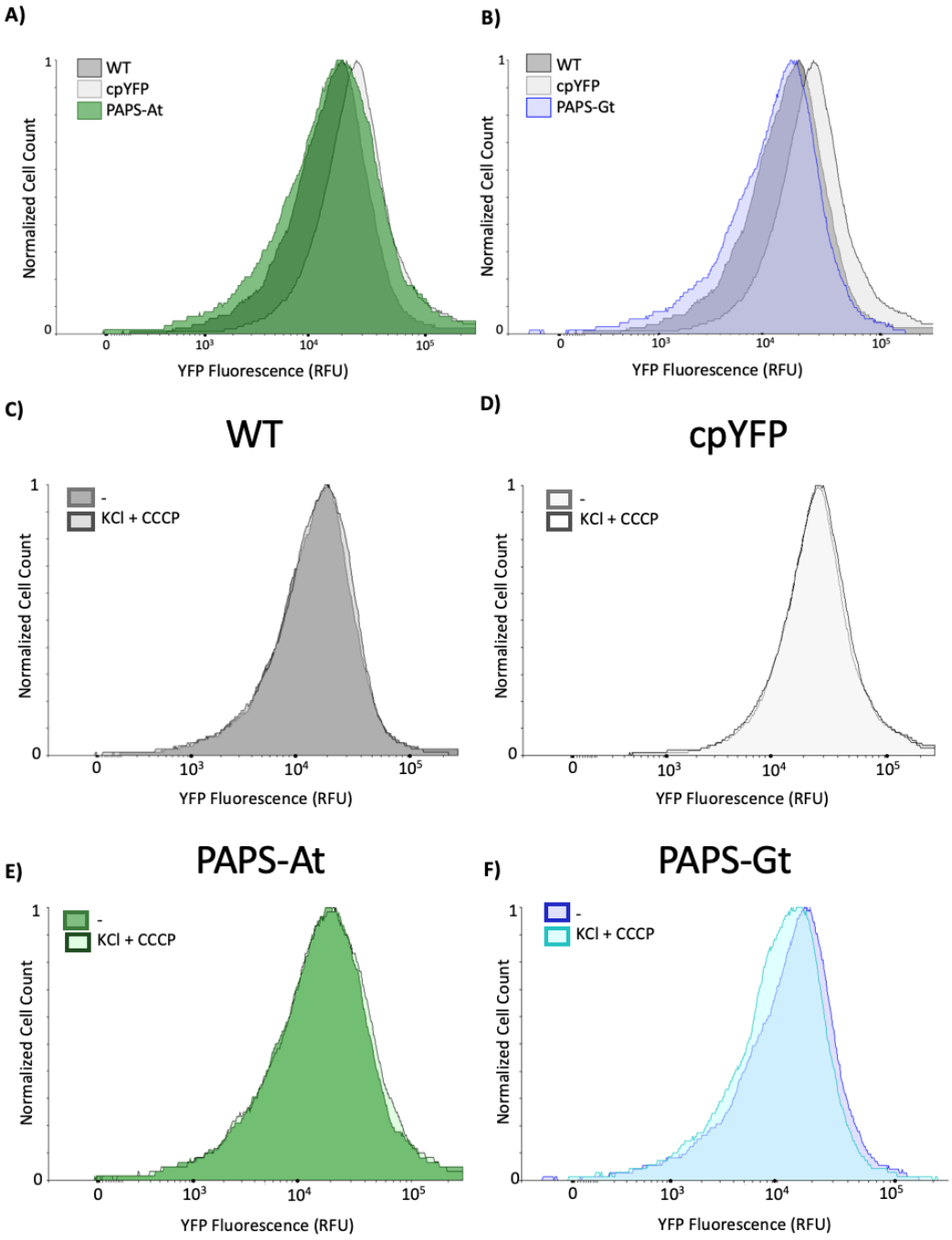

FIGURE 2.12: A-B) GFP intensity distribution at resting potential of PAPS-At (A) and PAPS-Gt (B), compared to the fluorescence distribution of the controls PY79 WT and PY79_cpYFP. C-F) GFP intensity distribution of PY79 WT (C), PY79_cpYFP (D), PY79_PAPS-At (E) and PY79_PAPS-Gt (F) before and after depolarization with KCl and CCCP. Figures adapted from Arthur Barker.

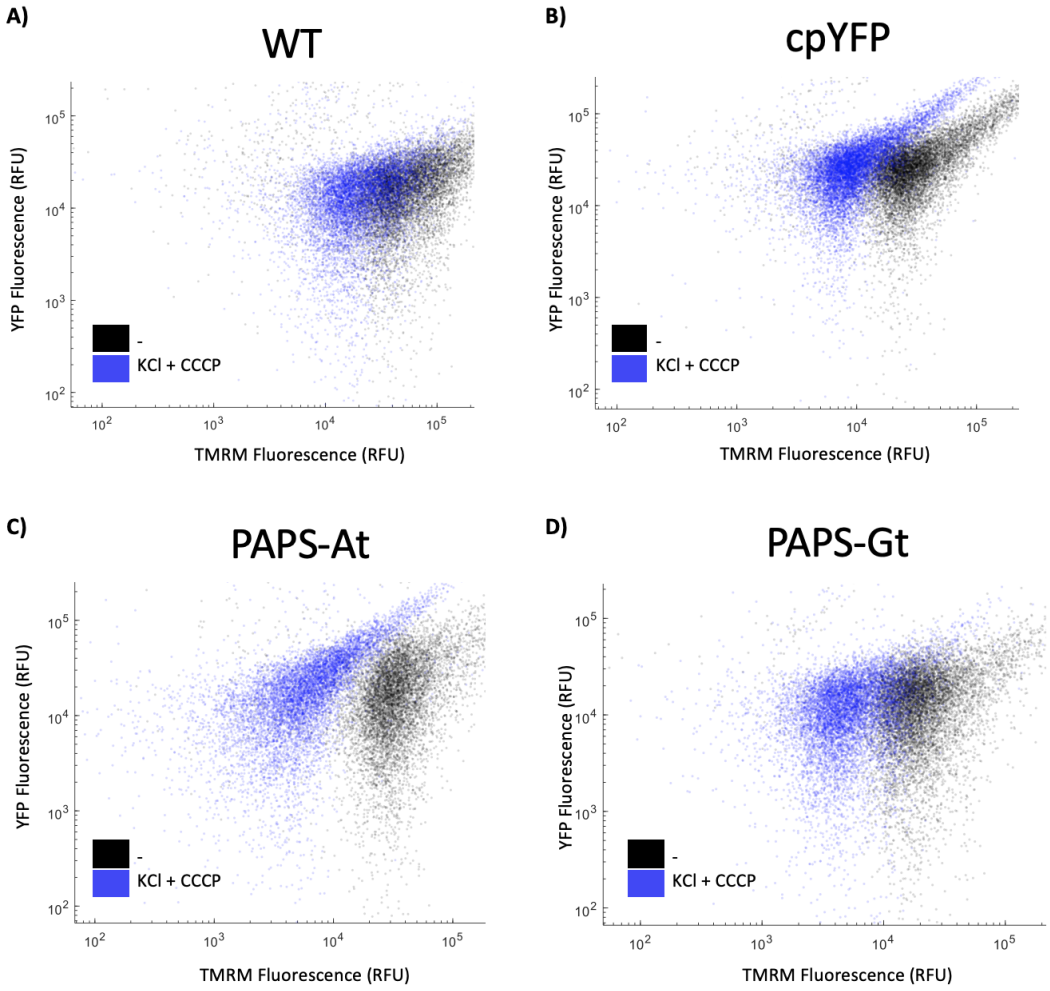

FIGURE 2.13: A-D) Plots showing how both YFP and TMRM fluorescence change in different PAPS constructs after depolarization with KCl and CCCP is obtained. Every PAPS population shows higher values of TMRM fluorescence at resting potential (black dots), lowering the TMRM intensity after depolarization (blue dots, shifted on the left). A vertical shift (YFP fluorescence) is not visually noticeable. PAPS-At shows a change of shape in the YFP-TMRM plot after depolarization. Figures adapted from Arthur Barker.

PAPS performance post-mutations

After performing random mutagenesis on S3 and S4 helices in PAPS-At and PAPS-Gt, 92 colonies of recombinant *B.subtilis* with PAPS-At mutants and 70 colonies with PAPS-Gt mutants were obtained. On the FACS machine, 192 single cells were selected for each PAPS mutant. Driven by the hypothesis that the cells showing the brightest signal would have the better chance to decrease fluorescence after cell depolarization, cells in the 90^{th} percentile of YFP-fluorescence intensity were picked. Each of the selected mutant was cultured overnight and the population analysed on

the flow cytometer before and after KCl cell depolarization. In Fig.2.14 is shown the comparison of the peak fluorescence change (%) before/after depolarization for the 192 PAPS-Gt selected mutants, after normalization on the fluorescence change showed by PY79 WT.

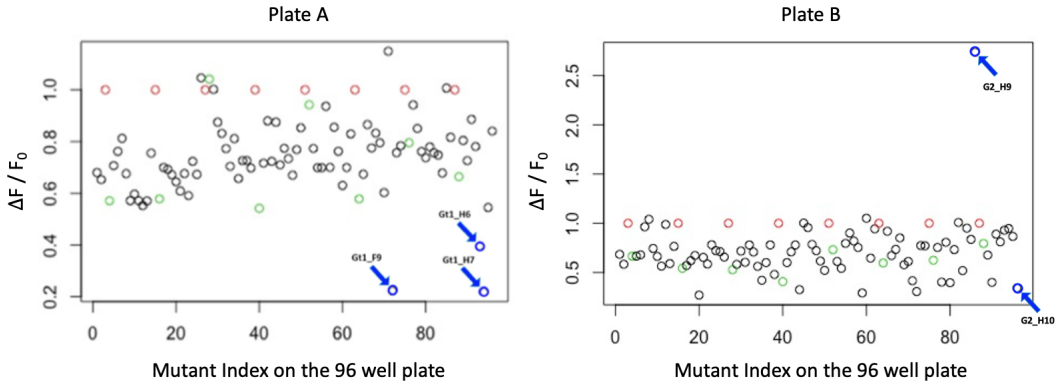

FIGURE 2.14: $\Delta F/F_0$ of peak GFP fluorescence from the 192 PAPS-Gt mutants after cell depolarization. Each $\Delta F/F_0$ was normalized on the $\Delta F/F_0$ of PY79 WT strains that were also analysed on each line of the 96 well plate (red dots). Green dots indicate PY79_cpYFP strains, also analysed in every line of each 96 well plate. Blue arrows indicate the 5 PAPS-Gt mutant strains that were selected because of the larger $\Delta F/F_0$ compared to PY79 WT.

The five PAPS-At strains that underwent the highest fluorescence change after cell depolarization, showed a percentual change of -80%, -60%, -55%, -50% and +35% after the signal was normalized on PY79_WT autofluorescence change.

The five most promising PAPS-Gt mutants, Gt1_F9, Gt1_H7, Gt1_H6, Gt2_H10 and Gt1_H9, showed a post-normalization fluorescence difference of -75%, -75%, -60%, -60% and +190%, respectively (Fig.2.14).

2.2.3 Sequencing

As seen in Sec.2.2.2, 5 recombinant strains obtained by random mutagenesis were selected for both PAPS-At and PAPS-Gt for showing a larger $\Delta F/F_0$ upon membrane depolarization, compared to the rest of the population. It was hypothesised that such a different behaviour could be due to amino acid substitution in PAPS helices, resulting in a change of the protein electrochemical properties. Sequencing analysis on the selected mutants showed that every PAPS-At mutant had lost the

VSD domain, with the cells expressing cpYFP. PAPS-Gt1_H6 and PAPS-Gt2_H10 showed two synonymous mutations each (I626I and A634A in Gt1_H6, V625V and A634A in Gt2_H10) and PAPS-Gt2_H9 showed a codon shift upstream of cpYFP. The only mutants showing an amino acid substitution were PAPS-Gt1_F9 and PAPS-Gt1_H7, with D342Y mutation on the S3 helix.

Further analysis on selected PAPS mutants

A further analysis of the fluorescence change was carried out on the mutants strains selected from the analysis described in Sec.2.2.2, after over night growth of the strains. Since PAPS-At mutants were shown to have become cpYFP proteins, only PAPS-Gt mutants were assessed. The further analysis showed fluorescence changes of -5.82%, -4.89%, -7.86%, -7.13% and +2.52% for PAPS-Gt1_F9, PAPS-Gt1_H7, PAPS-Gt1_H6, PAPS-Gt2_H10 and PAPS-Gt2_H9 respectively. This analysis was carried out in the same flow cytometer as the one used in Sec.2.2.2, but the cultures were grown and analysed in standard tubes instead of the 96-well plate.
A graph showing the correlation between $\Delta F/F_0$ computed from the analysis in the 96 well plate and the analysis in standard vessels is shown in Fig.2.15. From this plot it can be seen how, excluding H9 which showed a codon-shift, the strain samples form a strict line, suggesting a correlation between the data gathered in the different analyses. Such correlation indicates that the differences in magnitude were probably due to different machine calibration.

2.3 Discussion

Starting from the mammalian membrane potential reporter ASAP1, a prokaryotic reporter was developed. While gene codon optimization and the substitution of cpsfGFP-OPT with cpYFP slightly increased the SNR of the probe, the addition of the transmembrane domain t216 was necessary to increase membrane specificity of

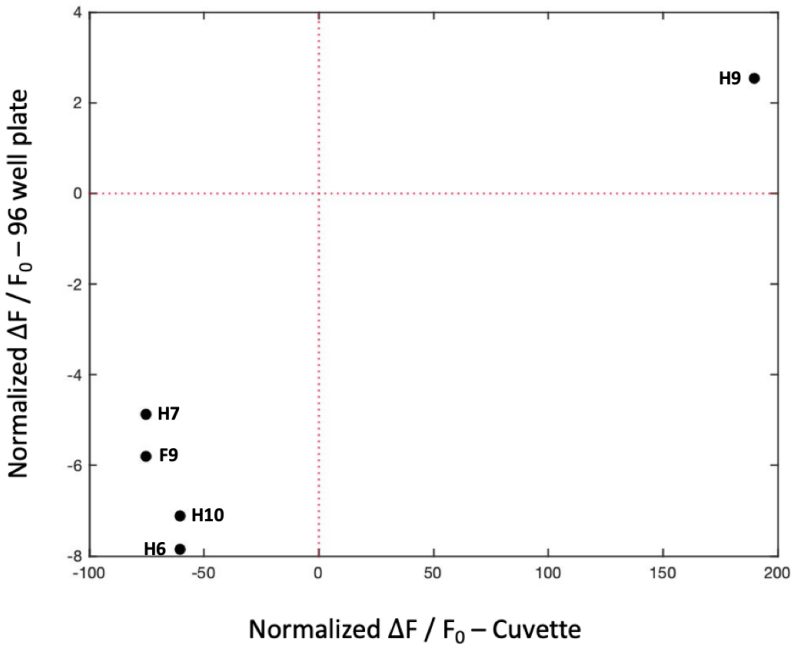

FIGURE 2.15: Plot showing the comparison between the $\Delta F/F_0$ measured from the selected PAPS-Gt mutants in the 96-well plate and in a standard cuvette after overnight growth.

the protein. Random mutagenesis on the most promising PAPS variants produced only lower-performing reporters. In Tab.2.3 are summarized the fluorescence intensity changes obtained by membrane-targeting PAPS after cell depolarization.

Strain	$\Delta F/F_0$ Microscope	$\Delta F/F_0$ 96WP	$\Delta F/F_0$ Cuvette	Mutation
(WT)	+0.6%	-	+1%	-
(cpYFP)	+0.8%	-	+4%	-
PAPS-At	+0.8%	-	+5.5%	-
PAPS-Gt	-6.3%	-	-13%	-
PAPS-J	-1.4%	-	-	-
PAPS-Gt1-F9	-	-75%	-5.82%	D342Y
PAPS-Gt1-H7	-	-75%	-4.89%	D342Y
PAPS-Gt1-H6	-	-60%	-7.86%	synonymous (it's Gt)
PAPS-Gt2-H10	-	-60%	-7.13%	synonymous (it's Gt)
PAPS-Gt2-H9	-	+190%	+2.52%	Codon shift after N366

TABLE 2.1: Summary of the different $\Delta F/F_0$ obtained with different experiments throughout the project.

2.3.1 PAPS development

Heterologous expression of eukaryotic proteins in prokaryotic cells is notoriously not trivial, given host dissimilarities in processes such as the expression machinery, protein folding, post-translational modifications and biochemical environment (Gomes, 2016). For an optimized expression, factors such as codon usage and choice of appropriate vector, promoter strength and host environment have all to be considered (Khow and Suntrarachun, 2012). In the realm of recombinant proteins, the heterologous expression of membrane proteins, in particular, is complicated. In fact, the different characteristics and size of cellular membranes and the high misfolding risk of hydrophobic domains pose additional challenges to the correct

protein expression (Bernaudat et al., 2011).

The fluorescence of the eukaryotic fusion protein ASAP1 in *B.subtilis* showed improvements in brightness after substitution of the sfGFP-OPT with YFP Venus and after performing codon optimization for the host (Fig2.7). Codon optimization has become a standard procedure for expression of recombinant proteins due to organisms codon usage bias (Plotkin and Kudla, 2011), therefore an increase of expression and consequent fluorescence was expected. On the other hand, the FP substitution benefit must be given by the 13 residues of difference between the two FPs. It is known that the same FP can have different brightness in different hosts (Sacchetti et al., 2001). It is then suggested that, while in mammalian cells ASAP1 fluorescence was higher with cpsfGFP-OPT rather than other tested FP (St-Pierre et al., 2014), the different residues of YFP played a role in how the chromophore is assembled in prokaryotes, after circular permutation of the protein and its fusion with the VSD.

The analysis of PAPS-G was affected by the mutations in the promoter region and should be repeated with a correct functioning promoter. On the other hand, the higher SNR coming from structures such as PAPS-A and PAPS-B, which have the cpYFP inside the cytoplasm, showed that such alternative design can be a viable one. However, the lack of membrane-specificity did not make these constructs a sensible choice for a membrane potential reporter. It was shown how the t216-VSD-YFP construct had high membrane specificity (Fig.2.4B). However, it was still unclear whether the VSD helices correctly became transmembrane, or they were still in the cytosol hanging from the membrane-targeting t216 helices. On this topic, a better analysis should be done to assess whether the S3-S4 loop is extracellular or cytoplasmic.

As mentioned, recombinant *E.coli* strains expressing PAPS-H and PAPS-Ht could not be obtained, which may be due to the toxicity of these constructs. As both PAPS-H and PAPS-Ht were designed to include the 'inverted VSD', it is hypothesised that such a topological change led to the formation of a toxic membrane

protein and eventually to cell death. The toxicity of the 'inverted VSD' is supported by the fact that all the successfully transformed constructs had a correct helices orientation. Since PAPS-J was successfully obtained and had a partial 'inverted VSD' (only S3 and S4, Fig.2.6), it was hypothesised that the toxicity of the 'inverted VSD' was given by S1-S2 and S2-S3 loops.

After the addition of t216 domain, PAPS-Gt did not show strong membrane localization, but its fluorescence showed the highest change after membrane depolarization (-6.3%) compared to membrane-targeting PAPS-At and PAPS-J (+0.8% change and -1.4% respectively) and control strains WT and cpYFP (+0.6% and +0.8% respectively). The change in fluorescence upon depolarization, regardless PAPS-Gt cytoplasmic localisation can be explained by hypothesising that the protein is overexpressed and gets localised both onto the membrane and in the cytosol, with only the membrane-targeting ones changing fluorescence. To test this hypothesis, it can be worth to decrease the gene expression level, for example by lowering the promoter strength.

As can be seen in Fig.2.7, the constructs targeting the cell membrane were also the ones showing the lowest SNR. Such result can be the consequence of a lower density of protein on the membrane compared to the cytoplasm and also to the higher difficulty of manually selecting a cell membrane on the microscope image compared to the cell cytoplasm. The use of a confocal microscope could have helped in determining and selecting the cell membrane.

In flow cytometer settings and with KCl depolarization, PAPS-Gt showed a bigger fluorescence change (-13%) compared to the controls (+1% and +4%). PAPS-Gt fluorescence change was also larger than the change of its D342Y variant (-5.35% in average) obtained with random mutagenesis. The D342Y mutation means that an aspartate residue has been substituted with tyrosine. Since D342 is one of the negative residues on S3 playing a role in forming the 'groove' hosting the S4 helix, its substitution with a large aromatic hydrophobic residue such as tyrosine potentially disrupted the groove affinity with S4. The decrease in fluorescence change

therefore agrees with the hypothesis that such a mutation decreased S4 movement upon membrane depolarization.

2.3.2 Depolarization methods

Valinomycin is an antibiotic which creates potassium-specific carriers in the cellular membrane (Margolin and Eisenbach, 1984).

Addition of KCl is a well-reported method to balance the electrochemical gradient across the membrane and disrupt the PMF. In particluar, complete cell depolarization is obtained when extracellular KCl concentration reaches 300 mM, matching the bacterium internal potassium concentration (Prindle et al., 2015). On the other hand, CCCP is a protonophore which increases the membrane permeability to protons, dissipating as well the electrochemical gradient and therefore depolarising the cell (Winkel et al., 2016). It was shown in Fig.2.11 that addition of CCCP depolarized *B.subtilis* membrane by a magnitude greater than KCl and CCCP together. It is hypothesised that, with the KCl and CCCP concentrations used, the PMF is disrupted by CCCP and at that point KCl has already reached chemical equilibrium between intracellular and extracellular environment. Therefore, a further addition of KCl does not modify the electrochemical gradient and the membrane potential further. However, only peak values were compared. A better comparison could show they are not statistically different.

2.3.3 Depolarization effects

The control strain cpYFP showed a +0.7% and +4.0% fluorescence increase upon depolarization in the microscope and flow cytometer, respectively. These changes can be explained with an increase of cytoplasmic pH following membrane depolarization. It is in fact known that FP are sensitive to pH changes; in particular, the fluorescence intensity increases at higher pHs (Elsliger et al., 1999).

PAPS-At showed to increase its fluorescence upon depolarization in both the microscope and the flow cytometer (+0.8% and +5.5%, respectively). The positive shift mirrors the behaviour of the control strains, in particular PY79_cpYFP, and is in contrast with the other PAPS, showing a negative shift post-depolarization. In PAPS-At, the cpYFP was inserted in the S2-S3 loop, which was not expected to undergo large conformational changes upon depolarization. Since the population-level analysis did not allow the computation of the standard deviation of the change, it cannot be stated whether the changes in PAPS-At are statistically-relevant. However, the similarity of the average increase and the consideration on the VSD dynamics suggest that PAPS-At fluorescence change is still due to pH changes.
On the other hand, PAPS-Gt reporter, regardless being cytoplasmic, showed a fluorescence change of -6.3% on the microscope with CCCP depolarization and of -13% on the flow cytometer with KCl depolarization. Considering that the controls were increasing the fluorescence after depolarization, the opposite behaviour of PAPS-Gt suggests the fluorescence difference is due to VSD conformational changes and candidate the construct as potential reporter.
However, to have a clearer idea of PAPS performance, the constructs should be tested in the same experiment with the state-of-the-art probe PROPS.

2.3.4 Comparison between TMRM data and PAPS data

From the 2D-plots comparing TMRM fluorescence with PAPS fluorescence (Fig.2.13) it is apparent how PAPS dynamic range is much smaller than TMRM dynamic range. In fact, after cell depolarization, the data population shifts an average of 30000 RFU on the TMRM axis and of an average of 4000 RFU on the YFP axis. Nonetheless, the population fluorescence is diverse and show asymmetrical distribution tails. In particular, from Fig.2.13C, it can be seen how PAPS-At fluorescence distribution changes from having a tail towards the lower fluorescence values (black dots projection on y-axis) to having a tail toward the higher fluorescence values

(blue dots projection on y-axis). This behaviour suggests that some cells are increasing their fluorescence after cell depolarization. However, the population-based analysis does not allow more accurate conclusions and a more accurate analysis of the fluorescence changes at single-cell level would be ideal.

2.3.5 Differences between Microscope and Flow Cytometry results

Tab.2.3 showed the differences between PAPS measurements in the 96-well plate of the flow cytometer and the measurements a few days later on the cell cultures in a standard cuvette of the same flow cytometer. As can be seen from Fig.2.15, when PAPS-Gt2.H9 is excluded from the analysis, the relationship between the two measurements suggests that there is an inverse correlation: the mutants which showed a larger fluorescence change during the first analysis showed a smaller change in the second analysis and vice-versa. During preliminary analysis, time difference between sample stimulation might have played a role in biasing the measurements. In fact, cells in the 96 well plate were chemically depolarized at the same time, but analysed by the automated machine at slightly different times. Even if control strains were put in every line to normalise the fluorescence coming from the cell of every line of the plate, the time difference could have made a difference in terms of cell stress. Depolarization obtained with chemical agents that are not soon removed from the cell environment would in fact induce high stress to the cells. For this reason, a single-cell analysis with a temporary cell depolarization would be ideal to better test the PAPS constructs.

To compare flow cytometry population data, peak fluorescence (the mode of the population) was used, but other parameters could have been considered, such as the mean value, the standard deviation of the asymmetrical distribution or other considerations on the population shape. For instance, PAPS-Gt construct peak shifted by

-13% but a larger shift from certain cells can be seen on the left-side of the population distribution, meaning a subpopulation was changing fluoresce by more than 13%.

2.3.6 Random Mutagenesis

It is apparent how only 4 out of the 20 mutants sent to sequencing were found with residue substitution on S3 and S4, including synonymous ones. Given the sequencing results on the random mutants, it is suggested to change the parameters of the PCR mutagenesis in order to obtain more mutations. Moreover, given the short size of the DNA to mutate (156bp-long for PAPS-At, 60bp-long for PAPS-Gt) it is recommended to repeat the PCR to increase the mutation rate. Perhaps, a pseudo-rational introduction of charged arginines, lysines or histidine in S4 helix would increase conformational shift after depolarization by providing higher ionic force. The phenylanine residue that initiates the VSD conformational change can be substituted by residues with similar aromatic, hydrophobic properties such as Tyrosine, Tryptophan. Nonetheless, the substitution possibilities are so many that a rational design based on the current scarce knowledge is discouraged, and a bigger mutant library and high-throughput analysis is advised.

2.3.7 Mutant selection

During the experimental design of mutant selection, it was decided to pick the brightest mutants to analyse their fluorescence change after cell depolarization. As we expected to see a decrease of fluorescence following depolarization, as seen in ASAP1, the rational for this selection choice was that the brighter the mutant, the larger the possible fluorescence decrease. However, a candidate showing high initial fluorescence can be associated to a high gene expression, or a higher internal pH. It is not necessarily associated to higher probability of undergoing a bigger conformational change. For this reason, the choice of depolarizing only the strains

showing a higher initial fluorescence might have missed other promising candidates. A different selection approach, following the initial mutant screening, might have been used. For instance, based on the PAPS-At dot plot in Fig.2.13C, mutants' population could have been analysed on the FACS machine before and after addition of the depolarizing agent, and the cells falling outside the population shape pre-depolarization been selected. A more sensible choice could have been to select cells in the top-right corner of the YFP-TMRM plot (Fig.2.13C). Another, more laborious and high-throughput, strategy would be instead to separate each cell of the heterogeneous mix in several 96-well plates and analyse the change in fluorescence of every well in a highly-automated system.

2.3.8 Further analysis

Starting from the presented results, further analyses and workflow corrections are proposed to future researchers, in order to to find the best PAPS candidate:

- Test PROPS under the same depolarization protocol, for a better comparison between PROPS and PAPS performance;
- Test the codon-optimized version of ASAP1 (without substitution of cpsfGFP-OPT with cpYFP);
- Test PAPS-A and PAPS-B under depolarization conditions, given that cytoplasmic PAPS-Gt was the constructs showing the biggest fluorescence change;
- Test PAPS-G after expression with correct promoter;
- Test different promoter strengths to better analyse constructs' membrane specificity.
- use a confocal microscope to better analyse constructs' membrane specificity;
- Create PAPS-J mutants and test them;
- Create bigger mutant library;

- Test constructs at single-cell level before/after depolarization, since population changes are of difficult interpretation and statistical power of the fluorescence change cannot be evaluated;
- In particular, perform more high-throughput analysis of mutants in automated system
- Test different expression levels of every protein;
- Have a more consistent analysis with potentiometric dyes: use only TMRM;
- Have a more consistent use of depolarizing agents: use only CCCP or KCl;
- Test the kinetics of the reporters with temporary depolarization (e.g. electrical stimulus);
- Use Mann-Whitney test as statistical test to compare fluorescence intensity when cell depolarization was obtained in unapaired, non-normal populations.

2.4 Conclusion

Bacterial electrophysiology is a field that has not been explored enough, especially considering the recent discoveries of its role in a multitude of cellular processes. To better study membrane potential dynamics, membrane potential reporters for prokaryotic hosts have to be expanded, as the current solutions are either toxic or they do not provide enough specificity and dynamic range required for meaningful studies. In this chapter, I have shown the effort to heterologously express the eukaryotic membrane potential reporter ASAP1, eventually leading to the creation of a different reporter called PAPS. In particular, I have shown the different processes undertaken to develop a GEVI for prokaryotic hosts, from ASAP1 to PAPS mutants (Fig.3.22).

After testing different PAPS variants, the one showing the greatest dynamic range over cell depolarization was PAPS-Gt. PAPS-Gt has the topology similar to ASAP1, with the substitution of cpsfGFP-OPT with cpYFP, the addition of the membrane-targeting domain t216 at the N-terminus and the codons optimised. Even if PAPS-Gt

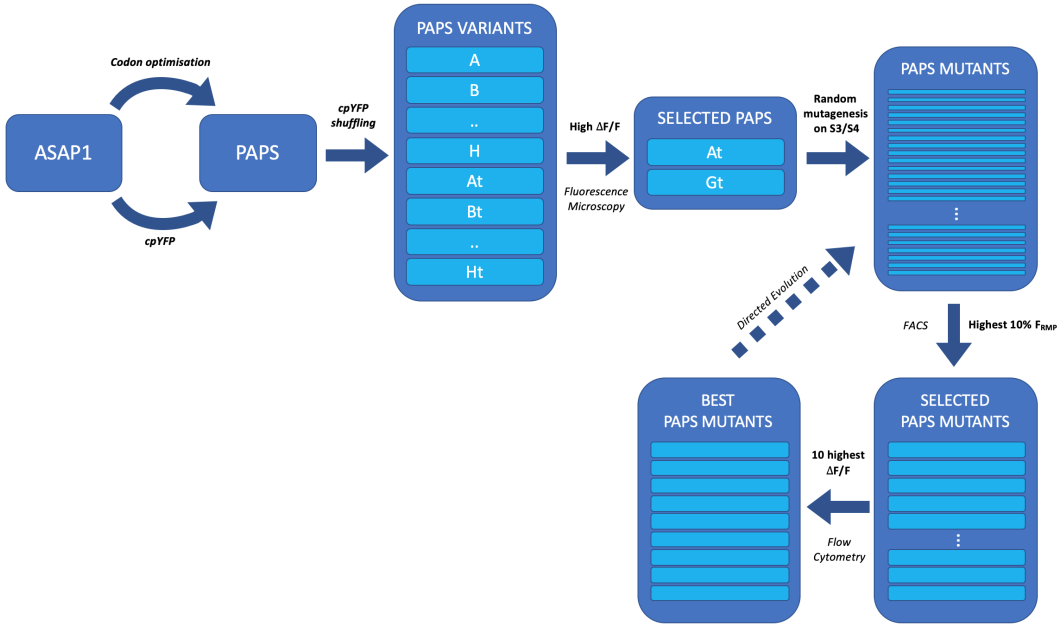

FIGURE 2.16: Development of PAPS variants from ASAP1 original gene sequence. Initial codon optimization and FP substitution were followed by the psuedo-rational development of different variants having cpYFP inserted in different positions. The two variants with the highest $\Delta F/F_0$ upon membrane depolarization were selected and random mutagenesis was performed on the S3-S4 helices of the selected constructs. The 384 brightest mutants were selected from the heterogeneous mix by FACS. The fluorescence coming from these mutant strains was measured in a Flow Cytometer before and after depolarization; the 10 samples showing the highest $\Delta F/F_0$ after depolarization were selected and their sequence analysed to find mutations responsible for the different behaviour

.

did not show a specific membrane localization, its fluorescence change upon complete membrane depolarization was -6.3% in the microscope analysis with 1uM CCCP and -13% in the flow cytometer with 150 mM KCl. Random mutagenesis resulted in a single meaningful mutant, PAPS-Gt D342Y, which showed a lower dynamic range of the original PAPS-Gt upon cell depolarization (average of -5.3% fluorescence change in flow cytometer conditions). The mutation was hypothesised to disrupt the ionic interactions happening between S3 and S4 helices during the VSD conformational change.

In order to develop a better membrane potential reporter, gene expression should be optimised and a bigger library of mutants should be created and analysed with high-throughput methodologies at the single-cell level. Complete rounds of directed evolution steps should be carried out by further mutate the better-performing initial

mutants.

The expression of the eukaryotic VSD showed poor specificity on the prokaryotic membrane. It is foreseen that finding a prokaryotic membrane domain that is homologous to the eukaryotic VSP's VSD would be a better option for a prokaryotic membrane potential reporter. As so far it has not been looked for, a genome-wide search in different prokaryotes could potentially find better candidates.

If a successful membrane potential reporter can be obtained for *B.subtilis*, it would allow long-term membrane potential tracking in big communities and biofilms, therefore allowing the potential discovery of electrophysiological mechanisms still unknown.

3 Development of a Voltage-Sensitive-Protease for Mammalian Cells

The recent development of optogenetics, magnetogenetics and sonogenetics has shown the advantages of controlling cellular processes with external stimuli such as light, magnetic fields and ultrasounds, respectively. On the other hand, the field of electrogenetics, i.e. the control of cellular processes with electrical stimuli, has lagged behind. While optogenetics, magnetogenetics and sonogenetics access biological functions by stimulating membrane proteins that are sensitive to the external stimulus, electrogenetic systems have so far relied only on the electrochemical activation of chemical inducers. The development of an electrogenetic system based on a voltage-sensitive-domain (VSD) would align electrogenetics to the mentioned technologies and constitute a self-contained, fast-acting electro-biological interface to better complement and enhance bioelectronic systems. In particular, the development of a family of Membrane potential-Activated Targetable Enzymes (MATEs) would allow an external electrical control of specific cellular processes.

In the present chapter I describe the first Membrane potential Activated Targeting Enzyme (MATE) obtained by coupling a voltage-sensitive domain with two halves of a protease. The resulting voltage-sensitive protease was meant to target the specific ENLYFQ/S peptide upon externally-induced cell depolarization.

3.1 Materials and Methods

3.1.1 Cell cultures

Strains

E.coli TOP10 (Invitrogen) were used for the assembly, the replication and the stock of every plasmid constructed. For the final expression and analysis of LOTEV constructs and protease reporters, *HeLa* and *HEK293* cells were used.

Culturing Conditions

E.coli were grown at $37°C$ for 15 hours either on lysogeny broth (LB) agar plate (1.5% w/v agar) or in liquid LB suspension (6 RCF). Both solid and liquid media were supplemented with $100\mu g/mL$ ampicillin when the cells had been transformed with a pcDNA3.1 plasmid.

HEK293 and *HeLa* cells were cultured in Dulbecco's Modified Eagle Medium (DMEM) with the addition of 10% fetal bovine serum, 100 units/mL penicillin G and $100\mu g/mL$ streptomycin. The cultures were grown in $75mm^2$ FalconTM Tissue Culture Treated Flasks (Fisher Scientific) at $37°C$ and with 5% CO_2 supplement. Cell passaging was carried out every 3 days by using 0.05% Trypsin/EDTA solution to dissociate the cells from the vessels.

3.1.2 Plasmid Design

Every gene expressed in this project was inserted into the high-copy-number pcDNA3.1 plasmid, following the CAG promoter for high gene expression (Hitoshi, Ken-ichi, and Jun-ichi, 1991) and preceding the bGH polyA terminator sequence. The insert's start codon ATG was placed after the consensus Kozak sequence GCCACC (Kozak, 1989) (Fig.B.1). The backbone contained the ampicillin resistance gene *bla* and the SV40 origin of replication (Fig.3.1).

LOTEVs and protease-reporters were inserted in two separated pcDNA3.1 plasmids. Transfection of the two plasmids in different ratios (3:1, 1:1, 1:3) was hypothesised to have a proportional effect on the LOTEV:reporters ratio present in a cell, because of the proportional mass of DNA that could be transcribed by the cell. Cells successfully transfected with a reporter plasmid could be seen in the microscope because of the reporter fluorescence. However, to make apparent which cells were expressing the non-fluorescent LOTEV or TEVp, a YFP followed by a Nuclear Localization Sequence repeated three times (3xNLS) was added to the design of the plasmids containing them. To be able to co-express protease-based constructs and YFP-3NLS cell-tag, pcDNA3.1 plasmid was made bicistronic with the insertion of a P2A sequence (Kim et al., 2011) between the protease construct and the YFP-3NLS tag (Fig.3.1D). P2A sequences allow the independent co-expression of two proteins; therefore, cells expressing LOTEVs on the membrane would have shown YFP fluorescence labelling the cell nucleus.

Software for construct design

Every DNA sequence was visualized and edited on Benchling (www.benchling.com). Benchling was used also to do sequence alignment and to design the primers for Gibson Assembly and sequencing reactions.
Protein 3D structures obtained from the Protein Data Bank (www.rcsb.org) were visualized and edited on PyMOL v1.7.4.5 or UCSF CHimera 1.13.1.. If the protein structure had not been solved, the protein folding was predicted on Robetta server (new.robetta.org).

3.1.3 Cloning

The pcDNA3.1 plasmid was linearized by digestion with HindIII and NotI restriction enzymes (Fig.B.1). Every cDNA to be assembled into a gene was obtained by Polymerase Chain Reaction (PCR) by using a PCR kit between PrimeSTAR Master

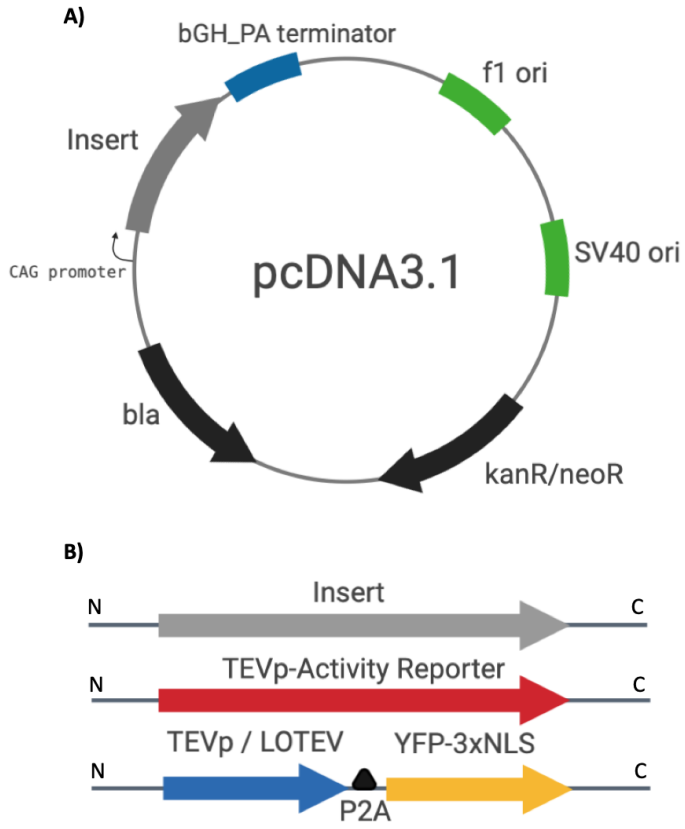

FIGURE 3.1: A) Schematic of the pcDNA3.1 plasmid where every construct (or pair of constructs) was inserted. B) In place of the "Insert" arrow shown on the plasmid, two types of assemblies were inserted: either a construct containing a fluorescent protein (e.g. protease reporter or LOTEV-YFP), or a non-fluorescent construct (e.g.LOTEV or TEVp) followed by P2A and YFP-3xNLS.

Mix (Takara) or Q5 Polymerase (NEB) on the appropriate template. When a template containing the sequence of interest was not present, DNA was synthesised by Integrated DNA Technologies or Genewiz. In App.B.0.1 are listed all the constructs sequences. Each primer used to amplify a sequence for Gibson Assembly (Gibson et al., 2009) included a sequence annealing to the template to amplify, and a 20bp-overhang homologous to the DNA sequence of the part to assemble with.

Each PCR-amplified cDNA was run on agarose gel (1% w/v agarose) and the bands confirming the expected cDNA length were purified from the gel (Gel Extraction Kit, NEB). The vector-insert(s) assembly was obtained by Gibson Assembly with Gibson Assembly Master Mix (NEB) after optimising the concentrations to a 1:3 molar ratio (backbone:insert). *E.coli* Top10 cells were made chemically competent

by using Mix&Go kit (ZymoGen) and the Gibson Assembly product was transformed into the competent cells by adding the assembly product to the cells as described in the protocol. The mix was then plated on warm LBA plates containing $100\mu g/mL$ ampicillin and the cells were left to grow overnight at $37°C$. The day after the transformation, three or four colonies per plate were screened by colonyPCR (SapphireAmp® Fast PCR Master Mix – Takara) by using primers AP634 and AP568, annealing to the DNA sequence flanking the insert. *E.coli* WT was used as negative control while *E.coli* pcDNA3.1_ASAP1 was used as positive control. The colonies showing DNA bands of the expected insert length on the agarose gel were grown overnight in liquid LB with $100\mu g/mL$ ampicillin ($37°C$, 6 RCF). Miniprep (Monarch Miniprep Kit – NEB) was performed the day after and each plasmid was sent for insert sequence confirmation to Source Bioscience plc or GATC (Eurofins). Liquid cultures of *E.coli* strains that showed a correct plasmid assembly were stored in cryogenic tubes at -80°C with 25% (v/v) glycerol.

The plasmids for mammalian cell transfection were obtained from the stored mutant *E.coli* by inoculating the appropriate strain from glycerol stock into liquid LB supplemented with $100\mu g/mL$ ampicillin. After being grown overnight for 15 hours, a miniprep was performed to extract the plasmid (Monarch Miniprep Kit – NEB) and the plasmid concentrations were measured by a NanoDropTM 2000/c Spectrophotometer (Thermo Scientific).

Every DNA sequence is reported in App.B.0.1.

3.1.4 Preparation for transfection in Mammalian Cells

Seeding for Chemical Depolarization experiment

Two days before a microscope experiment, *HeLa* or *HEK293* cells were seeded from the 75 mm^2 flask into a glass-bottom 8-well plate (μ-Slide 8 well glass bottom plate (Thisle Scientific). The wells were filled with $400\mu L$ of complete DMEM and a total of 700-1000 cells were seeded in each of them.

Seeding for Patch Clamp Experiment

Two days before a microscope experiment, 12 mm-glass cover slips (VWR) were dipped into 70%-EtOH, rinsed twice in PBS and suspended in DMEM-filled wells of a 6-well plate (CorningTM CostarTM Flat Bottom Cell Culture Plate 6-well Falcon). The wells were filled with 2 mL of complete DMEM and a total of 2 cover slips were added to each well, followed by suspension of 105 cells to have 70% confluency.

3.1.5 Transfection

The day before a microscope experiment, 15-24 hours after seeding, *HeLa* or *HEK293* cells were transfected. Transfection was carried out by following either calcium phosphate protocol or by using Lipofectamine®Transfection Reagent (Invitrogen) or jetPRIME®(Polyplus) kits. In the 6-well plates, $1\mu g$ of protease reporters and 300 ng of LOTEV construct or of TEVp were mixed with the reagents. In the 8-well ibidi plates, 100 ng of protease reporters and 30 ng of LOTEV construct or of TEVp were mixed with the reagents.

3.1.6 Microscopy data acquisition

The microscopes used were a Ti2 Eclipse (Nikon) and a Cleverscope (MCI Neuroscience) which was used for the patch clamp experiments.

The Eclipse microscope was equipped with a X-CITE®XLED 1 (Lumen Dynamics) light source, a oil-immersion CFI Plan Apochromat Lambda 100x/1.45 (Nikon) objective, a Zyla sCMOS (Andor) camera and it was interfaced on a Windows 7 computer through NIS-Elements AR 4.51.01 software. Cells were imaged in glass bottom μ-slide 8-well plate (Thisle Scientific) inside an incubator at $37°C$ and 5% CO_2. Brightfield, GFP and mCherry channels were acquired with 50ms, 100 ms and 100ms exposure, respectively.

The Cleverscope microscope was equipped with OptoLED Light Source (CAIRN),

a water-immersion LUMPlanFL N 60x/1.00 (Olympus) objective, a CFI Plan Apochromat Lambda 100x/1.45 (Nikon) objective and it was interfaced on a Windows XP computer through OptoFluor (CAIRN) software. Cells were imaged on a cover slip at room temperature on the microscope stage which was continuosly perfused with a Mammalian Physiological Solution (MPS: 124 mM $NaCl$, 26 mM $NaHCO_4$, 1.25 mM NaH_2PO_4, 3 mM KCl, 1 mM $MgSO_4$, 10 mM $D-glucose$, 2 mM $CaCl_2$) solution. MPS was bubbled with 95% O_2 and 5% CO_2 and was circulated by a pump system constituted by a P-1 Peristastic Pump (Amersham Biosciences) and a 323 Peristatic Pump (Watson Marlow). Brightfield, GFP and mCherry channels were acquired with 50 ms exposure each.

Chemical depolarization

Cell chemical depolarization was obtained by increasing the potassium concentration in the cell media. Three adapted versions of MPS buffer were prepared, each with a different KCl concentration: 3 mM KCl, 70 mM KCl and 140 mM KCl (details in App.B.1). Each solution was prepare to have a concentration of NaCl inversely proportional to KCl (140 mM, 70 mM and 3 mM, respectively) in order to maintain the buffer osmolarity constant. In each well of the 8-well dish, the transfection medium was manually substituted with each buffer with $[K^+]$-increasing order. For each medium present in the well, the cells were imaged every minute for 5 minutes after the substitution.

Patch clamp

The patch clamp system of the Cleverscope microscope was made of a CV 203BU Headstage (Axon Instruments) controlled by PatchStar Motorised Micromanipulators (Scientifica). The stimulus was provided to the cells by an Axopatch 200B (Axon CNS) microelectrode amplifier in voltage clamp mode and through an electrode made of Borosilicate glass Capillaries (World Precision Instruments,Inc.) that

had been pulled with a P-97 Micropipette Puller (Sutter Instruments Co.) for an estimated impedence of 1 MΩ. The electrode was filled with an internal solution (130 mM *KGluconate*, 10 mM *KCl*, 10 mM *EGTA*, 10 mM *HEPES*, 2 mM *CaCl*2). The reference electrode was put in contact with MPS in the stage where the cell sat. After a whole-cell patch was obtained between the microelecrode and a cell sequential stimuli of +60 mV, +80 mV and +100 mV were provided to the patched cell with the microelectrode amplifier. The voltages were kept for 60 seconds (+60 mV) or 30 seconds (+80 mV and +100 mV), followed by 30 seconds of no-stimulus before increasing the voltage. The first experiments on Cherry-Q and LOTEV2 also included a +40 mV stimulus of 30 seconds before the +60 mV stimulus (Fig.3.18). For each time-lapse recording during patch-clamp, mCherry channel was imaged every 3 seconds for the duration of the experiment.

3.1.7 Data Analysis

ImageJ was the software used to visualise the acquired data, manually-select an appropriate region of interest (ROI) inside the cells and measure the average fluorescence intensity of the ROI. The ROIs considered were: sections of the cell membrane, cytoplasmic regions and the cell nucleus, all visually-identified from the BrightField images.

The data collected from each ROI was then processed on Matlab R2016b. Three parameters were computed from the fluorescence of the transfected cells:

- Membrane to Cytoplasm Ratio (MCR), obtained by dividing the average intensity coming from a section on the membrane by the average intensity coming from an arbitrary cytoplasmic region;
- Nucleus to Membrane Ratio (NMR), obtained by dividing the average intensity coming from the nucleus by the average intensity coming from a section on the membrane;

- Nucleus to Cytoplasm Ratio (NCR), obtained by dividing the average intensity coming from the nucleus by the average intensity coming from an arbitrary cytoplasmic region.

NMR was used to estimate TEVp proteolytic activity with LckCherry reporter; NCR to estimate it with Cherry-Q reporter. With both reporters, the magnitude of the parameter is proportional to the protease activity.

Unpaired t-test was used to compare different constructs' localization; while paired t-test was used to compare the dynamic spatial changes of the same construct over time.

3.2 Results

3.2.1 Design of a MATE and its activity reporters

The first MATE: "LOTEV"

To pursue the idea of the Membrane potential-Activated Targeting Enzyme (MATE) introduced in Sec.1.5.4, it was necessary to couple a voltage sensitive domain (VSD) with an enzyme having a highly-specific cellular target.

As for the VSD, the voltage sensitive domain from *C.intestinalis* voltage sensitive phosphatase (Ci-VSD) was chosen, based on its modularity (Sec.1.1), the well characterized conformational changes (Sec.1.1.1) and the successful usage in other fusion proteins such as the GEVIs family (Sec.1.2). In particular, the variant with the R217Q mutation was chosen, given its inactive conformation at cell resting potential and the gradual activation upon cell depolarization (Dimitrov et al., 2007).

As for the enzyme, the Tobacco Etch Virus protease (TEVp) was considered, because of its very specific target substrate - the peptide ENLYFQ/S - and the orthogonality to mammalian cell processes (Wehr et al., 2006). The combination of these two characteristics suggested that an electrically-activated TEV protease would target only the processes engineered with the ENLYFQ/S peptide. In particular, the

S219V mutant of TEVp was chosen, given its higher stability (Kapust et al., 2001). Since the distance between Ci-VSD's termini is dependent on membrane potential shifts (Inagaki et al., 2017), it was hypothesised to exploit such a relationship to activate TEVp. In particular, inspired by the design of the membrane potential reporter LOTUS-V (Sec.1.2 and Fig.1.3c) it was proposed to couple the Ci-VSD termini with two halves of a TEVp. As already proved (Wehr et al., 2006), when a TEVp is split in half between the residues Q118-T119, the three amino acids forming its active site (H47, D82 and C152) are separated in such a way that proteolytic activity can rise only when the two TEVp halves (nTEVp and cTEVp) are kept close to each other. It was hypothesised that if the Ci-VSD was coupled with the two halves of a split TEVp, the distance between nTEVp and cTEVp and therefore the proteolytic activity would be controlled by VSD' membrane potential-dependent movements (Fig.3.2). Such a protein, inspired by LOTUS-V design and bearing a TEV protease, was called "LOTEV".

Membrane potential reporter LOTUS-V (Fig.1.3c) was modified to bear nTEVp in place of the NLuc8 luciferase and cTEVp in place of YFP Venus. The construct was called LOTEV1. The mirrored version, having nTEVp and cTEVp inverted, was called LOTEV2 (Fig.3.3).

It was known from literature that the D129R mutant of the Ci-VSD was voltage-insensitive (Tsutsui et al., 2013). Therefore, voltage-insensitive variants of LOTEV1 and LOTEV2 were created by modifying the original constructs with a corresponding mutation. The variants LOTEV1(D129R) and LOTEV2(D129R) could be used as controls to relate LOTEV proteolytic activity directly to VSD conformational changes.

LOTEV activity reporters

Two reporters were conceived to measure the proteolytic activity dynamics of LOTEV variants, both based on the red fluorescent protein mCherry. The first

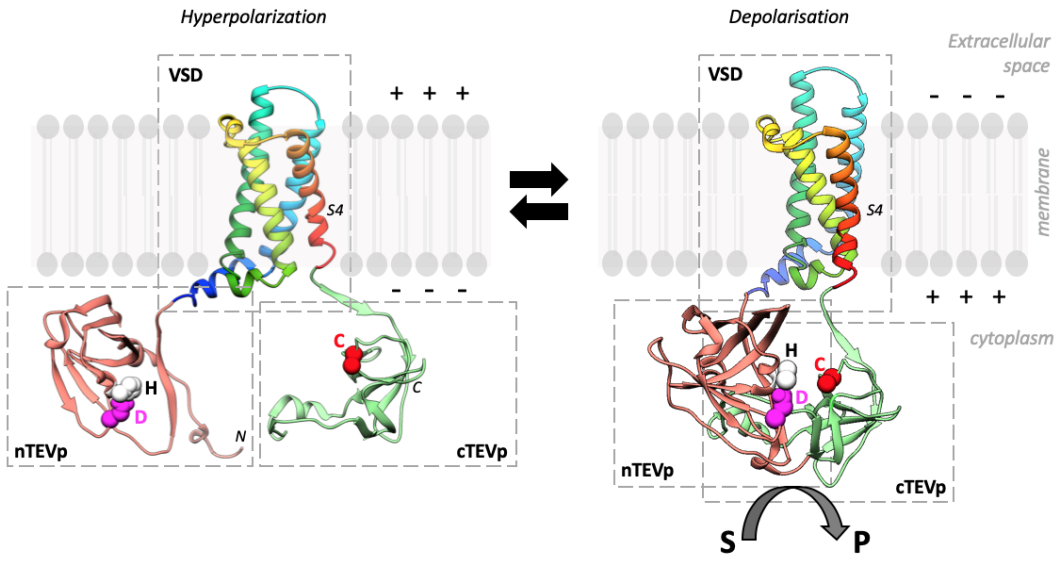

FIGURE 3.2: LOTEV1 protein, designed on UCSF Chimera 1.13.1 by using the VSD crystal structure 4G7V and TEVp crystal structure 1LVM obtained from Protein Data Bank (PDB). The first and the second half of the split TEVp are bond to the N and C termini of the VSD (light-red and light-green domains, respectively). The three residues of the TEVp active site are displayed as spheres: two of the residues (H47 and D82) are on the first half of TEVp, the third one (C152) is on the second half. At resting potential, nTEVp and cTEVp are distant enough to not show proteolytic activity (left); when membrane is depolarized, Ci-VSD's S4 movement brings the two TEVp halves closer, assembling the active site and triggering protease activity.

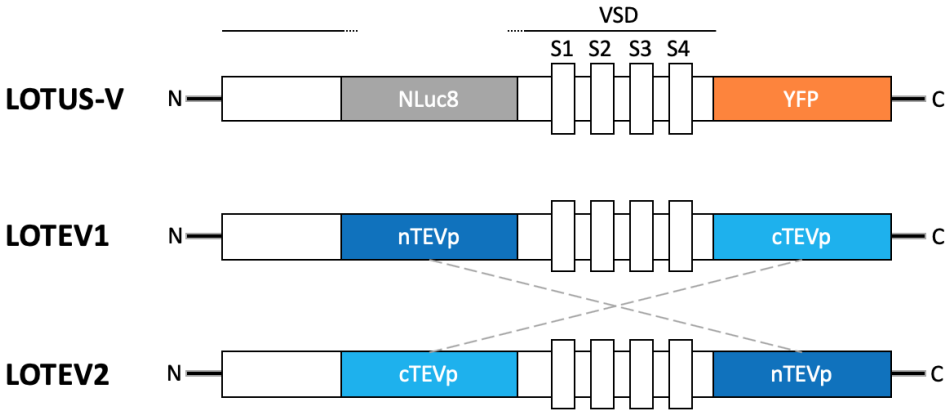

FIGURE 3.3: Cartoon of LOTEV1 and LOTEV2 domain assembly compared to LOTUS-V. NLuc8 luciferase was substituted by nTEVp and YFP Venus was substituted by cTEVp to create LOTEV1. LOTEV2 had the TEVp halves inverted.

reporter was designed to measure TEVp activity based on mCherry spatial distribution in the cell, the second one based on mCherry fluorescence intensity.

To obtain a TEVp-dependent spatial distribution of mCherry, the fluorescent protein was linked to the C-terminus of the membrane-targeting domain of Lck

protein (Benediktsson et al., 2005) through the TEV target peptide ENLYFQ/S. A Nuclear Localization Sequence repeated three times (3xNLS) was added to the C-terminus (Fig.3.4B). It was hypothesised that such a reporter, called "LckCherry", would have mCherry targeting the membrane in absence of TEVp activity and accumulate in the cell nucleus when TEVp cleaves the linker to the Lck domain. It would therefore measure TEVp activity by showing fluorescence going from cell membrane to cell nucleus with increasing TEVp activity (Fig.3.4C).

On the other hand, to obtain a reporter with the fluorescence intensity dependent on TEVp activity, a 27 amino acid quenching peptide from the transmembrane region of influenza M2 was considered (Nicholls et al., 2011). The quenching peptide sequence (CNDSSDPLVVAASIIGILHLILWILDRL) was linked to mCherry through the TEVp cleavage recognition site ENLYFQ/S (Fig.3.4D). Such a reporter, called "Cherry-Q", was hypothesised to have the fluorescence quenched in absence of active TEVp, and increasing fluorescence intensity upon proteolytic cleavage of the quencher (Fig.3.4E).

3.2.2 Analysis at resting potential

LOTUS-V shows membrane specificity in *HeLa* cells

When LOTUS-V was developed, it was shown that its localization was membrane specific. Regardless the fusion with luciferase and YFP, the Ci-VSD proved to target the cell membrane in *HEK293* cells (Inagaki et al., 2017). In this project, I aimed to fuse the Ci-VSD with two halves of TEVp and express the construct in *HeLa* cells, due to the larger cell size and the greater facility of patching the cell membrane. LOTUS-V protein was expressed in *HeLa* cells to assess whether the Ci-VSD was correctly trafficked to the membrane in *HeLa* cells as it was in HEK293 cells (Fig.3.5).

A comparison of the GFP Membrane to Cytoplasm Ratio (MCR) showed that

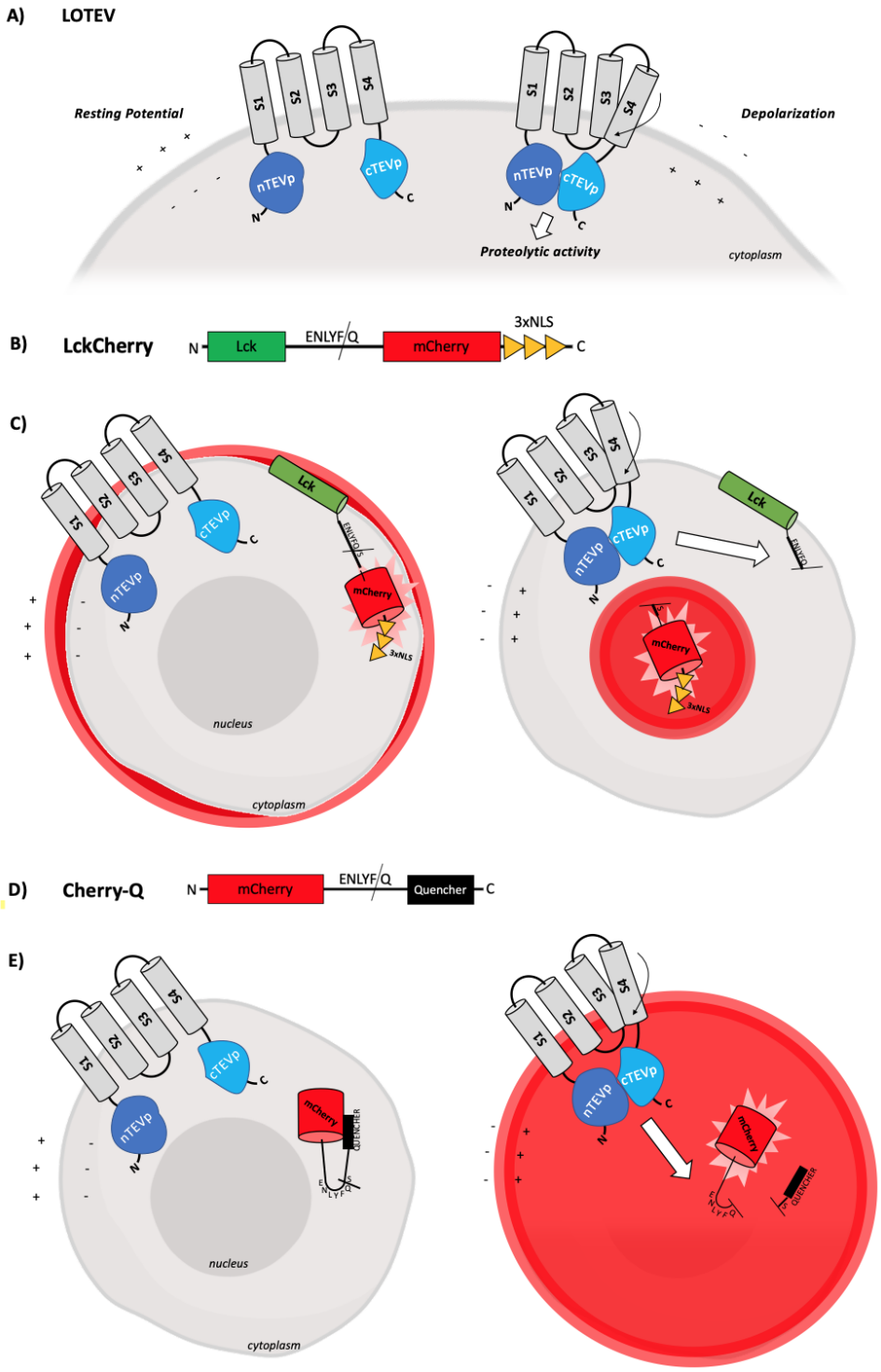

FIGURE 3.4: A) Simplified cartoon representation of LOTEV1, showing its activation by artificial cell depolarization. The VSD and its 4 transmembrane helices is represented by 4 grey cylinders connected by black lines representing the loops. The two halves of TEVp are represented by the dark blue and light blue blobs. B) Linear representation of LckCherry reporter assembly. C) LckCherry cell localization in absence (left) and presence (right) of TEVp activity. The fluorescence of mCherry (red cylinder) is expected to move from the cell membrane to the cell nucleus when the two halves of TEVp (blue blobs) are closer due to S4 conformational change. D) Linear representation of Cherry-Q reporter assembly. E) Cherry-Q fluorescence intensity in absence (left) and presence (right) of TEVp activity. The fluorescence of mCherry (red cylinder) would increase due to cleavage of a quencher peptide (black rectangle). Plus and minus signs refer to the cell membrane polarization.

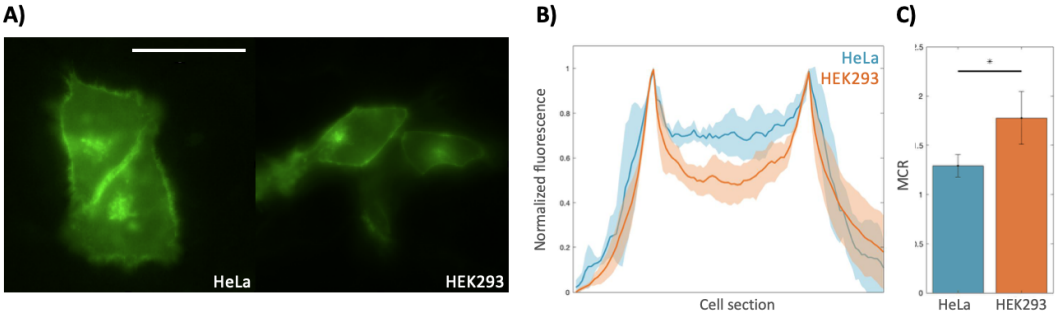

FIGURE 3.5: A) GFP signal from mammalian cells expressing LOTUS-V: *HeLa* cells (left) and *HEK293* cells (right); scale: $50\mu m$. B) Fluorescence intensity across *HeLa* and *HEK293* cell section, normalized in section length and fluorescence intensity (thicker line: mean value, shaded area: standard deviation, n=3, N=2). The fluorescence peaks identify the cell membrane, with the fluorescence in between coming from the cell cytoplasm. C) Membrane to Cytoplasm Ratio (MCR) of LOTUS-V fluorescence in *HeLa* and *HEK293* cells (p=0.045; n=3, N=2).

LOTUS-V had an higher fluorescence intensity on the cell membrane compared to the cytoplasm ($MCR_{HeLa} = 1.29$), even if the membrane specificity was higher in *HEK293* cells ($MCR_{HEK293} = 1.78$) (Fig.3.5C). It could also be seen that LOTUS-V formed aggregates in both cell lines (Fig.3.5A).

LOTEVs do not show membrane specificity in *HeLa* cells

To assess whether LOTEV constructs showed different membrane specificity in *HeLa* and *HEK293* cells as well, LOTEV1 and LOTEV2 were tagged with a YFP protein at their C-terminus. The YFP-tagged proteins were called LOTEV1-YFP and LOTEV2-YFP (Fig.3.6A)

When fusing two protein domains, the linker sequence plays the important role of separating the domains, as it is critical that the addition of another domain does not affect the folding of the first domain, and vice-versa. To confirm that both the LOTEV construct and the YFP were folding independently, two peptides with different flexibility were tested as linkers, with the hypothesis that a stiffer linker would have better separated the two domains. Linker1 was designed to be a sequence made of glycines and serines, known to form a highly flexibile peptide (Van Rosmalen, Krom, and Merkx, 2017); Linker2 was chosen from a linker database

for its low flexibility ("1CS6A" from https://synlinker.syncti.org)(Fig.3.6B).

LOTEV constructs showed different spatial distributions when expressed in *HeLa* and *HEK293* cells. As it can be seen from Fig.3.6, in *HeLa* cells, LOTEV1-YFP was homogeneously distributed in the cell when the flexible linker was used ($MCR = 1.05, SD = 0.01$), while it is suggested it was sequestrated by the endoplasmic reticulum (ER) when the rigid linker was used (MCR = 0.62, SD = 0.12). LOTEV2-YFP with the same rigid linker did not show membrane specificity (MCR = 0.66, SD = 0.51).

In *HEK293* cells, on the other hand, LOTEV1-YFP membrane localization was higher than in *HeLa* cells when the flexible linker was used (MCR = 1.21, SD = 0.46), becoming even higher with the use of the rigid linker (MCR = 1.29, SD = 0.12). When LOTEV2 was separated from YFP by the same rigid linker, it showed an heterogeneous distribution in the cell, with some preference for membrane localization (MCR = 1.21, SD = 0.13).

In summary, the more rigid Linker2 showed the best efficacy in separating the YFP tag from LOTEV constructs in *HEK293* cells. However, the use of such a linker did not help estimate membrane localization of LOTEV constructs in *HeLa* cells.

Even if no apparent localization of LOTEVs on *HeLa* cell membrane was found, the results suggested that the linker connecting YFP to LOTEV constructs was affecting the folding and the localization of LOTEVs in *HeLa* cells. For this reason, the further analyses were still carried out in this chosen chassis rather than in *HEK293* cells, motivated by the higher facility of carrying out patch clamp experiments.

Cherry-Q shows higher efficiency than LckCherry in reporting TEVp activity

To test the efficiency of the TEVp activity reporters introduced in Sec.3.2.1, LckCherry and Cherry-Q were expressed in *HeLa* cells alone or together with an active TEVp. As mentioned in Sec.3.1.2, to label the cells expressing TEVp, a YFP with a 3xNLS tag was co-expressed from the same plasmid (Fig.3.7 and Fig.3.8).

The analysis of LckCherry fluorescence distribution in absence and in presence of

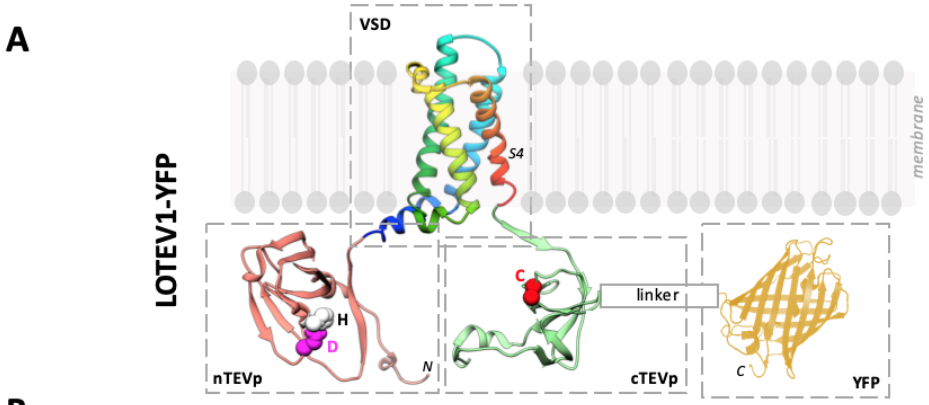

B

LINKER NAME	LINKER SEQUENCE	FLEXIBILITY	REFERENCE
Linker1	$SSSG(SG)_3$	High	van Rosmalen et al., 2017
Linker2	NPVPQ	Low	*https://synlinker.syncti.org*

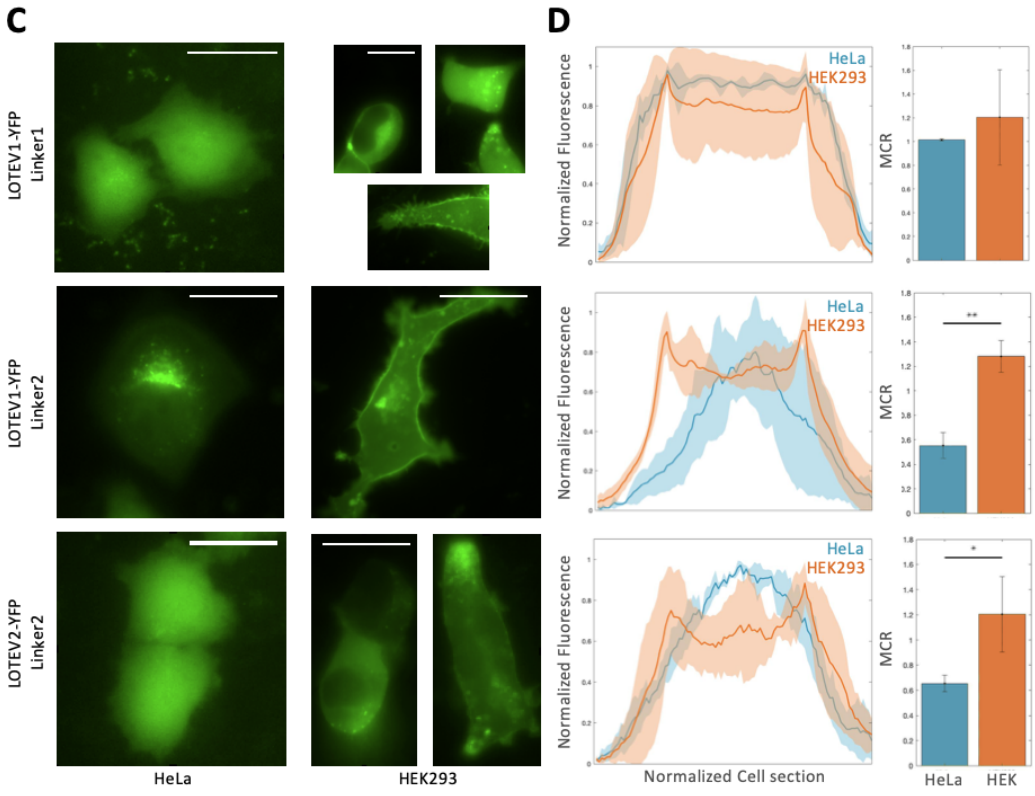

FIGURE 3.6: A) Cartoon showing LOTEV1 with YFP linked to its C-terminus. A linker peptide was inserted between the two fused proteins to separate the domains for independent protein folding. B) Table showing the two residue sequences tested as linkers, having high and low flexibility. C) GFP signal from mammalian cells expressing LOTEV1 and LOTEV2 constructs tagged with YFP through different linkers: *HeLa* cells (left), *HEK293* cells (right); scale: $50\mu m$. D) Normalized fluorescence intensity profile along normalized cell section, for both *HeLa* and *HEK293* cells (left); comparison of Membrane to Cytoplasm ratio (MCR) in *HeLa* and *HEK293* cells. Bars show average value, vertical lines the standard deviation (p: 0.450, 0.002, 0.036 from top to bottom; n=3, N=2).

a TEV protease showed that the Nucleus to Membrane Ratio (NMR) increases by +84% (from 0.87 to 1.60) when an active TEVp is present inside *HeLa* cells (Fig.3.7). The significance of the result (p=0.049) suggested that LckCherry was an efficient reporter of TEVp activity.

A comparison between the expected Cherry-Q fluorescence distribution in absence of TEVp (Fig.3.8A) and Cherry-Q fluorescence as measured from *HeLa* cells (Fig.3.8B) showed that the reporter was not behaving as hypothesised. In particular, the quencher peptide did not quench mCherry fluorescence in absence of TEVp, but made mCherry avoid the cell nucleus.

Even though Cherry-Q was not working as hypothesised, the difference in Nucleus to Cytoplasm Ratio (NCR) in absence (NMR = 0.71) and presence (NMR = 0.98) of TEVp was statistically significant (p = 0.025), therefore it was concluded that Cherry-Q could be used as an efficient TEVp-activity reporter.

LOTEV1 shows proteolytic activity at resting potential, LOTEV2 does not

Cherry-Q's NCR index showed to discriminate TEVp activity inside the cell better than LckCherry's NMR index ($p_{LckCherry} = 0.049$, $p_{CherryQ} = 0.025$); thus, it was chosen to measure LOTEV proteolytic activity at resting potential and after cell depolarization. If LOTEV constructs behaved as hypothesised, the proteolytic activity should have been absent at resting potential and increasing upon cell depolarization.

HeLa cells expressing both Cherry-Q and LOTEV1 showed Cherry-Q's NCR at resting potential to be non statistically different to the NCR from cells with active TEVp (p = 0.05). On the contrary, LOTEV2 showed a NCR dissimilar to both presence (p = 0.03 compared to CherryQ added to TEVp) and absence (p = 0.02 compared to CherryQ alone) of TEVp (Fig.3.9).

These data suggested that LOTEV1 had at resting potential a proteolytic activity that was already similar to an active TEVp. In other words, the two TEVp halves were already close enough to each other at resting potential to correctly assemble

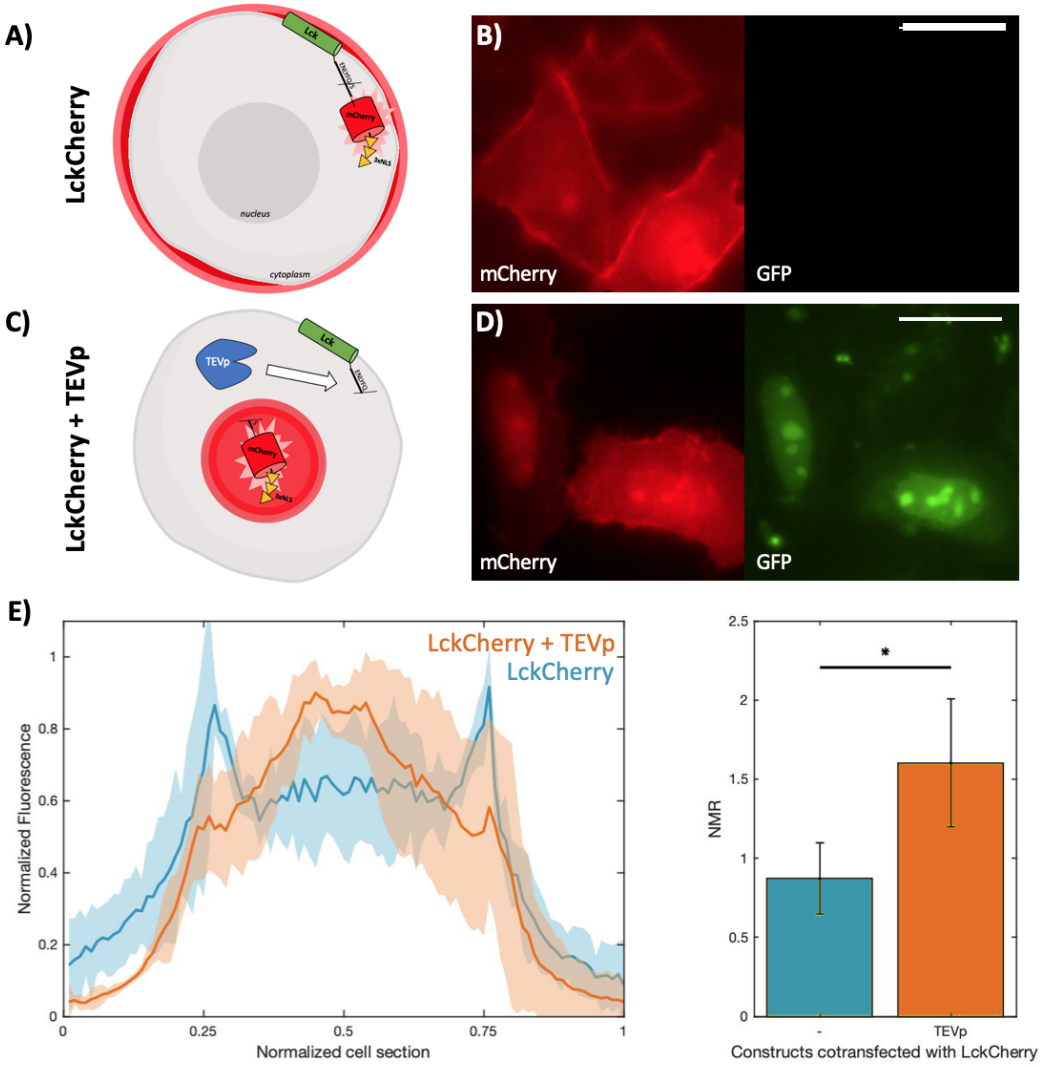

FIGURE 3.7: A) Cartoon of LckCherry expected fluorescence localization inside the cell, in absence of TEVp. LckCherry is represented as in Fig.3.4. B) mCherry (left) and GFP (right) fluorescence signal from *HeLa* cells transfected with LckCherry; scale: $50\mu m$. C) Cartoon of LckCherry expected fluorescence localization inside the cell, in presence of TEVp. Cleavage represented as in Fig.3.4, with an active TEVp (blue polygon) substituting LOTEV representation. D) mCherry (left) and GFP (right) fluorescence signal from *HeLa* cells transfected with LckCherry and TEVp; scale: $50\mu m$. The GFP signal from the nucleus labels the cells that are expressing TEVp. E) LckCherry intensity profile across cell section in absence (blue) and presence (orange) of TEVp. Think line represents the average, the shaded area the standard deviation (n = 3, N = 2). F) Comparison of the Nucleus to Membrane Ratio (NMR) fluorescence intensity of LckCherry in absence and presence of TEVp. Bars represent the average, the vertical lines the standard deviation (p: 0.049, n=3, N=2)

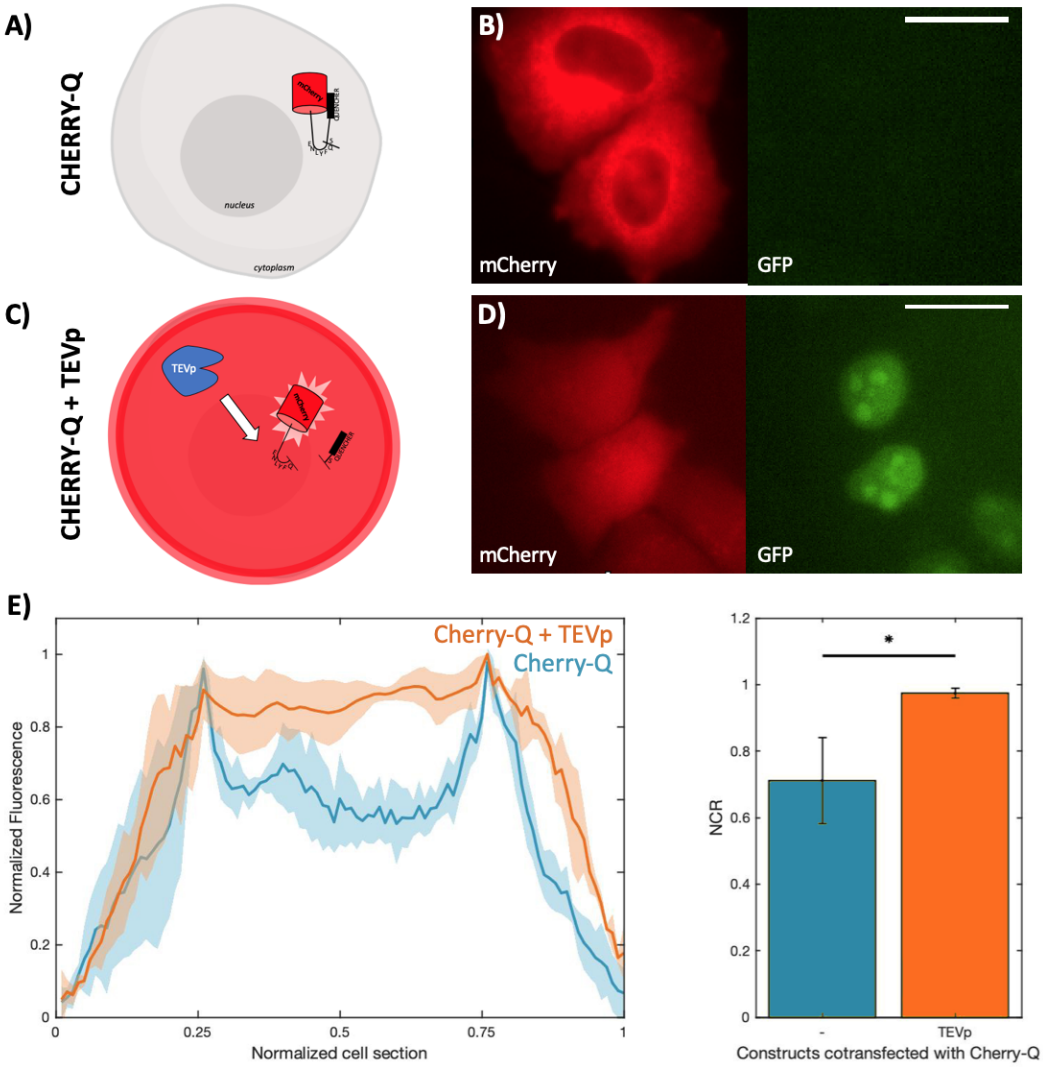

FIGURE 3.8: A) Cartoon of Cherry-Q expected fluorescence localization inside the cell, in absence of TEVp. Cherry-Q is represented as in Fig.3.4. B) mCherry (left) and GFP (right) fluorescence signal from *HeLa* cells transfected with Cherry-Q; scale: $50\mu m$. C) Cartoon of Cherry-Q expected fluorescence localization inside the cell, in presence of TEVp. Cleavage represented as in Fig.3.4, with an active TEVp (blue polygon) substituting LOTEV representation. D) mCherry (left) and GFP (right) fluorescence signal from *HeLa* cells transfected with Cherry-Q and TEVp; scale: $50\mu m$. The GFP signal from the nucleus labels the cells that are expressing TEVp. E) Cherry-Q intensity profile across cell section in absence (blue) and presence (orange) of TEVp. Thick line represents the average, the shaded area the standard deviation (n = 3, N = 2). F) Comparison of the Nucleus to Cytoplasm Ratio (NCR) fluorescence intensity of Cherry-Q in absence and presence of TEVp. Bars represent the average, the vertical lines the standard deviation (p: 0.025, n=3, N=2)

the protease active site (Fig.3.2, schematic on the right).

LOTEV2 did not show a high TEVp activity, therefore it was suggested that its conformation at resting potential was similar to the hypothesised one, with the TEVp halves far from each other (Fig.3.2, schematic on the left).

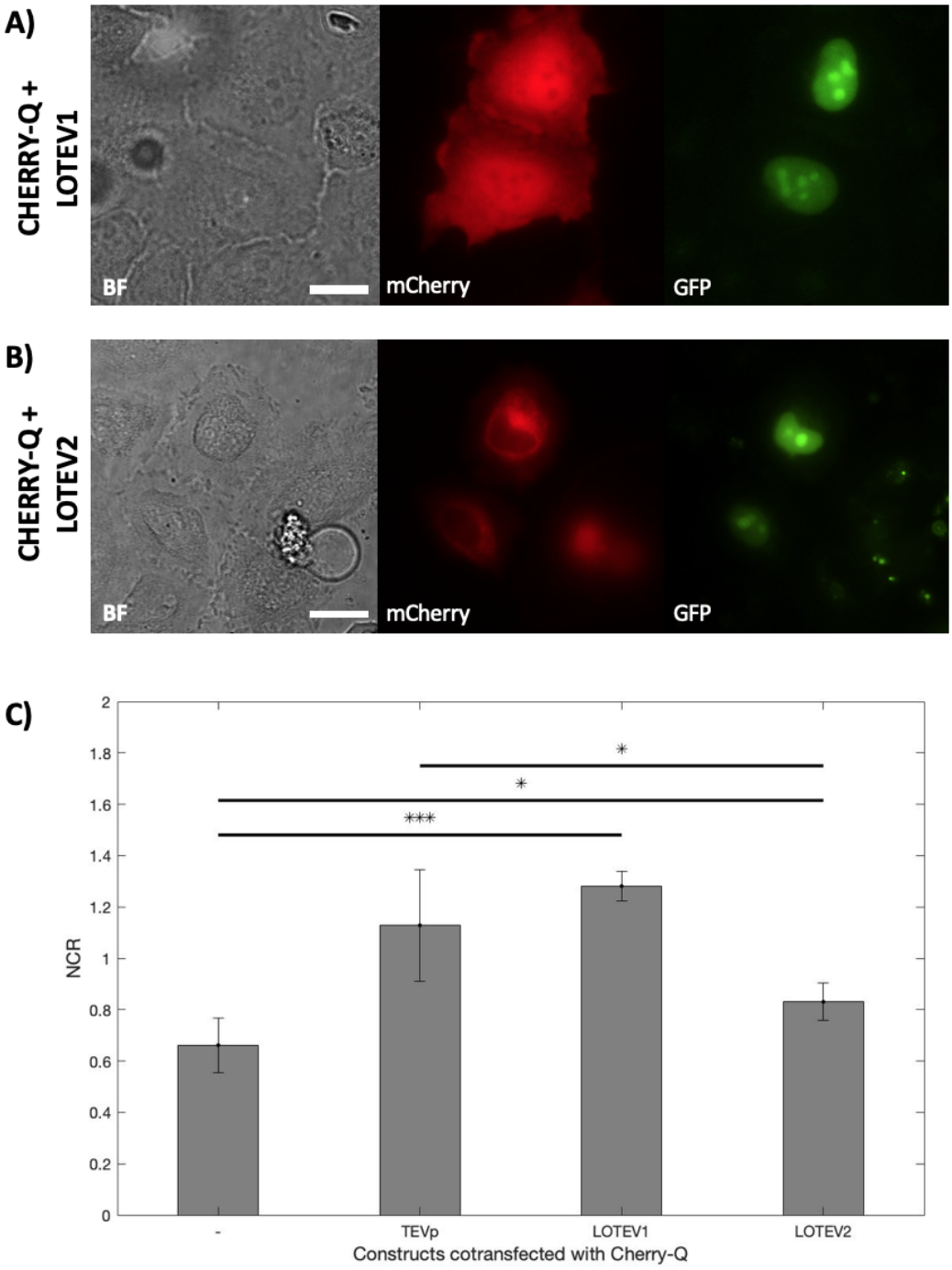

FIGURE 3.9: A-B) Cherry-Q reporter distribution in *HeLa* cells in presence of LOTEV1 (A) and LOTEV2 (B), at resting potential. Brightfield, mCherry and GFP channels; scale: $50\mu m$. The mCherry signal shows the cell distribution of Cherry-Q, the GFP signal labels the cells expressing LOTEV constructs. C) Comparison of Nucleus to Cytoplasm Ratio (NCR) of Cherry-Q alone and co-expressed with TEVp, LOTEV1 or LOTEV2. Bars show mean values, vertical lines standard deviations (n=3, N=2). At resting potential, Cherry-Q's NCR index in presence of LOTEV1 is not statistically different from TEVp presence (p=0.05), suggesting LOTEV1 proteolytic activity. Differently, NCR index in presence of LOTEV2 is statistically different from TEVp presence (p=0.03), but also to TEVp complete absence (p=0.02), suggesting LOTEV2 has limited proteolytic activity at resting potential.

Design of LOTEV variants by linker engineering

Since at resting potential LOTEV1 showed a high proteolytic activity and LOTEV2 showed a non-zero activity (Fig.3.9), it was hypothesised that appropriate modification of the linkers connecting Ci-VSD with the two protease halves could have better calibrated the distance between TEVp halves. It is known from literature (Wriggers, Chakravarty, and Jennings, 2005) and it was shown in LOTEV-YFP constructs (Sec.3.2.2) and in Cherry-Q (Sec.3.2.2) that the sequence of a linker is critical for the correct folding and dynamic behaviour of a protein. In particular, the amino acid sequence connecting the Ci-VSD to the original phosphatase domain was already known to influence the dynamics of the whole protein (Liu et al., 2008; Hobiger et al., 2012).

Therefore, it was hypothesised that changing the length and the amino acid sequence of LOTEVs linkers could affect the distance between TEVp halves. In particular, it was hypothesised that different linkers in LOTEV1 could lead to a better separation of TEVp halves at resting potential, therefore disassembling the protease active site and making LOTEV1 inactive without the depolarizing stimulus.

A library of LOTEV variants was designed for both LOTEV1 and LOTEV2. The linker at the N-terminus of Ci-VSD was designed to be shortened by 15, 12, 8 and 4 residues (versions were called 1a 1b, 1c and 1d respectively); the linker at the C-terminus was designed to be shortened by 12 or by 8 residues (versions called 2a and 2b respectively). Also two more rigid C-linkers were designed, both starting from linker 2a and adding $(AP)_2$ or $(AP)_4$ at the C-terminus (they were called 2AP2 and 2AP4, respectively) (Fig.3.10). Repeats of alanines-prolines were chosen because of the rigidity that proline-rich sequences provide to peptides (Breibeck and Skerra, 2018; Williamson, 1994).

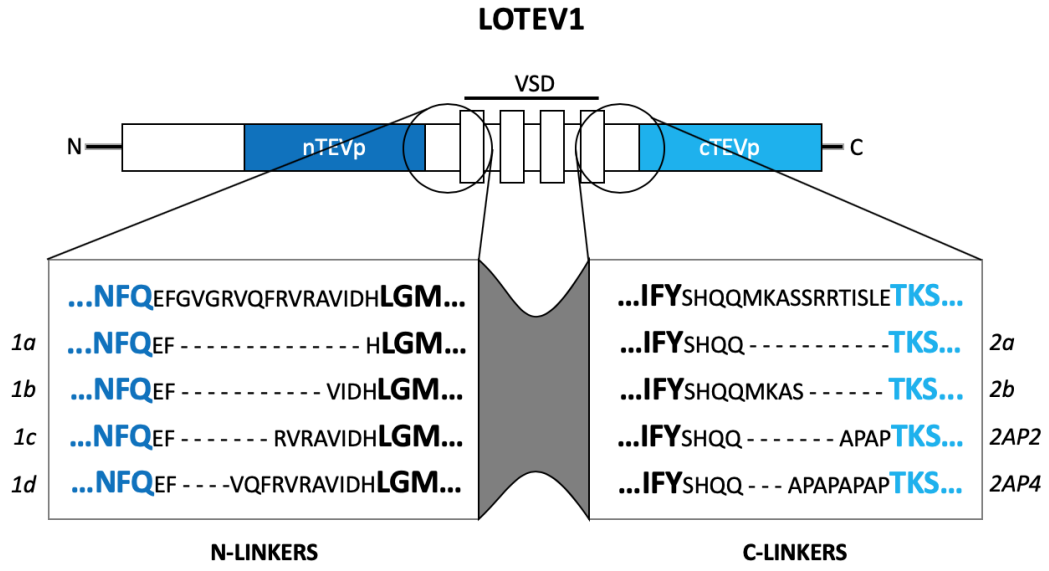

FIGURE 3.10: Schematic of the library made of N-linkers and C-linkers, showed for LOTEV1 construct as an example.

LOTEV variants at resting potential

Out of the 16 possible combinations of linker couples (the entire original linker was not considered), 3 variants were successfully assembled for LOTEV1 (LOTEV1-1a2a, LOTEV1-1a2AP2 and LOTEV1-1a2AP4) and 2 for LOTEV2 (LOTEV2-1a2a and LOTEV2-1a2AP2). These variants still gave the opportunity to assess whether a shorter N-linker and a shorter or stiffer C-linker were enough to modify LOTEV activity and dynamics.

As can be assessed from a visual analysis of Cherry-Q spatial distribution in Fig.3.11, cells transfected with a LOTEV1 variant showed a Cherry-Q intensity in the nucleus comparable or higher than in the cytoplasm in Fig.3.13. In fact, the NCR index was not significantly different from the cells transfected with TEVp ($p = 0.05, 0.09, 0.11, 0.06, 0.07$ for LOTEV1, LOTEV1(D129R), LOTEV1_1a2a, LOTEV1_1a2AP2, LOTEV1_1a2AP4, respectively). Such behaviour suggested proteolytic activity at resting potential of LOTEV1 constructs.

On the other hand, cells with LOTEV2 variants showed a Cherry-Q spatial distribution with an apparent intensity in the nucleus lower than in the cytoplasm (Fig.3.12).

Cherry-Q's NCR was significantly different from cells with TEVp (p = 0.03, 0.008, 0.04, 0.04 for LOTEV2, LOTEV2(D129R), LOTEV2_1a2a, LOTEV2_1a2AP2, respectively). As this result suggested absence of TEVp proteolytic activity, the fact that only LOTEV2(D129R) showed a NCR non statistically different to Cherry-Q expressed alone (p = 0.02, 0.06, 0.01, 0.01) suggested that only LOTEV2(D129R) was completely not active (Fig.3.13).

Out of all LOTEV1 variants, only LOTEV1-1a2AP4 showed a NCR at resting potential that was statistically different from the presence of a active TEV protease. This result suggested that shortening LOTEV1 linkers (1a2a and 1a2AP2 variants) did not result in a larger separation of TEVp halves, but the addition of 4 more residues (APAP) at the terminus decreased TEVp halves vicinity at resting potential.

On the contrary, every LOTEV2 variant showed an NCR lower than 1, meaning Cherry-Q fluorescence in the cell nucleus was lower than the fluorescence in the cytoplasm and thus that LOTEV2 variants had low proteolytic activity at resting potential. LOTEV2-1a2a and LOTEV2-1a2AP2 showed higher NCR values (0.93 and 0.92, respectively) than the original LOTEV2 (0.83), suggesting that substitution of Ci-VSD with shorter linkers brought the TEVp halves closer to each other, increasing the probability of proteolytic activity at resting potential. The NCR index of cells expressing LOTEV2(D129R) did not show statistical difference to the NCR of Cherry-Q alone (p = 0.18, n = 4), suggesting the TEVp halves were distant from each other and the proteolytic activity absent.

The absence of significant proteolytic activity at resting potential for LOTEV2 constructs was in accordance with the MATE idea, therefore these constructs were considered the most promising to be tested for cell depolarization.

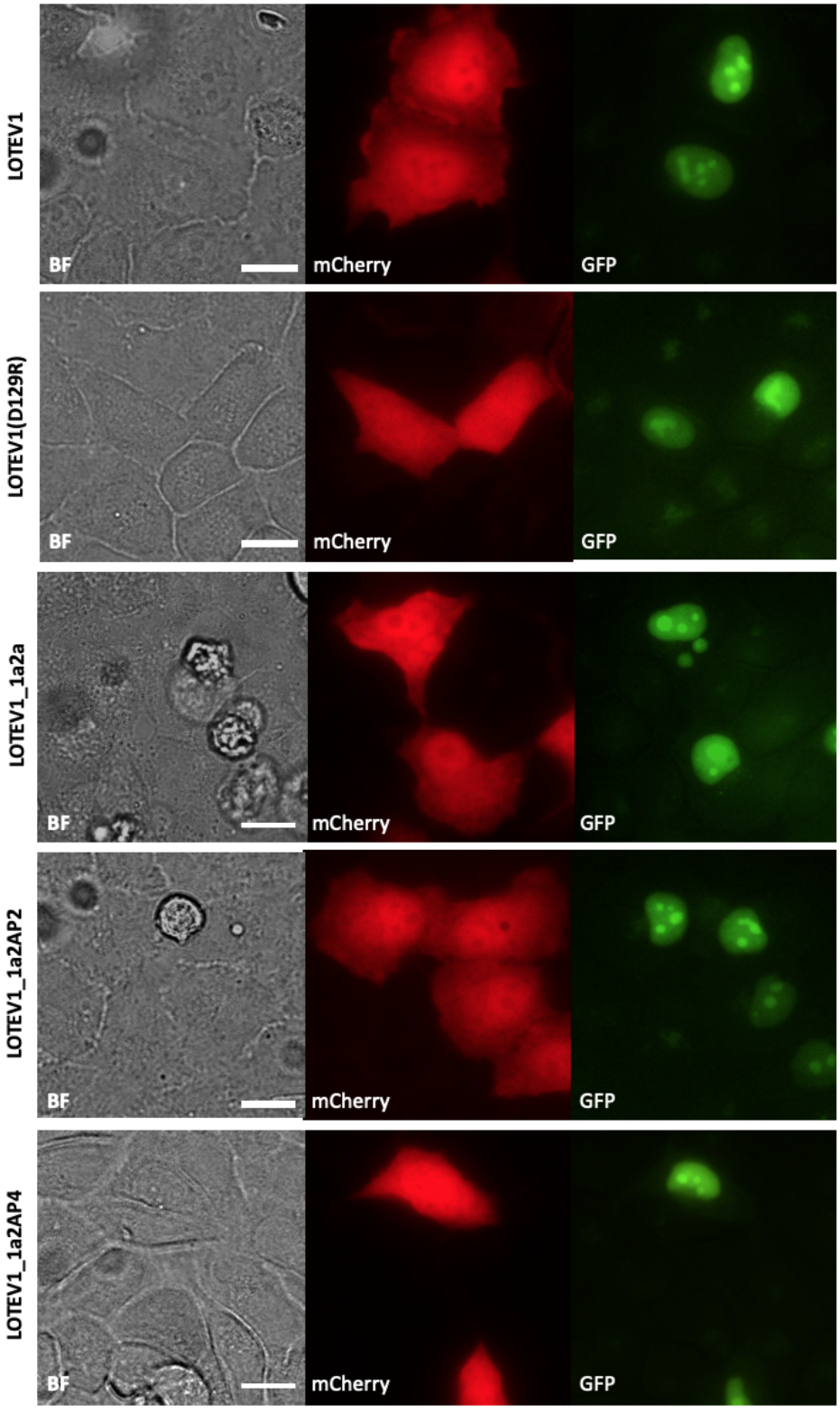

FIGURE 3.11: Microscope data from LOTEV1 variants. Every *HeLa* cell expressing both Cherry-Q and a LOTEV1 variant showed a Cherry-Q cell localization similar to Cherry-Q in presence of an active TEVp (Fig.3.8). Brighfield, mCherry and GFP channels; scale: $50\mu m$.

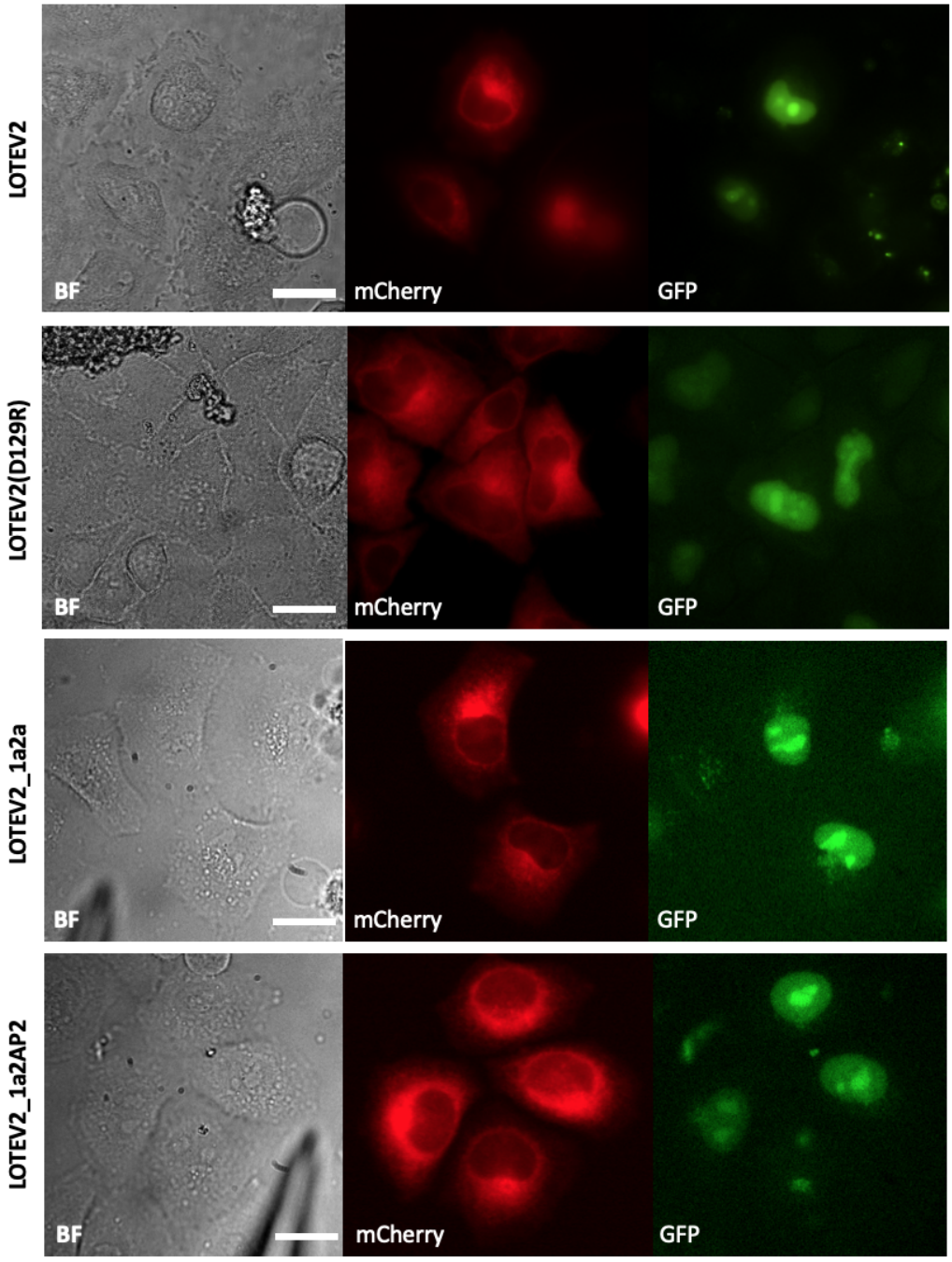

FIGURE 3.12: Microscope data from LOTEV2 variants. Every *HeLa* cell expressing both Cherry-Q and a LOTEV2 variant showed a Cherry-Q cell localization similar to Cherry-Q alone (Fig.3.8). Brighfield, mCherry and GFP channels; scale: $50\mu m$.

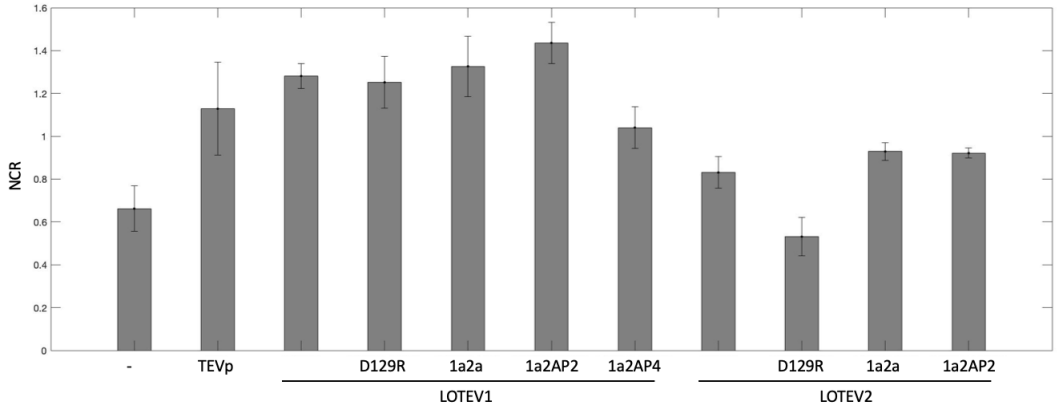

FIGURE 3.13: Comparison of the NCR of every LOTEV variants at resting potential. Bars show average NCR values and vertical bars the standard deviation (n=4 or 5, N=2)

3.2.3 Analysis upon Cell Depolarization

Addition of 70 mM KCl depolarizes cell membrane by 50 mV

Cell depolarization can be obtained by increasing $[K^+]$ in the extracellular environment, following Goldman Equation (Goldman, 1943). To test the magnitude of the depolarization brought by the potassium clamp, *HeLa* cells were stained with the potentiometric dye di-8-ANEPPS and $[K^+]$ was increased from 3 mM KCl to 70 mM KCl.

To estimate membrane potential from di-8-ANEPPS fluorescence, the ratio F_{450}/F_{500} had to be computed, where F_{450} was the fluorescence measured with 450ex/575em filters and F_{500} measured with 500ex/575em filters. As it is shown in Fig.3.14, when 70 mM KCl were added to the cell media, the F_{450}/F_{500} index decreased by 4.4%. According to di-8-ANEPPS calibration obtained with patch clamp on mice muscle cells (DiFranco, Quinonez, and Vergara, 2012), such a percentage decrease in di-8-ANEPPS fluorescence was associated to a +50 mV depolarization of *HeLa* cells.

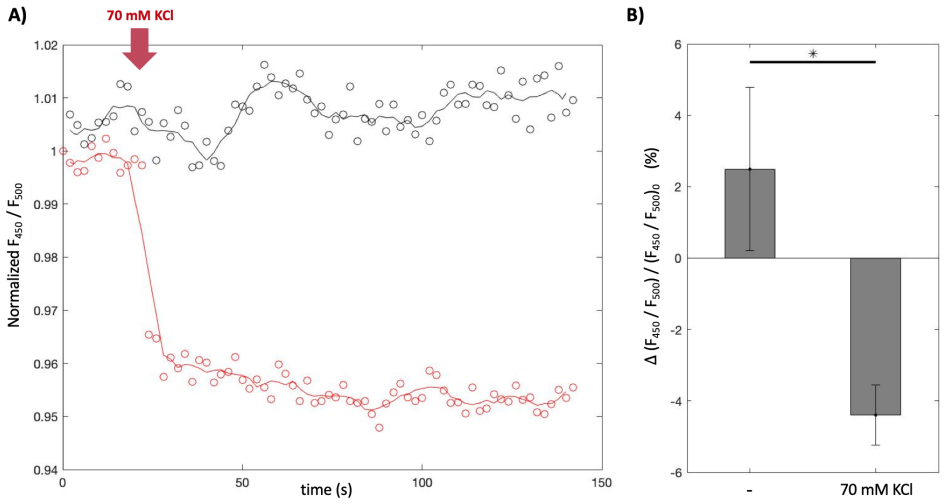

FIGURE 3.14: Fluorescence signal coming from *HeLa* cells stained with $2\mu M$ di-8-ANEPPS. A) Time trace of F_{450}/F_{500} fluorescence from cells without (black line) and with (red line) addition of 70 mM KCl (red arrow). B) Comparison of F_{450}/F_{500} fluorescence change between time 0s and 100s, for cells without and with KCl stimulus. Bars indicate the mean value, vertical lines the standard deviation (p = 0.008, n = 3).

Cherry-Q distribution changes after chemical depolarization when co-expressed with LOTEV2

Having assessed that cell depolarization could be achieved by increasing $[K^+]$, the same chemical stimulus was given to cells expressing Cherry-Q and LOTEV constructs. After 1 minute from the stimulus, the NCR was compared to the NCR before the depolarization.

The degree of proteolytic change induced in LOTEV constructs by the chemical depolarization obtained with 70 mM KCl was estimated by $(NCR_D - NCR_0)/NCR_0$ where NCR_D is the NCR after chemical depolarization and NCR_0 is the NCR before the initial NCR.

A comparison of the NCR change for different LOTEV constructs showed that for most LOTEV1 variants the NCR did not change after the +50 mV chemical depolarization of the cells. As LOTEV1 construct had already shown to have proteolytic activity at resting potential, this result was not surprising, meaning that Cherry-Q reporters had already been cleaved before cell depolarization. Only the LOTEV1 variant with shorter N-linker and the shorter and stiffer C-linker (LOTEV1-1a2AP2)

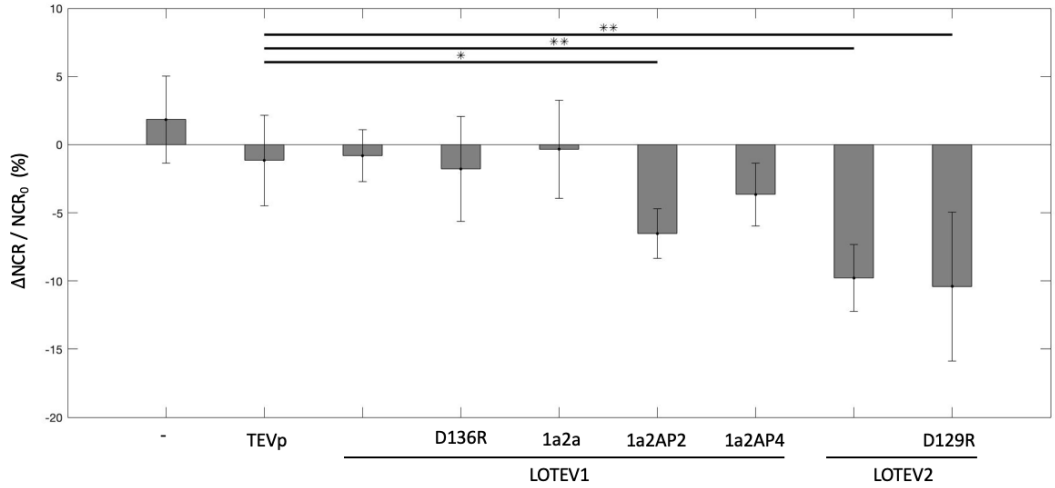

FIGURE 3.15: Comparison of Nucleus to Cytoplasm Ratio (NCR) change (%) after cell depolarization. Bars indicate the mean value, vertical lines the standard deviation (n = 3, N = 2). Out of the LOTEV1 and LOTEV2 variants, only LOTEV1_1a2AP2, LOTEV2 and LOTEV2(D129R) showed a NCR change significantly different from the controls (p = 0.009, 0.002, 0.004, respectively).

showed a change in NCR (-6.5%) significantly different from the controls (p = 0.009).

LOTEV2 constructs, on the other hand, did not show proteolytic activity at resting potential (Fig.3.13) and, after the +50 mV chemical depolarization of the cell membrane, they showed a statistically relevant NCR change. In particular, LOTEV2 NCR decreased by -9.79% and LOTEV2(D129R) decreased by -10.40% (p = 0.002 and 0.004 compared to TEVp, respectively).

Even if such a result suggested that depolarization was affecting LOTEV2 activity on Cherry-Q, the NCR change was negative, meaning Cherry-Q in the nucleus had decreased compared to the cytoplasm. This behaviour was the opposite of the expected one, suggesting a decrease rather than an increase of proteolytic activity (compare with Fig.3.8E).

However, the activity of a protease is not reversible and the production of novel, uncleaved Cherry-Q does not take one minute but tens of minutes (Patrick J. Macdonald, Yan Chen and Mueller, 2013). Therefore, it was not considered possible that the result indicated a decrease in LOTEV proteolytic activity. Moreover, since

LOTEV2(D129R) was not expected to change conformation upon cell depolarization (Tsutsui et al., 2013), it was suggested the NCR decrease was due to other reasons. It was noted that the medium substitution caused shrinking of *HeLa* cells. It was then hypothesised that such a change in cell shape was affecting Cherry-Q fluorescence assessment.

In order to avoid the artifacts obtained with chemical cell depolarization and have a better control on cell membrane potential, patch clamp technique was considered.

Patch clamp

Each of LOTEV1 variant showed proteolytic activity at resting potential, suggesting they could not represent the hypothesised MATE activated only upon cell depolarization.

On the other hand, no LOTEV2 showed proteolytic activity at resting potential, therefore patch clamp depolarization was performed on *HeLa* cells expressing Cherry-Q and LOTEV2 variants.

When a sequence of increasing electrical stimuli (+40 mV, +60 mV, +80 mV, +100 mV) was provided to the cells, the LOTEV2 variant with no shortened linkers showed the most promising results. In particular, as can be seen from the microscope images in Fig.3.16C and the time traces in Fig.3.18C, after the +60 mV stimulus, Cherry-Q fluorescence inside the cell nucleus (and the NCR index) increased. Such a behaviour was not observed in cells with Cherry-Q alone or with Cherry-Q in presence of an active TEVp (Fig.3.16A and B respectively), with the NCR increase at time t=150 being significantly larger (+0.5% the greatest change in the controls, +8.6% with LOTEV2, p=0.035, n=3, N=2)(Fig.3.19). It was therefore suggested that the reporter was cleaved by an increase of LOTEV2 proteolytic activity. As cells expressing the voltage-insensitive LOTEV2(D129R) variant did not show significant NCR increase, the change in NCR was suggested to be due to Ci-VSD conformational changes and TEVp halves brought closer. LOTEV2-1a2a showed a significant increase of proteolytic activity (+2.2% and +3.5% at time t=120s and

150s, p=0.03, 0.04 respectively, compared to TEVp)(Fig.3.19). On the other hand, LOTEV2-1a2AP2 did not show a significant NCR increase. Such a result suggested that the rigid linker $(AP)_2$ at the C-terminus of the Ci-VSD brought TEVp halves more distant from each other, making not possible the correct assembly of the protease even after Ci-VSD conformational change.

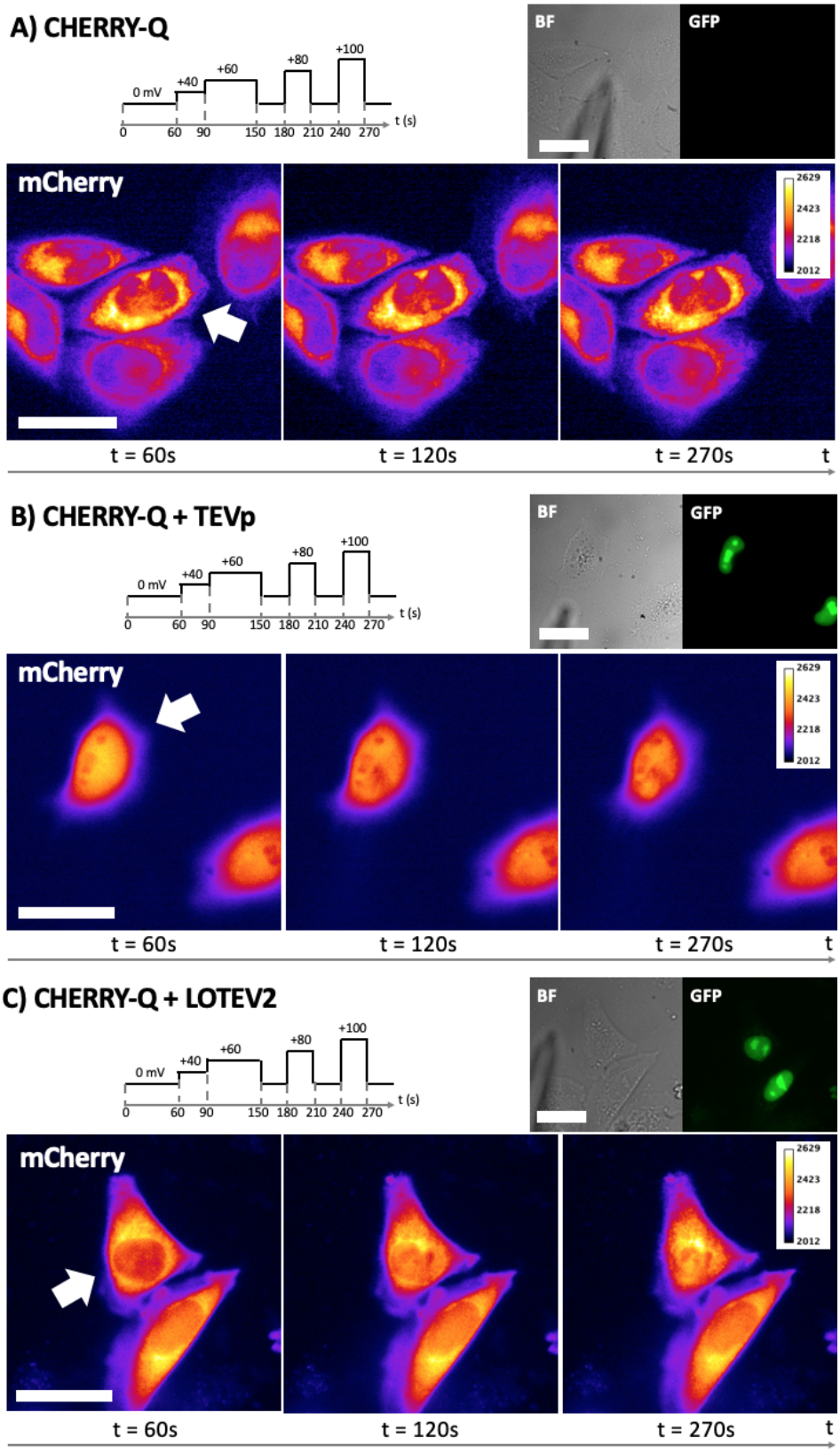

FIGURE 3.16: Microscope images of patch clamp depolarization of *HeLa* cells expressing Cherry-Q alone or together with TEVp or LOTEV2. Brighfield, GFP and mCherry channels; scale: 50 μm. The diagram shows the time trace of the voltage provided by the patch clamp microelectrode. GFP channel shows the YFP fluorescence coming from the nucleus of cells expressing TEVp or LOTEV2; mCherry channel (coloured with "fire" LUT) shows Cherry-Q fluorescence. The white arrow indicates the cell depolarized by patch clamp stimulation.

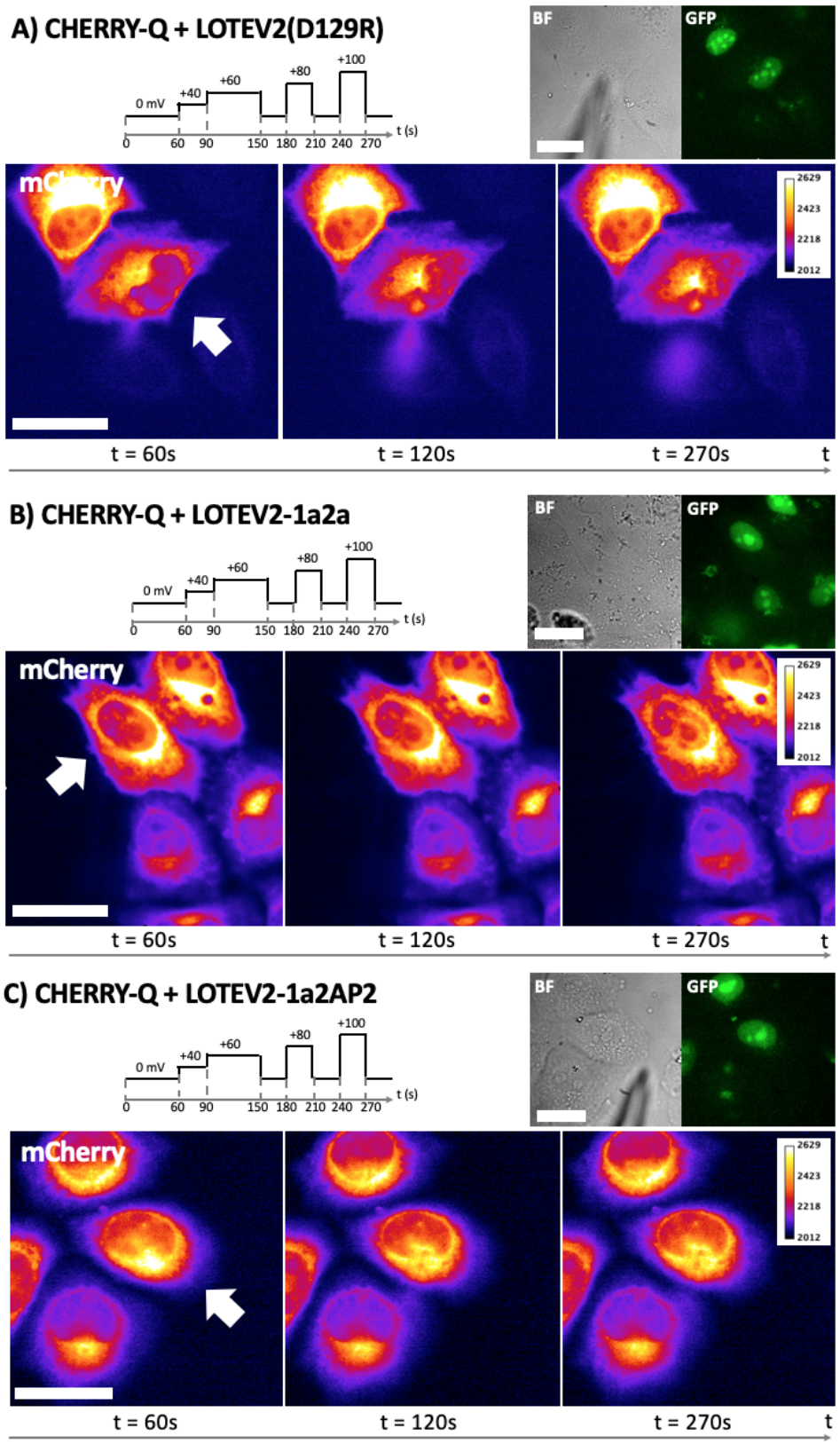

FIGURE 3.17: Microscope images of patch clamp depolarization of *HeLa* cells expressing Cherry-Q together with LOTEV2 variants. Brighfield, GFP and mCherry channels; scale: 50 μm. The diagram shows the time trace of the voltage provided by the patch clamp microelectrode. GFP channel shows the YFP fluorescence coming from the nucleus of cells expressing LOTEV2 constructs; mCherry channel (coloured with "fire" LUT) shows Cherry-Q fluorescence. The white arrow indicates the cell depolarized by patch clamp stimulation. Scale: 50 μm)

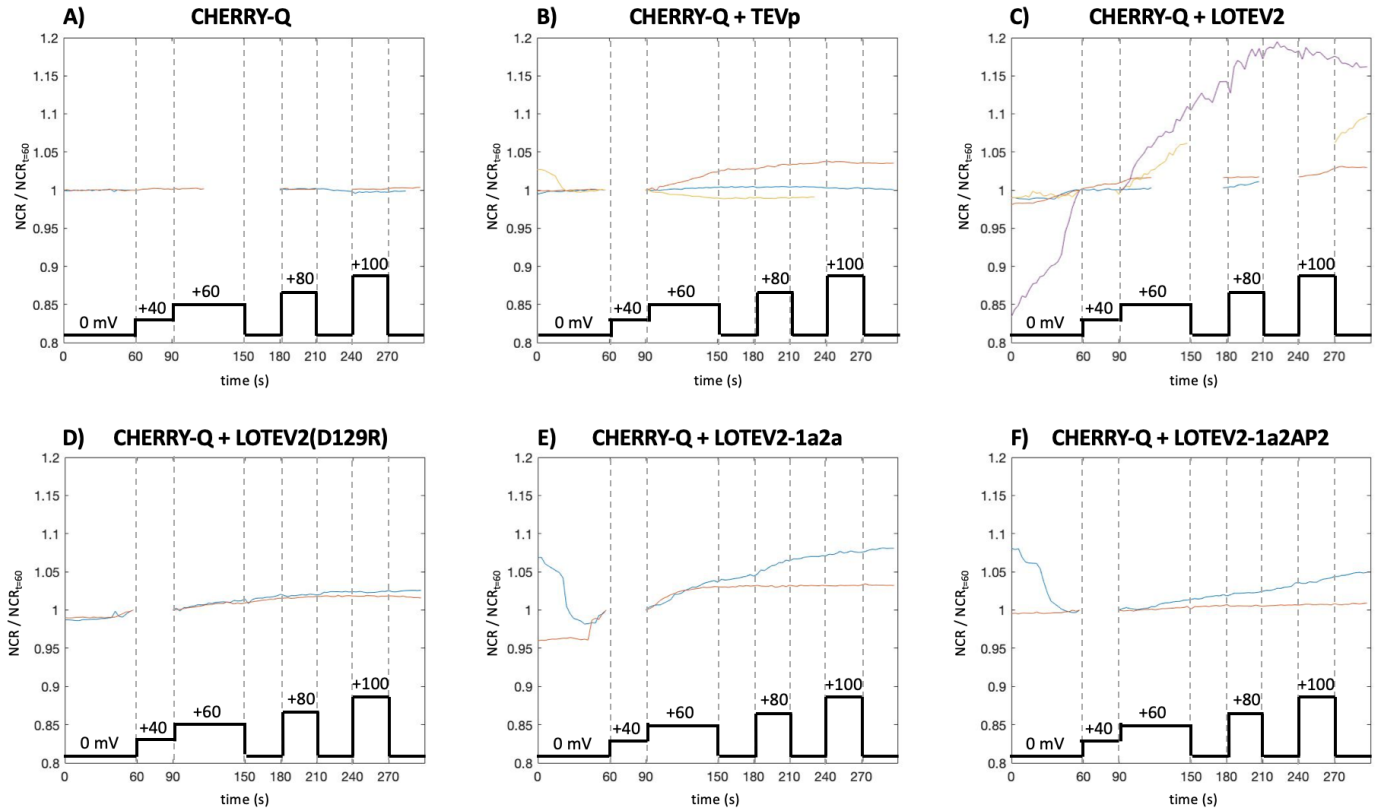

FIGURE 3.18: Time traces of Nucleus to Cytoplasm Ratio (NCR) from Cherry-Q expressed in *HeLa* cells upon patch clamp membrane depolarization. Each curve represents the NCR coming from the Cherry-Q expressed by a single cell, after normalization to the NCR at time t = 60 s when the first electrical stimulus was delivered. Absent data points in the time traces are due to different electrical stimulation pattern in some experiments

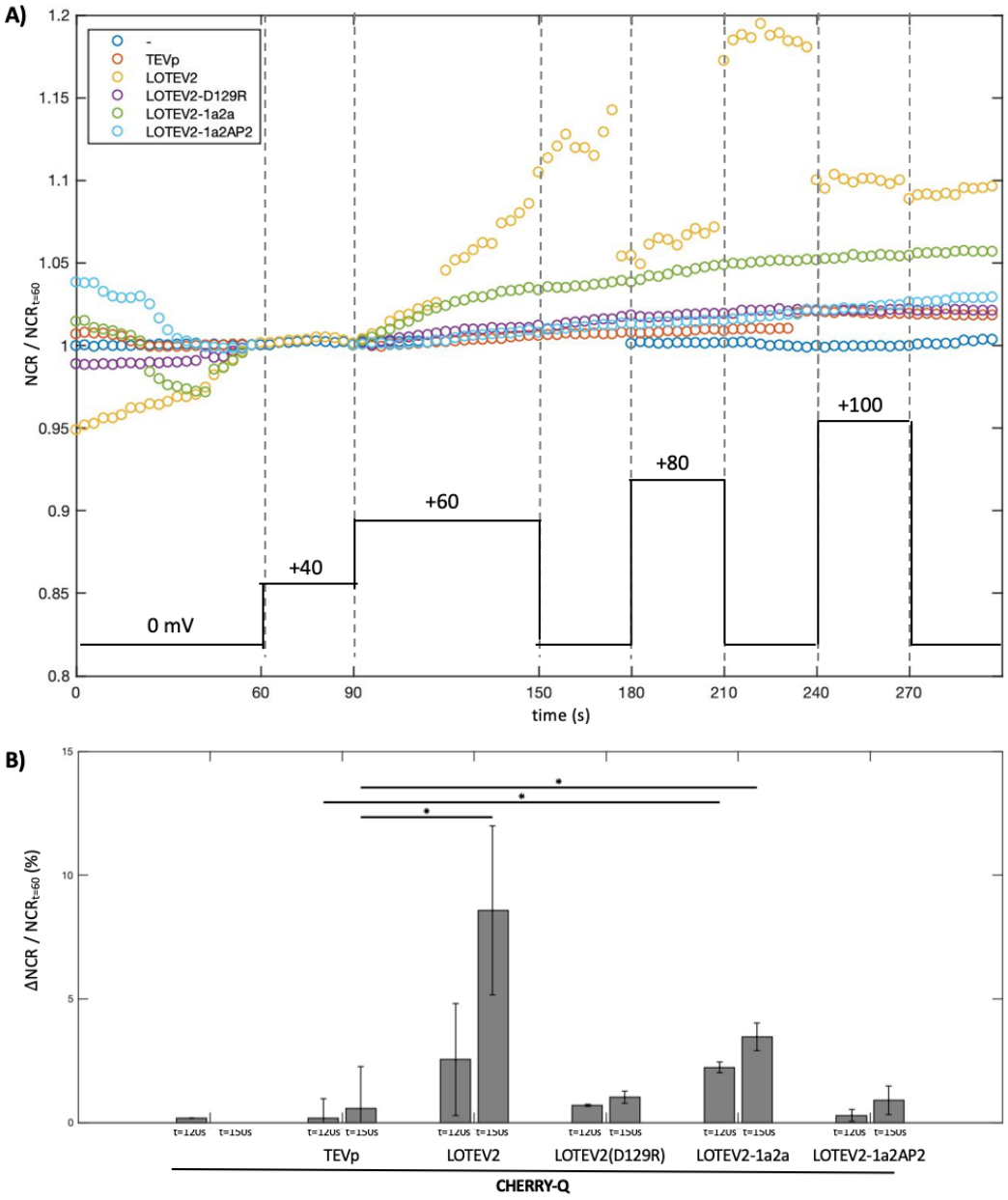

FIGURE 3.19: A) Average NCR time-traces of cells expressing the Cherry-Q reporter and either TEVp or a LOTEV2 construct, during patch clamp stimulation. Curves were normalized to the NCR at time t = 60 s when the first electrical stimulus was provided. Overlaid at the bottom the time-trace of the electrical stimulus given by the patch clamp microelectrode to the cell. Sudden jumps in LOTEV2 average curve are due to the average being computed from curves having different electrical stimulation pattern. In particular, 2 samples did not have the stimulation break between +60 mV - 80 mV and +80 mV - 100 mV (see curves in Fig.3.18C). B) Comparison of the NCR increase in different cells during the +60 mV stimulus, after 30 s and 60 s from the beginning of the stimulus. Bars indicate the average NCR, vertical lines the standard deviation (n = 2 or 3, N = 2)

3.3 Discussion

It is important to emphasise that this work represents the very first attempt to develop a direct interface between the electrical world and the biological world by exploiting voltage-sensitive conformational changes. Compared to natural systems made of a membrane domain and an enzymatic domain, such as the voltage-sensitive-phosphatase, the electrically-activated protease LOTEV provides specific control over a customizable target. The viral origin of TEVp ensures that the system is orthogonal to every other cellular process and does not interfere with proteins and pathways different from the labeled target.

While the first LOTEV candidates, LOTEV1 and its variants, showed to be enzymatically active at cell resting potential, the inversion of TEVp halves in LOTEV2 variants made the enzyme inactive in absence of electrical stimulation. Even if it is not clear whether the protein correctly targets the cell membrane in *HeLa* cells as much as it does in *HEK293* cells, LOTEV2 showed an estimated +8.6% increase of proteolytic activity, 150 s after an electrical stimulation of +60 mV. When the linkers connecting the VSD with the TEVp halves were shortened by 15 and 12 residues (N- and C- terminus, respectively) in LOTEV2-1a2a, the activity change under the same electrical stimulus decreased to +3.5%.

3.3.1 Protease reporters

To better analyse the localization of LckCherry and the membrane specificity change upon cell depolarization, a confocal microscope could have been used. In particular, the implementation of a confocal microscope with a patch clamp system is expected to provide high resolution on LckCherry behaviour.

On the other hand, Cherry-Q did not require a higher spatial resolution, as its localization was clearer. It was in fact apparent that the fluorescence of mCherry was not quenched by the attached peptide as expected (Nicholls et al., 2011). As seen from the results in Sec.3.2.2, the reporter fluorescence intensity at resting potential

was comparable with a non-quenched mCherry, showing it was avoiding only the cell nucleus. The different behaviour can be explained by the way the quencher peptide was reported to quench GFP. In fact, the hydrophobic amino acid sequence of the peptide is said to tetramerize the fluorescent protein, thus preventing the maturation of GFP's chromophore. It is hypothesised that the substitution of the GFP with an mCherry and the modification of the linker changed the way the FP was tetramerized, allowing the correct maturation of the mCherry chromophore. However, even if the fluorescence was not quenched, the tetramerization induced by the hydrophobic peptide increased the size of the FP complex from 26kDa (an mCherry monomer) to 104 kDa (an mCherry tetramer). Since passive diffusion of proteins inside the cell nucleus decreases for proteins larger than 60 kDa (Paine, Moore, and Horowitz, 1975; Ma et al., 2012), it is hypothesised that the presence of the "quencher peptide" did not allow the tetramerized mCherry to access the nucleus. The hypothesised novel behaviour of Cherry-Q is shown in Fig.3.20.

Cherry-Q showed to have a NCR index more significantly different in presence and absence of TEVp than LckCherry's NMR index and therefore it was selected as reporter to study LOTEV activity. However, the statistical test used was an unpaired t-test, implying populations with normal distributions and same variances. The normality hypothesis needed first to be tested with a Shapiro-Wilk test and, in case the distributions were not normal, the use of the Mann-Whitney test for unpaired samples would have been more suited. This consideration applies to every statistical test performed during this project.

3.3.2 LOTUS-V and LOTEVs localization

The significant difference of LOTUS-V localization (Fig.3.5) in *HeLa* and *HEK293* cells shows how the local cell environment can lead to different expression of the same protein.

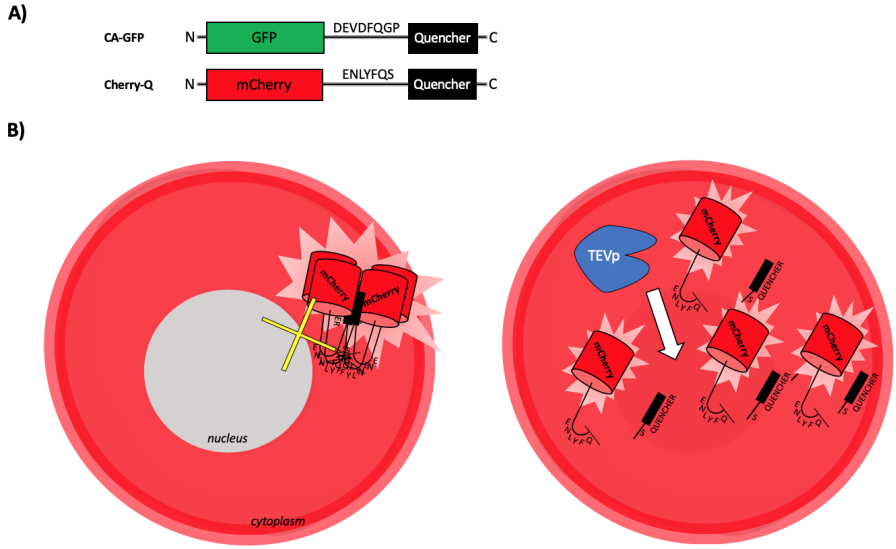

FIGURE 3.20: A) Comparison between the domain assembly of the original CA-GFP caspase-reporter which used the quenching peptide (Nicholls et al., 2011) and Cherry-Q structure. Differently from Cherry-Q, CA-GFP was based on a GFP and was linked to the quencher through the caspase-7 cleavage recognition site. B) Proposed new mechanism of action of Cherry-Q reporter, substituting the one shown in Fig.3.4E. Left: the original "quencher peptide" (black rectangle) still leads to mCherry tetramerization when linked to the mCherry (red cylinder), but it does not block chromophore maturation, letting mCherry to fluoresce. Instead, the tetramerization makes nucleus access difficult for the mCherry tetramer (yellow cross). Right: in presence of TEVp (blue polygon), the cleavage of the linker releases mCherry from the tetramer, and lets it access the nucleus.

It is hypothesised that in *HeLa* cells are present fewer chaperones involved in membrane protein folding than in *HEK293* cells. If this is true, the chaperones in *HeLa* cells would have difficulties to cope with the high membrane protein expression provided by the highly constituitive CAG promoter. Therefore, a high amount of correctly-folded construct can remain sequestered by the endoplasmic reticulum.

From an analysis of the microscope data on LOTEV localization (Fig.3.6), it can be seen how, in *HEK293* cells, the localization of LOTEV1-YFP Linker1 is heterogeneous across the cell population, while the localization of LOTEV1-YFP Linker2 is more consistent and correctly shows membrane specificity. Such a result suggests that the use of the stiffer Linker2 better separates the YFP domain from the LOTEV1 domain, while the flexible Linker1 was leading to incorrect protein folding in part of the cell population. Following this reasoning, the results from *HeLa* cells suggest that LOTEV1-YFP Linker1 still misfolds in the different cell line, while its version

with Linker2 should show a more correct cell localization, which is not on the cell membrane (Fig.3.21).

On the other hand, the results from LOTEV2-YFP Linker2 construct in *HeLa* and *HEK293* cells show a behaviour similar to what was seen with LOTEV1-YFP Linker1: an homogeneous intra-cell protein distribution in *HeLa* cells and an heterogeneous inter-cell protein distribution in *HEK293* cells. Given the similar behaviour of LOTEV2-YFP Linker2 to LOTEV1-YFP Linker1, it is hypothesised that also LOTEV2-YFP Linker2 is not folding properly in both cell lines, and that another linker to better separate YFP from LOTEV2 is needed to better localize LOTEV2 construct in *HeLa* cells.

It is to be noted that, following this reasoning, the stiff linker NPVPQ was successfully separating LOTEV1 from YFP, while it does not successfully separate LOTEV2 from YFP. As the protein domain at the C-terminus of LOTEV1 and LOTEV2 differ (in LOTEV1 is cTEVp, in LOTEV2 is nTEVp), it follows that the linker efficiency in separating LOTEV constructs from YFP depends on its position in LOTEV structure. A diagram showing the reasoning is shown in Fig.3.21.

LOTEV2 localization was not proved to be membrane-specific in *HeLa* cells, while in *HEK293* cells the protein was showing a better membrane trafficking. For this reason, it is hypothesised that analysis of LOTEV1 and LOTEV2 behaviour in *HEK293* cells rather than *HeLa* cells would have removed uncertainties on misexpression of the protein. However, while LOTUS-V localization assay was carried out at the beginning of the project, LOTEV localization experiments were conducted in a later stage of the project, when several experiments in *HeLa* cells had been conducted. Therefore, it was decided to keep analysing *HeLa* cells, following the hypothesis that the linkers were affecting protein folding and LOTEV2 was correctly targeting the membrane.

In order to increase the understanding of protein localization and membrane specificity, a confocal microscope could have been used.

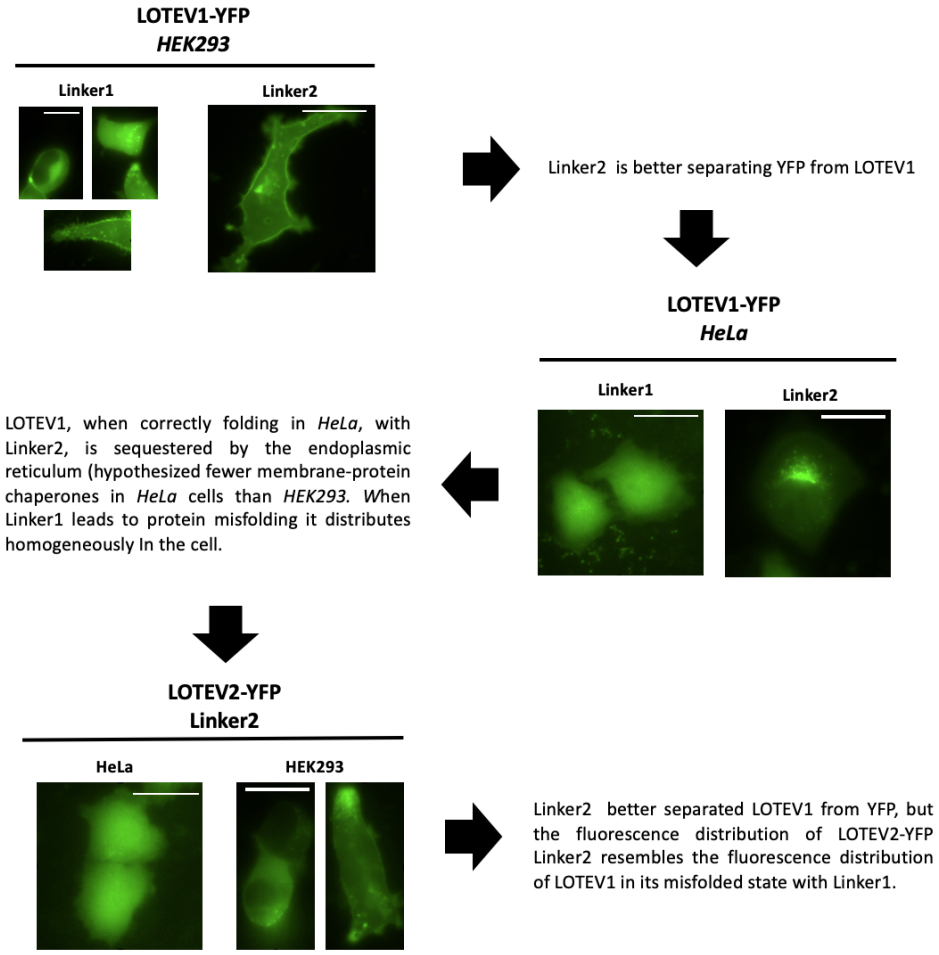

FIGURE 3.21: The results obtained during LOTEV localization experiments can be explained by hypothesising that Linker2 better separates YFP domain from LOTEV1 but not from LOTEV2. Moreover, fewer membrane-protein chaperones in *HeLa* cells than in *HEK293* cells would not be able to cope with the high amount of correctly-folded LOTEV1 in *HeLa*, resulting in ER sequestration.

LOTEV activity at resting potential

The fluorescence data from Cherry-Q reporter shown in Fig.3.9 and Fig.3.11 suggested that at resting potential LOTEV1 constructs had a high proteolytic activity while LOTEV2 has a low proteolytic activity. The difference in these two behaviours shows how the association of the TEVp halves to the Ci-VSD termini had the effect of determining the activation (LOTEV1) or inactivation (LOTEV2) of the proteolytic activity at resting potential. There are three hypotheses for such a behaviour in LOTEV1:

- the relative orientation of nTEVp and cTEVp, when connected respectively to

the N- and C-terminus of a correctly-folded Ci-VSD, resulted in the assembly of the protease active site at resting potential;

- TEVp halves on different LOTEV1 on the cell membrane assembled with each other and activated proteolytic activity inter-protein;
- LOTEV1 was partially misfolding, leading to protease halves assembly, independently from the VSD.

The second hypothesis can be rejected by noticing that Ci-VSD is a monomer and would not form dimers or more complex structures with other Ci-VSDs (Murata and Okamura, 2007). Moreover, it was shown by Wehr that, once split, TEVp halves do not assemble except in the presence of an external force pulling them together (Wehr et al., 2006).

As the first hypothesis can still hold, the results from LOTEV1 localization experiments (Fig.3.6) and the reasoning shown in Fig3.21 suggest that LOTEV1 did not reach the cellular membrane in *HeLa* cells, therefore the two protease halves could assemble independently from the membrane potential.

3.3.3 LOTEV activity upon cell depolarization

Cell chemical depolarization had the effect of shrinking the cells, therefore biasing the analysis. While one hypothesis is that the osmolarity of the buffers was not the same, even if it had always been checked, another hypothesis is that the depolarization was higher than expected and it was leading to cell apoptosis. In fact, the estimation of +50 mV depolarization with 70 mM KCl came from a calibration curve of di-8-ANEPPS that was performed on a different type of cell line and in the different conditions of a patch clamp. A better choice would have been to calibrate di-8-ANEPPS on *HeLa* cells and in conditions similar to the chemical depolarization settings.

Patch clamp stimulation solved the problem with chemical depolarization and provided a way to precisely control cell membrane potential changes. The results from

patch clamp experiments suggest that LOTEV2 construct is the best performing LOTEV protein out of all the variants created. In particular, upon +60 mV stimulus, Cherry-Q NCR increased significantly more than the reporter alone, suggesting an increase of proteolytic activity was happening. Moreover, the greater increase of Cherry-Q NCR compared also to the voltage-insensitive LOTEV2(D129R) suggest that the proteolytic activity increase is due to the VSD conformational changes.
LOTEV2 variants 1a2a and 1a2AP2 showed that the efficiency of the MATE decreased when the linkers were shortened. It was already known that the linker connecting the VSD with the original phosphatase in Ci-VSP was critical for the VSP functionality (Hobiger et al., 2012). In the case of LOTEV2, it is confirmed that the linker length and composition are critical for the correct coupling of the protease halves.

3.3.4 Issues encountered and Further Analysis

Several failed attempts of experimental design were not presented in the present document. In particular:

- expression of LOTEV and LOTEV reporters from the same bicistronic plasmid. Since the reporter showed cleavage at resting potential, the reporter and LOTEV constructs were separated on different plasmids to be able to tune the ratio of transfect plasmid to better control expression ratio;
- creation of bicistronic plasmids with a different fluorescent protein in place of the final YFP-3NLS. Creating P2A_mCherry led to DNA misfolding, P2A_ECFP could not be well measured by the microscope filter set;
- creation of an Arduino-based pumping system to better liquid substitution during chemical depolarization experiments. It was successfully obtained but successively abandoned.

Given the limited time available, several more experiments were planned but not carried out. In particular:

- expression and test of the constructs in *HEK293* cells where the localization experiments showed a higher membrane-specificity of LOTEVs;
- better characterization of LOTEV response to stimuli with different intensity, duration and frequency;
- characterization of re-usability of LOTEV after a single electrical stimulus;
- test of a reporter based on a protease-triggered release of a transcription factor from the membrane. Such a reporter would prove that LOTEV system can trigger gene expression with an electrical stimulus.

3.4 Conclusions

The development of an electrogenetic system based on the voltage-sensitive conformational changes of a transmembrane domain is a critical step to achieve a fast connection between biology and electricity.

Following the MATE idea conceptualized in Sec.1.5.4, in this chapter I presented the development of the first MATE: the voltage-sensitive TEV protease "LOTEV". The stages followed for the development of LOTEV are summarized in Fig.3.22. After testing two different VSD-protease coupling orientation and different linker

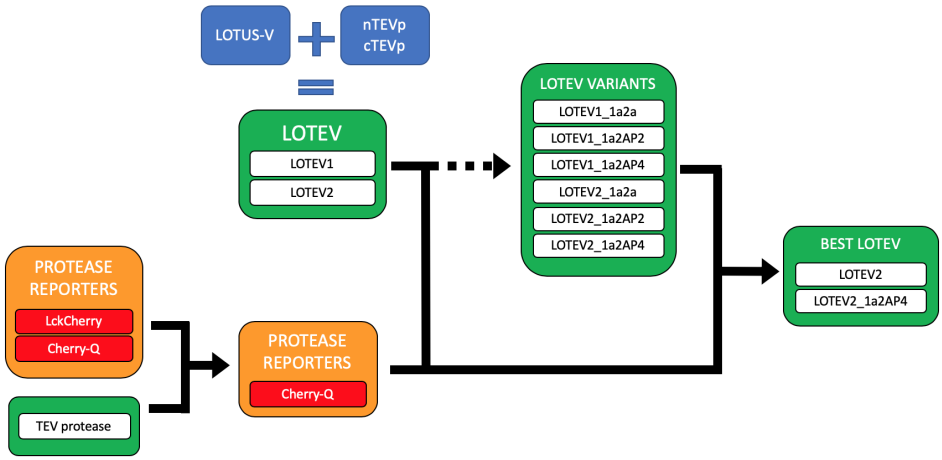

FIGURE 3.22: Overview of the LOTEV development path.

lengths, LOTEV2 constructs showed to be the best MATE developed so far. In

particular, when the cell is provided a +60 mV stimulus, LOTEV2 increases its proteolytic activity by +8.6% after 1 minute.

To conclude, protease-based systems are not the only option suitable for MATE concept. Even if a TEV protease was chosen for its high characterization, its very specific target and the orthogonality to the mammalian chassis, protease activity is not reversible. In fact, after the target peptide is cleaved by LOTEV, the electrically-induced system can be used again only after a novel, uncleaved, target is expressed again. The need of such a "recovery time" can constitute a limit in the usability of LOTEV, for instance in settings where a more frequent electro-biological crosstalk is wanted.

Thus, it can be valuable to explore other enzymes to make voltage sensitive through the use of a VSD, such as target-specific phosphatases, kinases or transcription factors. In particular, the expansion of the MATE family with orthogonal voltage-sensitive phosphatases and kinases could lead the way to a precise and reversible control of a variety of cellular processes.

4 General Discussion

In Chapter 1 it was presented the Voltage Sensitive Domain of the Voltage Sensitive Phosphatase. In particular, its unique characteristic of modularity was described, together with its past uses in fluorescent proteins.
Throughout this thesis, I presented the efforts to extend the uses of the voltage-sensitive conformational changes:

- from mammalian cells to prokaryotic cells (Chapter 2);
- from reporters to actuators (Chapter 3).

The prokaryotic expression of a mammalian membrane protein proved to be particularly complicated given the very different environments and cell membrane composition. However, the construct PAPS-Gt showed a fluorescence change of -6.3% in the microscope and -13% in the flow cytometer upon +50 mV of estimated chemical depolarization.
As the localization of the VSD was not specific to the prokaryotic membrane, it is suggested that its eukaryotic origin was not fit for the microbial membrane. A genome-wide search in every prokaryote for a membrane domain homologous to the eukaryotic VSP's VSD could have provided a better VSD candidate than the Ci-VSD. Finding a microbial membrane domain that undergoes conformational changes and that it is independent from other linked domains would be an important step towards the development of better prokaryotic GEVIs.

On the other hand, the novel concept of a voltage-sensitive enzyme for mammalian cells led to the development of LOTEV, a TEV protease that increases its activity

by +8.6% upon +60 mV stimulation.

It was shown that the length of the linkers connecting the VSD to the TEVp halves is critical for the TEVp activation upon cell depolarization. A more high-throughput search for the linkers optimizing the functionality of LOTEV could lead to larger activation of the protease. Computational protein design could restrict the search space by simulating the minimal distance needed between nTEVp and cTEVp to have an assembled active site and excluding linkers that would not allow such distance.

Further improvements of LOTEV, or more in general a MATE system, could in future lead to several applications such as:

- Enhancement of bioelectronic devices: electrogenetics could be the perfect complement to enhance bioelectronic devices and create stabilizing feedback-loops between the biological and the electronic world. For instance, the tattoo-based glycemic sensor (Bandodkar et al., 2015) could measure the interstitial glucose and, if needed, electrically stimulate release of insulin in the body through MATE-engineered cells.

  Goding et al. functionalised electrodes with conductive hydrogel to incorporate neural cells on the surface and improve prosthetic implants (Goding et al., 2019). Engineering these neurons with MATE would allow drug production and release in the body and solve the current challenges of drug delivery.

  Inspired by Mimee's work on ingestible bacterial-electronic system to detect gastrointestinal biomarkers (Mimee et al., 2018), cells in an ingested device can be MATE-engineered in order to control the release of a compound with a wireless external system.

- As an alternative induction system for industrial biomass production and research experiments: constitutive gene expression generates a metabolic burden on the energy sources of an engineered cell, leading to an overall lower yield of protein production. For this reason, regulated inducing systems are

used for industrial biomass production (Valdez-Cruz et al., 2010). Biochemical inducers are costly and require particular conditions (Donovan, Robinson, and Click, 1996). Electrogenetics would present an advantage over optogenetic, magnetogenetics and sonogenetics, by requiring an easier equipment implementation and a more energy-efficient approach.

- Creation of tissues with spatial gene-expression patterns: With the advent of nanopillar technology (Xie et al., 2012) it will be possible to change cell membrane potential precisely without the invasiveness of patch clamp, making the cell sit and integrate on a board of metallic pins interfaced with electronics. The ability to create sophisticated electric spatial patterns would be translated by MATE-engineered cells into spatial patterns of activated cellular processes. This technology should prove useful for the design of genetically-programmable organ-on-a-chip systems. A tissue of spatially-programmable cells would allow to test different biological situations for drug testing with a click. For future purposes of synthetic biology, linking such electronic board interface with grow factor expression could be used to drive tissue or organism growth in customized spatial directions.
- As a complement to optogenetics: since optogenetics links a light stimulus to membrane potential shift and electrogenetics couples a membrane potential shift with a customizable cellular process, expressing both a rhodopsin protein and the novel voltage-sensitive system in a cell would potentially trigger the target cellular process with light stimulus, enhancing optogenetics with novel functionalities.
- As a reporter for membrane potential monitoring *in vivo*. Currently, every membrane potential probe uses fluorescence or luminescence as measurable output. The novel electrogenetic system would be able to link membrane potential level with a cellular process. This ability gives the option of reporting the membrane potential change with a variety of substance production such as cell pigmentation. By providing the electrogenetic protein for example with

viral vectors, this capability can be useful for future applications of monitoring abnormal membrane potential behaviour of particular cells *in vivo*, avoiding the use of professional equipment to image fluorescent reporters.

- Development of condition-triggered gene circuits inside excitable cells. Appropriate calibration of the electrogenetic protein in excitable cells could potentially link abnormal activity of excitable cells to in-cell release of therapeutic proteins. Whenever neurons or myocardiac cells present an unnatural firing that represent a symptomatic condition, the electrogenetic system would act as a feedback system to act immediately and treat the cell.
- Gene therapy for cancer cells: Different studies showed how cancer development is linked to ion channel activity. In particular, it has been shown that cancer cells have a depolarized membrane which favours cancer progression (Yang and Brackenbury, 2013). Delivering a plasmid with a depolarization-triggered electrogenetic system and a gene circuit producing a drug upon activation from the electrogenetic system would make the drug active only in depolarized cells. This solution could represent a potential application for cancer treatment that bypasses the problem of targeting cancer receptors – which are highly variable in tumorous cells – by targeting the common characteristic of membrane depolarization.

An appropriate calibration of stimuli's magnitude, duration and frequency will allow tightly integrated electro-biological technologies. In fact, membrane potential is involved in many cellular processes and it is important that the electric signal triggering the electrogenetic system does not interfere with vital biological pathways. At the same time, the novel electrogenetic system, based on voltage-sensitive conformational changes, will have to be calibrated to respond to the external stimulus. A one-to-one relationship will have to be established between the external stimulus and the engineered cellular response.

Both PAPS and LOTEV suggest that further exploration of Ci-VSD can originate

novel technologies at the interface between electricity and biology. It has been shown how membrane potential regulation is critical for both prokaryotes and mammalian cells; now it is important to understand it fully and exploit such interface for novel uses in synthetic biology. We hope that this work can be of inspiration for future generations of researchers on cell electrophysiology and bioelectronics.

Bibliography

Anikeeva, Polina and Alan Jasanoff (2016). “Physical limits to magnetogenetics”. In: *eLife* 5.AUGUST, pp. 3–5. ISSN: 2050084X. DOI: 10.7554/eLife.17210.

Arter, Jessica A et al. (2010). “Virus-PEDOT Nanowires for Biosensing”. In: pp. 4858–4862. DOI: 10.1021/nl1025826.

Bai, Peng et al. (2019). “A fully human transgene switch to regulate therapeutic protein production by cooling sensation”. In: *Nature Medicine*. ISSN: 1546170X. DOI: 10.1038/s41591-019-0501-8. URL: http://dx.doi.org/10.1038/s41591-019-0501-8.

Baker, B. J. et al. (2007). “Three fluorescent protein voltage sensors exhibit low plasma membrane expression in mammalian cells”. In: *Journal of Neuroscience Methods* 161.1, pp. 32–38. ISSN: 01650270. DOI: 10.1016/j.jneumeth.2006.10.005.

Bandodkar, Amay J. et al. (2015). “Tattoo-based noninvasive glucose monitoring: A proof-of-concept study”. In: *Analytical Chemistry* 87.1, pp. 394–398. ISSN: 15206882. DOI: 10.1021/ac504300n.

Barnett, L et al. (2012). “A Fluorescent, Genetically-Encoded Voltage Probe Capable of Resolving Action Potentials”. In: *PLoS One*. DOI: 10.1371/journal.pone.0043454.g00110.1371/journal.pone.0043454.g002.

Baron, S (1996). “Medical Microbiology ? Chapter 27: Pseudomonas Galveston (4th Edition) ”. In:

Barton, Scott Calabrese, Josh Gallaway, and Plamen Atanassov (2004). “Enzymatic biofuel cells for implantable and microscale devices”. In: *Chemical Reviews* 104.10, pp. 4867–4886. ISSN: 00092665. DOI: 10.1021/cr020719k.

Benediktsson, Adrienne M. et al. (2005). "Ballistic labeling and dynamic imaging of astrocytes in organotypic hippocampal slice cultures". In: *Journal of Neuroscience Methods* 141.1, pp. 41–53. ISSN: 01650270. DOI: 10.1016/j.jneumeth.2004.05.013.

Bernaudat, F et al. (2011). "Heterologous expression of membrane proteins: choosing the appropriate host". In: *PLoS One* 6.12, e29191. DOI: 10.1371/journal.pone.0029191. URL: http://www.ncbi.nlm.nih.gov/pubmed/22216205.

Bezanilla, Francisco (2008). "How membrane proteins sense voltage". In: *Nature Reviews Molecular Cell Biology* 9.4, pp. 323–332. ISSN: 14710072. DOI: 10.1038/nrm2376.

Blackiston, Douglas J., Kelly A. McLaughlin, and Michael Levin (2009). "Bioelectric controls of cell proliferation: Ion channels, membrane voltage and the cell cycle". In: *Cell Cycle* 8.21, pp. 3527–3536. ISSN: 15514005. DOI: 10.4161/cc.8.21.9888. arXiv: NIHMS150003.

Bojar, Daniel et al. (2018). "Caffeine-inducible gene switches controlling experimental diabetes". In: *Nature Communications* 9.1. ISSN: 20411723. DOI: 10.1038/s41467-018-04744-1. URL: http://dx.doi.org/10.1038/s41467-018-04744-1.

Boyden, Edward S. et al. (2005). "Millisecond-timescale, genetically targeted optical control of neural activity". In: *Nature Neuroscience* 8.9, pp. 1263–1268. ISSN: 10976256. DOI: 10.1038/nn1525. arXiv: 9809069v1 [arXiv:gr-qc].

Breibeck, Joscha and Arne Skerra (2018). "The polypeptide biophysics of proline/alanine-rich sequences (PAS): Recombinant biopolymers with PEG-like properties". In: *Biopolymers* 109.1, pp. 1–12. ISSN: 10970282. DOI: 10.1002/bip.23069.

Cabantous, Stéphanie, Thomas C. Terwilliger, and Geoffrey S. Waldo (2005). "Protein tagging and detection with engineered self-assembling fragments of green fluorescent protein". In: *Nature Biotechnology* 23.1, pp. 102–107. ISSN: 10870156. DOI: 10.1038/nbt1044.

Chen, L.B. (1988). "Mitochondrial membrane potential in living cells". In: *Annual Review of Cell Biology* 4, pp. 155–81.

Chernet, Brook T. and Michael Levin (2013). "Transmembrane voltage potential is an essential cellular parameter for the detection and control of tumor development in a Xenopus model". In: *DMM Disease Models and Mechanisms* 6.3, pp. 595–607. ISSN: 17548403. DOI: 10.1242/dmm.010835.

Chifflet, Silvia, Julio A. Hernández, and Silvina Grasso (2005). "A possible role for membrane depolarization in epithelial wound healing". In: *American Journal of Physiology - Cell Physiology* 288.6 57-6, pp. 1420–1430. ISSN: 03636143. DOI: 10.1152/ajpcell.00259.2004.

Choi, Yongki and Gregory A Weiss (2012). "Single-Molecule Lysozyme Dynamics". In: 319. DOI: 10.1126/science.1214824.

Clegg, Robert M. (1992). "Fluorescence resonance energy transfer and nucleic acids". In: *Methods in Enzymology* 211.C, pp. 353–388. ISSN: 15577988. DOI: 10.1016/0076-6879(92)11020-J.

Clement, Marc, Gwenaelle Daniel, and Mario Trelles (2005). "Optimising the design of a broad-band light source for the treatment of skin". In: *Journal of Cosmetic and Laser Therapy* 7.3-4, pp. 177–189. ISSN: 1462883X. DOI: 10.1080/14764170500344575.

Collier, Joel H and Milan Mrksich (2006). "Engineering a biospecific communication pathway between cells and electrodes". In: 2005, pp. 5–9.

Cone, Clarence D. (1971). "the Role of the Surface Electrical Transmembrane Potential in Normal and Malignant Mitogenesis". In: *Annals of the New York Academy of Sciences* 238.1, pp. 420–435. ISSN: 17496632. DOI: 10.1111/j.1749-6632.1974.tb26808.x.

Cracknell, James A., Kylie A. Vincent, and Fraser A. Armstrong (2008). "Enzymes as working or inspirational electrocatalysts for fuel cells and electrolysis". In: *Chemical Reviews* 108.7, pp. 2439–2461. ISSN: 00092665. DOI: 10.1021/cr0680639.

Cundall R; Davies, A; Morris P; Williams J (1981). “Factors influencing the Photosensitivity Properties and ?Photoluminesence of Thioflavin T”. In:

Davies, Angela M., Uri Weinberg, and Yoram Palti (2013). “Tumor treating fields: A new frontier in cancer therapy”. In: *Annals of the New York Academy of Sciences* 1291.1, pp. 86–95. ISSN: 17496632. DOI: 10.1111/nyas.12112.

Deckers, Roel et al. (2009). “Image-guided, noninvasive, spatiotemporal control of gene expression”. In: *Proceedings of the National Academy of Sciences of the United States of America* 106.4, pp. 1175–1180. ISSN: 00278424. DOI: 10.1073/pnas.0806936106.

DiFranco, Marino, Marbella Quinonez, and Julio L. Vergara (2012). “The delayed rectifier potassium conductance in the sarcolemma and the transverse tubular system membranes of mammalian skeletal muscle fibers”. In: *The Journal of General Physiology* 140.2, pp. 109–137. ISSN: 0022-1295. DOI: 10.1085/jgp.201210802.

Dimitrov, D et al. (2007). “Engineering and Characterization of an Enhanced Fluorescent Protein Voltage Sensor”. In: *PLoS One*. DOI: 10.1371/journal.pone.0000440.g00110.1371/journal.pone.0000440.g00210.1371/journal.pone.0000440.t001.

Diss, J. K.J. et al. (2005). “A potential novel marker for human prostate cancer: Voltage-gated sodium channel expression in vivo”. In: *Prostate Cancer and Prostatic Diseases* 8.3, pp. 266–273. ISSN: 13657852. DOI: 10.1038/sj.pcan.4500796.

Djamgoz, Mustafa et al. (2001). “Directional movement of rat prostate cancer cells in direct-current electric field”. In: *Journal of Cell Science* 114, pp. 2697–2705. ISSN: 1477-9137.

Donovan, R. S., C. W. Robinson, and B. R. Click (1996). “Review: Optimizing inducer and culture conditions for expression of foreign proteins under the control of the lac promoter”. In: *Journal of Industrial Microbiology* 16.3, pp. 145–154. ISSN: 01694146. DOI: 10.1007/BF01569997.

Elsliger, Marc André et al. (1999). "Structural and spectral response of green fluorescent protein variants to changes in pH". In: *Biochemistry* 38.17, pp. 5296–5301. ISSN: 00062960. DOI: 10.1021/bi9902182.

Fraser, Scott P. et al. (2005). "Voltage-gated sodium channel expression and potentiation of human breast cancer metastasis". In: *Clinical Cancer Research* 11.15, pp. 5381–5389. ISSN: 10780432. DOI: 10.1158/1078-0432.CCR-05-0327.

Friedrich, Carol L. et al. (2000). "Antibacterial action of structurally diverse cationic peptides on gram- positive bacteria". In: *Antimicrobial Agents and Chemotherapy* 44.8, pp. 2086–2092. DOI: 10.1128/AAC.44.8.2086-2092.2000.

Garcia, Paulo A., Rafael V. Davalos, and Damijan Miklavcic (2014). "A numerical investigation of the electric and thermal cell kill distributions in electroporation-based therapies in tissue". In: *PLoS ONE* 9.8. ISSN: 19326203. DOI: 10.1371/journal.pone.0103083.

Gášková, D. et al. (1999). "Factors and processes involved in membrane potential build-up in yeast: diS-C3(3) assay". In: *International Journal of Biochemistry and Cell Biology* 31.5, pp. 575–584. ISSN: 13572725. DOI: 10.1016/S1357-2725(99)00002-3.

Gautam, S G et al. (2009). "Exploration of fluorescent protein voltage probes based on circularly permuted fluorescent proteins". In: *Front Neuroeng* 2, p. 14. DOI: 10.3389/neuro.16.014.2009. URL: http://www.ncbi.nlm.nih.gov/pubmed/19862342.

Gibson, Daniel G. et al. (2009). "Enzymatic assembly of DNA molecules up to several hundred kilobases". In: *Nature Methods* 6.5, pp. 343–345. ISSN: 15487091. DOI: 10.1038/nmeth.1318.

Goding, Josef et al. (2019). "A living electrode construct for incorporation of cells into bionic devices". In: 7.3, pp. 487–495. DOI: 10.1557/mrc.2017.44.

Goldman, David E. (1943). "Potential, impedance, and rectification in membranes". In: *Journal of General Physiology* 27.1, pp. 37–60. ISSN: 15407748. DOI: 10.1085/jgp.27.1.37.

Gomes, A R (2016). "An Overview of Heterologous Expression Host Systems for the Production of Recombinant Proteins et al". In: 4.4, pp. 346–356. ISSN: 1588292622. DOI: 10.1016/j.revmic.2007.02.006.

Green, Alexander A. et al. (2017). "Complex cellular logic computation using ribocomputing devices". In: *Nature* 548.7665, pp. 117–121. ISSN: 14764687. DOI: 10.1038/nature23271. URL: http://dx.doi.org/10.1038/nature23271.

Guilhon, E. et al. (2003). "Spatial and temporal control of transgene expression in vivo using a heat-sensitive promoter and MRI-guided focused ultrasound". In: *Journal of Gene Medicine* 5.4, pp. 333–342. ISSN: 1099498X. DOI: 10.1002/jgm.345.

Hall, Mary P. et al. (2012). "Engineered luciferase reporter from a deep sea shrimp utilizing a novel imidazopyrazinone substrate". In: *ACS Chemical Biology* 7.11, pp. 1848–1857. ISSN: 15548929. DOI: 10.1021/cb3002478.

Heijne, G von (2006). "Membrane-protein topology". In: *Nat Rev Mol Cell Biol* 7.12, pp. 909–918. DOI: 10.1038/nrm2063. URL: http://www.ncbi.nlm.nih.gov/pubmed/17139331.

Hitoshi, Niwa, Yamamura Ken-ichi, and Miyazaki Jun-ichi (1991). "Efficient selection for high-expression transfectants with a novel eukaryotic vector". In: *Gene* 108.2, pp. 193–199. ISSN: 03781119. DOI: 10.1016/0378-1119(91)90434-D.

Hobiger, K et al. (2012). "Coupling of Ci-VSP modules requires a combination of structure and electrostatics within the linker". In: *Biophys J* 102.6, pp. 1313–1322. DOI: 10.1016/j.bpj.2012.02.027. URL: http://www.ncbi.nlm.nih.gov/pubmed/22455914.

Hodgkin, A L and P Horowicz (1960). "THE EFFECT OF SUDDEN CHANGES IN IONIC CONCENTRATIONS ON THE MEMBRANE POTENTIAL OF SINGLE MUSCLE FIBERS". In: pp. 370–385.

Hosoi, S H I G E R U, N O R I K O Mochizuki, and Michiki Kasai (1980). "<Hosoi et al., 1980 (pH & Em).PDF>". In: 600, pp. 844–852.

Huang, Heng et al. (2010). "Remote control of ion channels and neurons through magnetic-field heating of nanoparticles". In: *Nature Nanotechnology* 5.8, pp. 602–606. ISSN: 17483395. DOI: 10.1038/nnano.2010.125.

Huckstepp, Robert T.R. et al. (2010). "Connexin hemichannel-mediated CO2-dependent release of ATP in the medulla oblongata contributes to central respiratory chemosensitivity". In: *Journal of Physiology* 588.20, pp. 3901–3920. DOI: 10.1113/jphysiol.2010.192088.

Humphries, Jacqueline et al. (2017). "Species-Independent Attraction to Biofilms through Electrical Signaling". In: *Cell* 168.1-2, 200–209.e12. ISSN: 10974172. DOI: 10.1016/j.cell.2016.12.014.

Ibsen, Stuart et al. (2015). "Sonogenetics is a non-invasive approach to activating neurons in Caenorhabditis elegans". In: *Nature Communications* 6, pp. 1–12. DOI: 10.1038/ncomms9264. URL: http://dx.doi.org/10.1038/ncomms9264.

Idevall-Hagren, Olof et al. (2012). "Optogenetic control of phosphoinositide metabolism". In: *Proceedings of the National Academy of Sciences of the United States of America* 109.35. ISSN: 00278424. DOI: 10.1073/pnas.1211305109.

Inagaki, S et al. (2017). "Genetically encoded bioluminescent voltage indicator for multi-purpose use in wide range of bioimaging". In: *Sci Rep* 7, p. 42398. DOI: 10.1038/srep42398. URL: http://www.ncbi.nlm.nih.gov/pubmed/28205521.

Jarmer, H et al. (2001). "Transcriptome analysis documents induced competence of B subtilis during nitrogen limiting conditions". In: *FEMS Microbiol Lett*.

Jeerapan, Itthipon et al. (2016). "Stretchable biofuel cells as wearable textile-based self-powered sensors". In: *Journal of Materials Chemistry A* 4.47, pp. 18342–18353. ISSN: 20507496. DOI: 10.1039/C6TA08358G. URL: http://dx.doi.org/10.1039/C6TA08358G.

Jin, L et al. (2012). "Single action potentials and subthreshold electrical events imaged in neurons with a fluorescent protein voltage probe". In: *Neuron* 75.5, pp. 779–785. DOI: 10.1016/j.neuron.2012.06.040. URL: http://www.ncbi.nlm.nih.gov/pubmed/22958819.

Kang, Seung Kyun et al. (2016). "Bioresorbable silicon electronic sensors for the brain". In: *Nature* 530.7588, pp. 71–76. ISSN: 14764687. DOI: 10.1038/nature16492. URL: http://dx.doi.org/10.1038/nature16492.

Kapust, R B et al. (2001). "Tobacco etch virus protease: mechanism of autolysis and rational design of stable mutants with wild-type catalytic proficiency". In: *Protein Engineering*.

Khow, Orawan and Sunutcha Suntrarachun (2012). "Strategies for production of active eukaryotic proteins in bacterial expression system". In: *Asian Pacific Journal of Tropical Biomedicine* 2.2, pp. 159–162. ISSN: 22211691. DOI: 10.1016/S2221-1691(11)60213-X.

Kim, J H et al. (2011). "High cleavage efficiency of a 2A peptide derived from porcine teschovirus-1 in human cell lines, zebrafish and mice". In: *PLoS One* 6.4, e18556. DOI: 10.1371/journal.pone.0018556. URL: http://www.ncbi.nlm.nih.gov/pubmed/21602908.

Kim, Jayoung et al. (2018). "Wearable Bioelectronics: Enzyme-Based Body-Worn Electronic Devices". In: *Accounts of Chemical Research* 51.11, pp. 2820–2828. ISSN: 15204898. DOI: 10.1021/acs.accounts.8b00451.

Klinkert, Birgit et al. (2012). "Thermogenetic tools to monitor temperature-dependent gene expression in bacteria". In: *Journal of Biotechnology* 160.1-2, pp. 55–63. ISSN: 01681656. DOI: 10.1016/j.jbiotec.2012.01.007. URL: http://dx.doi.org/10.1016/j.jbiotec.2012.01.007.

Konermann, S et al. (2009). "Optical Control of Mammalian Endogenous Transcription and Epigenetic States". In: 5.6, pp. 1–8. DOI: 10.4172/2157-7633.1000305.Improved.

Koo, Jahyun et al. (2018). "Wireless bioresorbable electronic system enables sustained nonpharmacological neuroregenerative therapy". In: *Nature Medicine* 24.12, pp. 1830–1836. ISSN: 1546170X. DOI: 10.1038/s41591-018-0196-2. URL: http://dx.doi.org/10.1038/s41591-018-0196-2.

Kozak, M. (1989). "The scanning model for translation: An update". In: *Journal of Cell Biology* 108.2, pp. 229–241. ISSN: 00219525. DOI: 10.1083/jcb.108.2.229.

Kralj, J M et al. (2011). "Electrical spiking in Escherichia coli probed with a fluorescent voltage-indicating protein". In: *Science* 333.6040, pp. 345–348. DOI: 10.1126/science.1204763. URL: http://www.ncbi.nlm.nih.gov/pubmed/21764748.

Kuchina, Anna et al. (2011). "Reversible and noisy progression towards a commitment point enables adaptable and reliable cellular Decision-Making". In: *PLoS Computational Biology* 7.11. ISSN: 1553734X. DOI: 10.1371/journal.pcbi.1002273.

Kuhlman, Sandra J. and Douglas G. McMahon (2004). "Rhythmic regulation of membrane potential and potassium current persists in SCN neurons in the absence of environmental input". In: *European Journal of Neuroscience* 20.4, pp. 1113–1117. ISSN: 0953816X. DOI: 10.1111/j.1460-9568.2004.03555.x.

Lavine (1972). "Electric Enhancement of Bone Healing". In: *Science*.

Levin, Michael (2007). "Large-scale biophysics: ion flows and regeneration". In: *Trends in Cell Biology* 17.6, pp. 261–270. ISSN: 09628924. DOI: 10.1016/j.tcb.2007.04.007.

– (2014). "Reprogramming cells and tissue patterning via bioelectrical pathways : Molecular Mechanisms and Biomedical Opportunities". In: 5.6, pp. 657–676. DOI: 10.1002/wsbm.1236.Reprogramming.

Levin, Michael et al. (2002). "Asymmetries in H+/K+-ATPase and cell membrane potentials comprise a very early step in left-right patterning". In: *Cell* 111.1, pp. 77–89. ISSN: 00928674. DOI: 10.1016/S0092-8674(02)00939-X.

Lewis, Rebecca et al. (2011). "The role of the membrane potential in chondrocyte volume regulation". In: *Journal of Cellular Physiology* 226.11, pp. 2979–2986. ISSN: 00219541. DOI: 10.1002/jcp.22646.

Li, Q et al. (2014). "Structural mechanism of voltage-dependent gating in an isolated voltage-sensing domain". In: *Nat Struct Mol Biol* 21.3, pp. 244–252. DOI: 10.1038/nsmb.2768. URL: http://www.ncbi.nlm.nih.gov/pubmed/24487958.

Lister, Philip D., Daniel J. Wolter, and Nancy D. Hanson (2009). "Antibacterial-resistant Pseudomonas aeruginosa: Clinical impact and complex regulation of chromosomally encoded resistance mechanisms". In: *Clinical Microbiology Reviews* 22.4, pp. 582–610. ISSN: 08938512. DOI: 10.1128/CMR.00040-09.

Liu, Jingyu; et al. (2008). "Electro-chemical coupling in the voltage-dependent phosphatase Ci-VSP". In: *Proc IEEE Int Conf Acoust Speech Signal Process* 6.10.1109/ICASSP, pp. 449–452. ISSN: 1552-4469. DOI: 10.1038/nchembio.349.Electro-chemical. arXiv: NIHMS150003.

Liu, Yi et al. (2017). "Electrochemistry for bio-device molecular communication: The potential to characterize, analyze and actuate biological systems". In: *Nano Communication Networks* 11, pp. 76–89. ISSN: 18787789. DOI: 10.1016/j.nancom.2017.01.002. URL: http://dx.doi.org/10.1016/j.nancom.2017.01.002.

Lo, W C et al. (2012). "CPred: a web server for predicting viable circular permutations in proteins". In: *Nucleic Acids Res* 40.Web Server issue, W232–7. DOI: 10.1093/nar/gks529. URL: http://www.ncbi.nlm.nih.gov/pubmed/22693212.

Lobo, Daniel, Wendy S. Beane, and Michael Levin (2012). "Modeling planarian regeneration: A primer for reverse-engineering the worm". In: *PLoS Computational Biology* 8.4. ISSN: 1553734X. DOI: 10.1371/journal.pcbi.1002481.

Lungu, Oana I. et al. (2012). "Designing Photoswitchable Peptides Using the AsLOV2 Domain". In: *Chemistry and Biology* 19.4, pp. 507–517. ISSN:

10745521. DOI: 10.1016/j.chembiol.2012.02.006. URL: http://dx.doi.org/10.1016/j.chembiol.2012.02.006.

Ma, Jiong et al. (2012). "Self-regulated viscous channel in the nuclear pore complex". In: *Proceedings of the National Academy of Sciences of the United States of America* 109.19, pp. 7326–7331. ISSN: 00278424. DOI: 10.1073/pnas.1201724109.

MacFarlane, Stacey Nee and Harald Sontheimer (2000). "Changes in ion channel expression accompany cell cycle progression of spinal cord astrocytes". In: *Glia* 30.1, pp. 39–48. ISSN: 08941491. DOI: 10.1002/(SICI)1098-1136(200003)30:1<39::AID-GLIA5>3.0.CO;2-S.

Mack, D. et al. (2006). "Biofilm formation in medical device-related infection". In: *International Journal of Artificial Organs* 29.4, pp. 343–359. ISSN: 03913988.

Madio, David P. et al. (1998). "On the feasibility of MRI-guided focused ultrasound for local induction of gene expression". In: *Journal of Magnetic Resonance Imaging* 8.1, pp. 101–104. ISSN: 10531807. DOI: 10.1002/jmri.1880080120.

Marbach, Anja and Katja Bettenbrock (2012). "Lac operon induction in Escherichia coli: Systematic comparison of IPTG and TMG induction and influence of the transacetylase LacA". In: *Journal of Biotechnology* 157.1, pp. 82–88. ISSN: 01681656. DOI: 10.1016/j.jbiotec.2011.10.009. URL: http://dx.doi.org/10.1016/j.jbiotec.2011.10.009.

Margolin, Y. and M. Eisenbach (1984). "Voltage clamp effects on bacterial chemotaxis". In: *Journal of Bacteriology* 159.2, pp. 605–610. ISSN: 00219193.

Marszalek, P, D S Liu, and T Y Tsong (1990). "Schwan equation and transmembrane potential induced by alternating electri field". In: *Bioph*.

Marszalek, Piotr (1990). "Schwan equation and transmembrane potential induced by". In: 58.October, pp. 1053–1058.

Mathews, A P (2019). "Electrical polarity in the hydroids". In: pp. 294–299.

Messenger, N. J. and A. E. Warner (2000). "Primary neuronal differentiation in Xenopus embryos is linked to the $\beta 3$ subunit of the sodium pump". In: *Developmental Biology* 220.2, pp. 168–182. ISSN: 00121606. DOI: 10.1006/dbio.2000.9646.

Mimee, Mark et al. (2018). "An ingestible bacterial-electronic system to monitor gastrointestinal health". In: 918.May, pp. 915–918.

Moreau, Christophe J et al. (2008). "Coupling ion channels to receptors for biomolecule sensing". In: 3.October, pp. 2–7. DOI: 10.1038/nnano.2008.242.

Murata, Yoshimichi and Y Okamura (2007). "Depolarization activates the phosphoinositide phosphatase Ci-VSP, as detected in Xenopus oocytes coexpressing sensors of PIP2". In: *J Physiol* 583.Pt 3, pp. 875–889. DOI: 10.1113/jphysiol.2007.134775. URL: http://www.ncbi.nlm.nih.gov/pubmed/17615106.

Murata, Yoshimichi et al. (2005). "Phosphoinositide phosphatase activity coupled to an intrinsic voltage sensor". In: *Nature* 435.7046, pp. 1239–1243. DOI: 10.1038/nature03650. URL: http://www.ncbi.nlm.nih.gov/pubmed/15902207.

Mycielska, Maria E. and Mustafa Djamgoz (2004). "Cellular mechanisms of direct-current electric field effects: Galvanotaxis and metastatic disease". In: *Journal of Cell Science* 117.9, pp. 1631–1639. ISSN: 00219533. DOI: 10.1242/jcs.01125.

Namdari, Mehrdad et al. (2017). "Recent advances in magnetoliposome for heart drug delivery". In: *Artificial Cells, Nanomedicine and Biotechnology* 45.6, pp. 1051–1057. ISSN: 2169141X. DOI: 10.1080/21691401.2017.1299159.

Newell, P. C. (1978). "Genetics of cellular communication during aggregation of Dictyostelium". In: *Birth Defects: Original Article Series* 14.2, pp. 507–526. ISSN: 05476844.

Nicholls, Samantha B. et al. (2011). "Mechanism of a genetically encoded dark-to-bright reporter for caspase activity". In: *Journal of Biological Chemistry* 286.28, pp. 24977–24986. ISSN: 00219258. DOI: 10.1074/jbc.M111.221648.

Noguchi, Takako et al. (2012). "Fibroblast circadian rhythms of PER2 expression depend on membrane potential and intracellular calcium". In: *Chronobiology*

International 29.6, pp. 653–664. ISSN: 07420528. DOI: 10.3109/07420528.2012.679330.

Nuccitelli, Richard (1988). "Physiological Electric Fields can Influence Cell Motility, Growth, and Polarity". In: *Advances in Molecular and Cell Biology* 2.C, pp. 213–233. ISSN: 15692558. DOI: 10.1016/S1569-2558(08)60435-X.

Paine, P L, L C Moore, and S B Horowitz (1975). "Nuclear envelope permeability". In: 1.

Palomares, L, S Estrada-Mondaca, and O Ramirez (1987). "Production of Recombinant Proteins". In: *Annals of the New York Academy of Sciences* 509.1, pp. 82–88. ISSN: 17496632. DOI: 10.1111/j.1749-6632.1987.tb30986.x.

Pan, Yijia et al. (2018). "Mechanogenetics for the remote and noninvasive control of cancer immunotherapy". In: *Proceedings of the National Academy of Sciences* 115.5, pp. 992–997. ISSN: 0027-8424. DOI: 10.1073/pnas.1714900115.

Pan, Yongchun et al. (2019). "Near-infrared upconversion–activated CRISPR-Cas9 system: A remote-controlled gene editing platform". In: *Science Advances* 5.4, eaav7199. ISSN: 2375-2548. DOI: 10.1126/sciadv.aav7199. URL: http://advances.sciencemag.org/lookup/doi/10.1126/sciadv.aav7199.

Patrick J. Macdonald, Yan Chen and Joachim D. Mueller (2013). "Chromophore maturation and fluorescence fluctuation spectroscopy". In: *Analytical Biochemistry* 421.1, pp. 291–298. DOI: 10.1016/j.ab.2011.10.040.Chromophore.

Pavšelj, Nataša and Damijan Miklavčič (2008). "Numerical modeling in electroporation-based biomedical applications". In: *Radiology and Oncology* 42.3, pp. 159–168. ISSN: 15813207. DOI: 10.2478/v10019-008-0008-2.

Pietak, Alexis et al. (2019). *Neural control of body-plan axis in regenerating planaria*. Vol. 15. 4, e1006904. ISBN: 1111111111. DOI: 10.1371/journal.pcbi.1006904.

Piraner, Dan I et al. (2016). "tunable thermal bioswitches for in vivo control of microbial therapeutics". In: *Nature Chemical Biology* November, pp. 1–8. ISSN:

1552-4450. DOI: 10.1038/nchembio.2233. URL: http://dx.doi.org/10.1038/nchembio.2233.

Platisa, Jelena et al. (2017). "Directed Evolution of Key Residues in Fluorescent Protein Inverses the Polarity of Voltage Sensitivity in the Genetically Encoded Indicator ArcLight". In: *ACS Chemical Neuroscience* 8.3, pp. 513–523. ISSN: 19487193. DOI: 10.1021/acschemneuro.6b00234.

Plotkin, Joshua B and Grzegorz Kudla (2011). "Synonymous but not the same". In: *National Review of Genetics* 12.1, pp. 32–42. DOI: 10.1038/nrg2899.Synonymous.

Prindle, A et al. (2015). "Ion channels enable electrical communication in bacterial communities". In: *Nature* 527.7576, pp. 59–63. DOI: 10.1038/nature15709. URL: http://www.ncbi.nlm.nih.gov/pubmed/26503040.

Ravikumar, Sambandam et al. (2015). "Engineering Escherichia coli to sense acidic amino acids by introduction of a chimeric two-component system". In: *Korean Journal of Chemical Engineering* 32.10, pp. 2073–2077. ISSN: 02561115. DOI: 10.1007/s11814-015-0024-z.

Reid, Brian and Min Zhao (2014). "The Electrical Response to Injury: Molecular Mechanisms and Wound Healing". In: *Advances in Wound Care* 3.2, pp. 184–201. ISSN: 2162-1918. DOI: 10.1089/wound.2013.0442.

Rocha, Paulo R.F. et al. (2015). "Low frequency electric current noise in glioma cell populations". In: *Journal of Materials Chemistry B* 3.25, pp. 5035–5039. ISSN: 2050750X. DOI: 10.1039/c5tb00144g.

Sacchetti, Andrea et al. (2001). "Green fluorescent protein variants fold differentially in prokaryotic and eukaryotic cells". In: *Journal of Cellular Biochemistry* 81, pp. 117–128. ISSN: 07302312. DOI: 10.1002/jcb.1091.

Sakai, R et al. (2001). "Design and characterization of a DNA-encoded, voltage-sensitive fluorescent protein". In: *European Journal of Neuroscience*.

Sakata, Souhei and Yasushi Okamura (2014). "Phosphatase activity of the voltage-sensing phosphatase, VSP, shows graded dependence on the extent of activation of the voltage sensor". In: *Journal of Physiology* 592.5, pp. 899–914. ISSN: 00223751. DOI: 10.1113/jphysiol.2013.263640.

Scaduto, Russell C. and Lee W. Grotyohann (1999). "Measurement of mitochondrial membrane potential using fluorescent rhodamine derivatives". In: *Biophysical Journal* 76.1 I, pp. 469–477. ISSN: 00063495. DOI: 10.1016/S0006-3495(99)77214-0.

Selvamani, Vidhya et al. (2017). "Engineering chimeric two-component system into Escherichia coli from Paracoccus denitrificans to sense methanol". In: *Biotechnology and Bioprocess Engineering* 22.3, pp. 225–230. ISSN: 19763816. DOI: 10.1007/s12257-016-0484-y.

Seo, Daeha et al. (2016). "A mechanogenetic toolkit for interrogating cell signaling in space and time". In: *Cell* 165.6, pp. 1507–1518. ISSN: 10974172. DOI: 10.1016/j.cell.2016.04.045. URL: http://dx.doi.org/10.1016/j.cell.2016.04.045.

Shaner, Nathan C., Paul A. Steinbach, and Roger Y. Tsien (2005). "A guide to choosing fluorescent proteins". In: *Nature Methods* 2.12, pp. 905–909. ISSN: 15487091. DOI: 10.1038/nmeth819.

Shimizu-Sato, Sae et al. (2002). "A light-switchable gene promoter system". In: *Nature Biotechnology* 20.10, pp. 1041–1044. ISSN: 10870156. DOI: 10.1038/nbt734.

Siegel, M S and E Y Isacoff (1997). "A Genetically Encoded Optical Probe of Membrane Potential". In: *Neuron*.

Sirec, Teja et al. (2019). "Electrical Polarization Enables Integrative Quality Control during Bacterial Differentiation into Spores". In: *iScience* 16, pp. 378–389. ISSN: 25890042. DOI: 10.1016/j.isci.2019.05.044. URL: https://doi.org/10.1016/j.isci.2019.05.044.

Smart, Ashley D. et al. (2017). "Engineering a light-activated caspase-3 for precise ablation of neurons in vivo". In: *Proceedings of the National Academy of Sciences of the United States of America* 114.39, E8174–E8183. ISSN: 10916490. DOI: 10.1073/pnas.1705064114.

Song, Yang, Jiapeng Wang, and Siu-tung Yau (2014). "Controlled glucose consumption in yeast using a transistor-like device". In: pp. 1–7. DOI: 10.1038/srep05429.

St-Pierre, F et al. (2014). "High-fidelty optical reporting of neuronalelectrical activity with an ultrafast fluorescent voltage sensor". In: *Nat Neurosci*.

Strahl, H. and L. W. Hamoen (2010). "Membrane potential is important for bacterial cell division". In: *Proceedings of the National Academy of Sciences* 107.27, pp. 12281–12286. ISSN: 0027-8424. DOI: 10.1073/pnas.1005485107. arXiv: arXiv:1408.1149. URL: http://www.pnas.org/cgi/doi/10.1073/pnas.1005485107.

Stratford, James P et al. (2019). "Electrically induced bacterial membrane-potential dynamics correspond to cellular proliferation capacity". In: *MICROBIOLOGY BIOPHYSICS AND COMPUTATIONAL BIOLOGY*. DOI: 10.1073/pnas.1901788116.

Strickland, Devin et al. (2012). "biology". In: 9.4, pp. 379–384. DOI: 10.1038/nmeth.1904.TULIPs.

Thomsen, Louiza Bohn, Maj Schneider Thomsen, and Torben Moos (2015). "Targeted drug delivery to the brain using magnetic nanoparticles". In: *Therapeutic Delivery* 6.10, pp. 1145–1155. ISSN: 20416008. DOI: 10.4155/tde.15.56.

Tschirhart, T et al. (2017). "Electronic control of gene expression and cell behaviour in Escherichia coli through redox signalling". In: *Nat Commun* 8, p. 14030. DOI: 10.1038/ncomms14030. URL: http://www.ncbi.nlm.nih.gov/pubmed/28094788.

Tschirhart, Tanya et al. (2016). "Electrochemical Measurement of the β-Galactosidase Reporter from Live Cells: A Comparison to the Miller Assay".

In: *ACS Synthetic Biology* 5.1, pp. 28–35. ISSN: 21615063. DOI: 10.1021/acssynbio.5b00073.

Tseng, Ai Sun et al. (2010). "Induction of vertebrate regeneration by a transient sodium current". In: *Journal of Neuroscience* 30.39, pp. 13192–13200. ISSN: 15292401. DOI: 10.1523/JNEUROSCI.3315-10.2010.

Tsong, T Y (1990). "Electrical Modulation of Membrane Proteins: Enforced Conformational Oscillations and Biological Energy and Signal Transductions". In: *Biophys J*.

Tsutsui, Hidekazu et al. (2013). "Optically detected structural change in the N-terminal region of the voltage-sensor domain". In: *Biophysical Journal* 105.1, pp. 108–115. ISSN: 00063495. DOI: 10.1016/j.bpj.2013.05.051. URL: http://dx.doi.org/10.1016/j.bpj.2013.05.051.

Valdez-Cruz, Norma A. et al. (2010). "Production of recombinant proteins in E. coli by the heat inducible expression system based on the phage lambda pL and/or pR promoters". In: *Microbial Cell Factories* 9, pp. 1–16. ISSN: 14752859. DOI: 10.1186/1475-2859-9-18.

Van Rosmalen, Martijn, Mike Krom, and Maarten Merkx (2017). "Tuning the Flexibility of Glycine-Serine Linkers to Allow Rational Design of Multidomain Proteins". In: *Biochemistry* 56.50, pp. 6565–6574. ISSN: 15204995. DOI: 10.1021/acs.biochem.7b00902.

Vandenberg, Laura N., Ryan D. Morrie, and Dany Spencer Adams (2011). "V-ATPase-dependent ectodermal voltage and Ph regionalization are required for craniofacial morphogenesis". In: *Developmental Dynamics* 240.8, pp. 1889–1904. ISSN: 10588388. DOI: 10.1002/dvdy.22685.

Villalba-Galea, C A (2012). "Voltage-Controlled Enzymes: The New JanusBifrons". In: *Front Pharmacol* 3, p. 161. DOI: 10.3389/fphar.2012.00161. URL: http://www.ncbi.nlm.nih.gov/pubmed/22993507.

Villaverde, Antonio et al. (1993). "Continuous Culture of Recombinant Escherichia coli". In: *Notes* 59.10, pp. 3485–3487.

Watson, Helen (2015). "Biological membranes". In: *Essays in Biochemistry* 59, pp. 43–70. ISSN: 00711365. DOI: 10.1042/BSE0590043.

Weaver, James C. (1993). "Electroporation: A general phenomenon for manipulating cells and tissues". In: *Journal of Cellular Biochemistry* 51.4, pp. 426–435. ISSN: 10974644. DOI: 10.1002/jcb.2400510407.

Weber, Wilfried et al. (2009). "A synthetic mammalian electro-genetic transcription circuit". In: *Nucleic Acids Res* 37.4, e33. DOI: 10.1093/nar/gkp014. URL: http://www.ncbi.nlm.nih.gov/pubmed/19190091.

Wehr, M C et al. (2006). "Monitoring regulated protein-protein interactions using split TEV". In: *Nat Methods* 3.12, pp. 985–993. DOI: 10.1038/nmeth967. URL: http://www.ncbi.nlm.nih.gov/pubmed/17072307.

Wheeler, Michael A et al. (2016). "Genetically targeted magnetic control of the nervous system_Supplementary information". In: *Nat Neurosci* advance on.2016, pp. 511–517. ISSN: 1546-1726. DOI: 10.1038/nn.4265. URL: http://dx.doi.org/10.1038/nn.4265{\%}5Cn10.1038/nn.4265{\%}5Cnhttp://www.nature.com/neuro/journal/vaop/ncurrent/abs/nn.4265.html{\#}supplementary-information.

Williamson, M P (1994). "The structure and function of proline-rich regions in proteins". In: *Biochemical Journal* 297.2, pp. 249–260. ISSN: 0264-6021. DOI: 10.1042/bj2970249. arXiv: sureshgovindarajan. URL: http://biochemj.org/lookup/doi/10.1042/bj2970249.

Winkel, J. Derk te et al. (2016). "Analysis of antimicrobial-triggered membrane depolarization using voltage sensitive dyes". In: *Frontiers in Cell and Developmental Biology* 4.APR, pp. 1–10. ISSN: 2296634X. DOI: 10.3389/fcell.2016.00029.

Wriggers, Willy, Sugoto Chakravarty, and Patricia A Jennings (2005). "Control of Protein Functional Dynamics by Peptide Linkers". In: 80.2005, pp. 736–746. DOI: 10.1002/bip.20291.

Xie, Chong et al. (2012). “Intracellular recording of action potentials by nanopillar electroporation”. In: *Nature Nanotechnology* 7.3, pp. 185–190. ISSN: 17483395. DOI: 10.1038/nnano.2012.8. URL: http://dx.doi.org/10.1038/nnano.2012.8.

Xiong, Xiaobing et al. (2015). “Remote spatiotemporally controlled and biologically selective permeabilization of blood-brain barrier”. In: *Journal of Controlled Release* 217, pp. 113–120. ISSN: 18734995. DOI: 10.1016/j.jconrel.2015.08.044. URL: http://dx.doi.org/10.1016/j.jconrel.2015.08.044.

Xu, Lizhi et al. (2014). “3D multifunctional integumentary membranes for spatiotemporal cardiac measurements and stimulation across the entire epicardium”. In: *Nature Communications* 5, pp. 1–10. ISSN: 20411723. DOI: 10.1038/ncomms4329. URL: http://dx.doi.org/10.1038/ncomms4329.

Yang, Ming and William J. Brackenbury (2013). “Membrane potential and cancer progression”. In: *Frontiers in Physiology* 4 JUL.July, pp. 1–10. ISSN: 1664042X. DOI: 10.3389/fphys.2013.00185.

Yang, Shou Jing et al. (2004). “Ultrastructural study of depolarization-induced translocation of NRF-2 transcription factor in cultured rat visual cortical neurons”. In: *European Journal of Neuroscience* 19.5, pp. 1153–1162. ISSN: 0953816X. DOI: 10.1111/j.1460-9568.2004.03250.x.

Zhao, Min et al. (2006). “Electrical signals control wound healing through phosphatidylinositol-3-OH kinase-γ and PTEN”. In: *Nature* 442.7101, pp. 457–460. ISSN: 14764687. DOI: 10.1038/nature04925.

Zhou, Ming et al. (2012). “A self-powered "sense-act-treat" system that is based on a biofuel cell and controlled by boolean logic”. In: *Angewandte Chemie - International Edition* 51.11, pp. 2686–2689. ISSN: 14337851. DOI: 10.1002/anie.201107068.

A Appendix

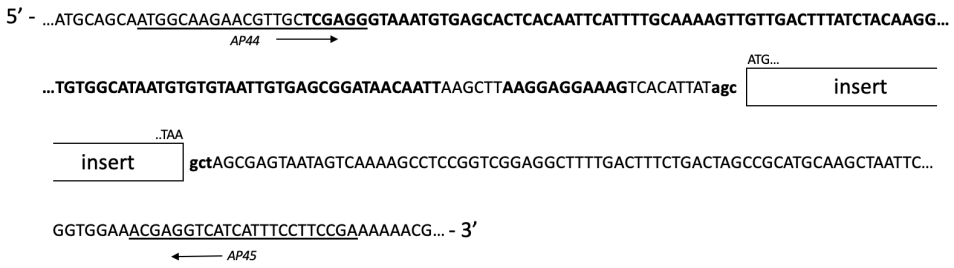

FIGURE A.1: Insert site in JDE131 plasmid. Upper case and bold: PHyperspank promoter; Ribosome Binding Site (RBS). Lower case and bold: restriction sites for AfeI, split on the two sides of the insert. Underlined: primers used for sequencing: AP44 and AP45. Every inserted gene began with "ATG" start codon and ended with "TAA" stop codon.

A.0.1 DNA Templates

Here are listed all the DNA sequences, from the 5'-end to the 3'-end.

A.0.2 JDE131 backbone

```
   1 GCTAGCGAGT AATAGTCAAA AGCCTCCGGT CGGAGGCTTT TGACTTTCTG
  51 ACTAGCCGCA TGCAAGCTAA TTCGGTGGAA ACGAGGTCAT CATTTCCTTC
 101 CGAAAAAACG GTTGCATTTA AATCTTACAT ATGTAATACT TTCAAAGACT
 151 ACATTTGTAA GATTTGATGT TTGAGTCGGC TGAAAGATCG TACGTACCAA
 201 TTATTGTTTC GTGATTGTTC AAGCCATAAC ACTGTAGGGA TAGTGGAAAG
 251 AGTGCTTCAT CTGGTTACGA TCAATCAAAT ATTCAAACGG AGGGAGACGA
 301 TTTTGATGAA ACCAGTAACG TTATACGATG TCGCAGAGTA TGCCGGTGTC
 351 TCTTATCAGA CCGTTTCCCG CGTGGTGAAC CAGGCCAGCC ACGTTTCTGC
 401 GAAAACGCGG GAAAAAGTGG AAGCGGCGAT GGCGGAGCTG AATTACATTC
```

```
 451 CCAACCGCGT GGCACAACAA CTGGCGGGCA AACAGTCGTT GCTGATTGGC
 501 GTTGCCACCT CCAGTCTGGC CCTGCACGCG CCGTCGCAAA TTGTCGCGGC
 551 GATTAAATCT CGCGCCGATC AACTGGGTGC CAGCGTGGTG GTGTCGATGG
 601 TAGAACGAAG CGGCGTCGAA GCCTGTAAAG CGGCGGTGCA CAATCTTCTC
 651 GCGCAACGCG TCAGTGGGCT GATCATTAAC TATCCGCTGG ATGACCAGGA
 701 TGCCATTGCT GTGGAAGCTG CCTGCACTAA TGTTCCGGCG TTATTTCTTG
 751 ATGTCTCTGA CCAGACACCC ATCAACAGTA TTATTTTCTC CCATGAAGAC
 801 GGTACGCGAC TGGGCGTGGA GCATCTGGTC GCATTGGGTC ACCAGCAAAT
 851 CGCGCTGTTA GCGGGCCCAT TAAGTTCTGT CTCGGCGCGT CTGCGTCTGG
 901 CTGGCTGGCA TAAATATCTC ACTCGCAATC AAATTCAGCC GATAGCGGAA
 951 CGGGAAGGCG ACTGGAGTGC CATGTCCGGT TTTCAACAAA CCATGCAAAT
1001 GCTGAATGAG GGCATCGTTC CCACTGCGAT GCTGGTTGCC AACGATCAGA
1051 TGGCGCTGGG CGCAATGCGC GCCATTACCG AGTCCGGGCT GCGCGTTGGT
1101 GCGGATATCT CGGTAGTGGG ATACGACGAT ACCGAAGACA GCTCATGTTA
1151 TATCCCGCCG TCAACCACCA TCAAACAGGA TTTTCGCCTG CTGGGGCAAA
1201 CCAGCGTGGA CCGCTTGCTG CAACTCTCTC AGGGCCAGGC GGTGAAGGGC
1251 AATCAGCTGT TGCCCGTCTC ACTGGTGAAA AGAAAAACCA CCCTGGCGCC
1301 CAATACGCAA ACCGCCTCTC CCCGCGCGTT GGCCGATTCA TTAATGCAGC
1351 TGGCACGACA GGTTTCCCGA CTGGAAAGCG GGCAGTGAGC GCAACGCAAT
1401 TAATGTGAGT TAGGATCCTG AGCGCCGGTC GCTACCATTA CCAGTTGGTC
1451 TGGTGTCAAA AATAATAATA ACCGGGCAGG CCATGTCTGC CCGTATTTCG
1501 CGTAAGGAAA TCCATTATGT ACTATTTCGA TCAGACCAGT TTTTAATTTG
1551 TGTGTTTCCA TGTGTCCAGT TTGGAATACT CTTAACCTCA TTGGAAATCG
1601 CGGCATAATC ACTGGTGGTA TGATTGATGA CCGCGTCAAC AATGACCTTT
1651 ATGCCATATT CTTCAGCGGC TGCACACATT TCTTTAAATT CTTGTTCAGT
1701 ACCTAAGTAA CGGTTGCCAA TTTGATACGA TGTCGGCTGA TACAGCCAGT
1751 ACCAGTTCGA CATGCTTTTA TCTCCTTGAT TCCCTTCCTT TACTTGGTTA
1801 ATCGGAGATG TCTGAATGGC TGTATATCCT GCATCATGAA TATCCTTCAT
1851 ATTGTGTTTT AACGTATTGA ACGACCAATT CCATGCATGA AGAATGGTTC
```

1901 CGCTTTTGAT CGACGGTGCT GTAAGCTCAT TCGATTTGTT CGCCGTTTCA

1951 GCACTCGCAG CCGCCGGTCC TGCCAGAACC AAATGAAACA GCAATAAAAA

2001 TCCAGCGAAT AACGGCAGTA AAGAGGTTTT GAATCGTTTT GCAAACATTC

2051 TTGACACTCC TTATTTGATT TTTTGAAGAC TTACTTCGGA GTCAAAAATC

2101 CCTCTTACTT CATTCTTCCG CTTCCTCCTT TCAAACCGAT GTGAAGACTG

2151 GAGAATTTTG TTAATTCTTG AAGACGAAAG GGCCTCGTGA TACGCCTATT

2201 TTTATAGGTT AATGTCATGA TAATAATGGT TTCTTAGACG TCAGGTGGCA

2251 CTTTTCGGGG AAATGTGCGC GGAACCCCTA TTTGTTTATT TTTCTAAATA

2301 CATTCAAATA TGTATCCGCT CATGAGACAA TAACCCTGAT AAATGCTTCA

2351 ATAATATTGA AAAAGGAAGA GTATGAGTAT TCAACATTTC CGTGTCGCCC

2401 TTATTCCCTT TTTTGCGGCA TTTTGCCTTC CTGTTTTTGC TCACCCAGAA

2451 ACGCTGGTGA AAGTAAAAGA TGCTGAAGAT CAGTTGGGTG CACGAGTGGG

2501 TTACATCGAA CTGGATCTCA ACAGCGGTAA GATCCTTGAG AGTTTTCGCC

2551 CCGAAGAACG TTTTCCAATG ATGAGCACTT TTAAAGTTCT GCTATGTGGC

2601 GCGGTATTAT CCCGTGTTGA CGCCGGGCAA GAGCAACTCG GTCGCCGCAT

2651 ACACTATTCT CAGAATGACT TGGTTGAGTA CTCACCAGTC ACAGAAAAGC

2701 ATCTTACGGA TGGCATGACA GTAAGAGAAT TATGCAGTGC TGCCATAACC

2751 ATGAGTGATA ACACTGCGGC CAACTTACTT CTGACAACGA TCGGAGGACC

2801 GAAGGAGCTA ACCGCTTTTT TGCACAACAT GGGGGATCAT GTAACTCGCC

2851 TTGATCGTTG GGAACCGGAG CTGAATGAAG CCATACCAAA CGACGAGCGT

2901 GACACCACGA TGCCTGCAGC AATGGCAACA ACGTTGCGCA AACTATTAAC

2951 TGGCGAACTA CTTACTCTAG CTTCCCGGCA ACAATTAATA GACTGGATGG

3001 AGGCGGATAA AGTTGCAGGA CCACTTCTGC GCTCGGCCCT TCCGGCTGGC

3051 TGGTTTATTG CTGATAAATC TGGAGCCGGT GAGCGTGGGT CTCGCGGTAT

3101 CATTGCAGCA CTGGGGCCAG ATGGTAAGCC CTCCCGTATC GTAGTTATCT

3151 ACACGACGGG GAGTCAGGCA ACTATGGATG AACGAAATAG ACAGATCGCT

3201 GAGATAGGTG CCTCACTGAT TAAGCATTGG TAACTGTCAG ACCAAGTTTA

3251 CTCATATATA CTTTAGATTG ATTTAAAACT TCATTTTTAA TTTAAAAGGA

3301 TCTAGGTGAA GATCCTTTTT GATAATCTCA TGACCAAAAT CCCTTAACGT

3351 GAGTTTTCGT TCCACTGAGC GTCAGACCCC GTAGAAAAGA TCAAAGGATC

3401 TTCTTGAGAT CCTTTTTTTC TGCGCGTAAT CTGCTGCTTG CAAACAAAAA

3451 AACCACCGCT ACCAGCGGTG GTTTGTTTGC CGGATCAAGA GCTATCAACT

3501 CTTTTTCCGA AGGTAACTGG CTTCAGCAGA GCGCAGATAC CAAATACTGT

3551 CCTTCTAGTG TAGCCGTAGT TAGGCCACCA CTTCAAGAAC TCTGTAGCAC

3601 CGCCTACATA CCTCGCTCTG CTAATCCTGT TACCAGTGGC TGCTGCCAGT

3651 GGCGATAAGT CGTGTCTTAC CGGGTTGGAC TCAAGACGAT AGTTACCGGA

3701 TAAGGCGCAG CGGTCGGGCT GAACGGGGGG TTCGTGCACA CAGCCCAGCT

3751 TGGAGCGAAC GACCTACACC GAACTGAGAT ACCTACAGCG TGAGCTATGA

3801 GAAAGCGCCA CGCTTCCCGA AGGGAGAAAG GCGGACAGGT ATCCGGTAAG

3851 CGGCAGGGTC GGAACAGGAG AGCGCACGAG GGAGCTTCCA GGGGGAAACG

3901 CCTGGTATCT TTATAGTCCT GTCGGGTTTC GCCACCTCTG ACTTGAGCGT

3951 CGATTTTTGT GATGCTCGTC AGGGGGGCGG AGCCTATGGA AAAACGCCAG

4001 CAACGCGGCC CGACCTCGAG CTGGATACTT CCCGTCCGCC AGGGGGACAT

4051 GCCGGCGATG CTGAAGGTCG CGCGCATTCC CGATGAAGAG GCCGGTTACC

4101 GCCTGTTTGA GGATATAGTA ATCTTTCTAA ATAGCTTTGG ATTGGAGGAG

4151 TATGGCCACT AATACTAAGT TCAGCTAATA AAAAAATTTG CTAAAGAACT

4201 CCAGCTGGAT TTCACTGATG AGAATATCGT CGGAGATAAA TATAATAATT

4251 CCACGGACTA TAGACTATAC TAGTATACTC CGTCTACTGT ACGATACACT

4301 TCCGCTCAGG TCCTTGTCCT TTAACGAGGA TTGTTACGTA CGCTAATGGC

4351 GTCAAAACAA AGACTCTAGA CCTAGGCCTT AAGATCTGAT CATATGCATC

4401 CGCGGGCCCG GGTTAACGCG TAATCCATGG ATCAAGAGAC AGGATGAGGA

4451 TCGTTTCGCA TGATTGAACA AGATGGATTG CACGCAGGTT CTCCGGTGCC

4501 CTGAATGAAC TGCAGAAAGA GCTGGTAGTT GGCGCACTGT TCGAAGAACT

4551 GCCGATGTCC AGTAAGATTC TTACTATGCT GGTTGAACCG GATGCTGGTA

4601 AAGCTACTTG GGTTGCTGCT TCTACTTATG GTACCGATAC AACTACTGGT

4651 GAGGAAGTTA AAGGAGCTCT TAAAGAAATC CACTTCAGTA GGTGGCCCGG

4701 CTCCATGCAC CGCGACGCAA CGCGGGGAGG CAGACAAGGT ATAGGGCGGC

4751 GCCTACAATC CATGCCAACC CGTTCCATGT GCTCGCCGAG GCGGCATAAA

4801 TCGCCGTGAC GATCAGCGGT CCAGTGATCG AAGTTAGGCT GGTAAGAGCC

4851 GCGAGCGATC CTTGAAGCTG TCCCTGATGG TCGTCATCTA CCTGCCTGGA

4901 CAGCATGGCC TGCAACGCGG GCATCCCGAT GCCGCCGGAA GCGAGAAGAA

4951 TCATAATGGG GAAGGCCATC CAGCCTCGCG TCGCGACTAA GAAAATGCCG

5001 TCAAATCCGC TCGCCATGAC TTCACTAACG ATGCCTTTGA AAATCTTCAA

5051 GTTCTTTTCT ACTAATTCAA GGCGTGTCTC ACCAGGTTTT TGGTTTGCTC

5101 CGGCGCAAAT GCAGACAATA TCAGCATCCT TGCAGGGTAT GTTTCTCTTT

5151 GATGTCTTTT TGTTTGTGAA GTATTTCACA TTTATATTGT GCAACACTTC

5201 ACAAACTTTT GCAAGAGAAA AGTTTTGTCT GATTTATGAA CAAAAAAGAA

5251 ACCATCATTG ATGGTTTCTT TCGGTAAGTC CCGTCTAGCC TTGCCCTCAA

5301 TGGGGAAGAG AACCGCTTAA GCCCGAGTCA TTATATAAAC CATTTAGCAC

5351 GTAATCAAAG CCAGGCTGAT TCTGACCGGG CACTTGGGCG CTGCCATTAT

5401 TAAAAATCAC TTTTGCGTTG GTTGTATCCG TGTCCGCAGG CAGCGTCAGC

5451 GTGTAAATTC CGTCTGCATT TTTAGTCATT GGTTTTCCAG GCCAAGATCC

5501 GGTCAATTCA ATTACTCGGC TCCCATCATG TTTATAGATA TAAGCATTTA

5551 CCTGGCTCCA ATGATTCGGA TTTTGATAGC CGATGGTTTT GGCCGACGCT

5601 GGATCTCTTT TAACAAAACT GTATTTCTCG GTCCTCGTTA CACCATCACT

5651 GTTCGTTCCT TTTAACATGA TGGTGTATGT TTTGCCAAAT TGGATCTCCT

5701 TTTCCGATTG TGAATTGATC TCCATCCTTA AACGCCTGTC GTCTGGTCCA

5751 TTATTGATTT GATAAACGGC TTTTGTTGTA TTCGCATCTG CACGCAAGGT

5801 AATCGTCAGT TGATCATTGA AAGAATGTGT TACACCTGTT TTGTAATTCT

5851 CAAGGAAAAC ATGAGGCGCT TTTGCAATAT CATCAGGATA AAGCACAGCT

5901 ACAGACCTGG CATTGATCGT GCCTGTCAGT TTACCATCGT TCACTTGAAA

5951 TGAACCCGCT CCAGCTTTAT TGTCATACCT GCCATCAGGC AATTTTGTTG

6001 CCGTATTGAT AGAGACAGAG GATGAACCTG CATTTGCCAG CACAACGCCA

6051 TGTGAGCCGC GCTGATTCAT AAATATCTGG TTGTTTCCAT TCGGGTTCGA

6101 GAGTTCCTCA GGCTGTCCAG CCATCACATT GTGAAATCTA TTGACCGCAG

6151 TGATAGCCTG ATCTTCAAAT AAAGCACTCC CGCGATCGCC TATTTGGCTT

6201 TTCCCCGGGA ACCTCACACC ATTTCCGCCT CCCTCAGGTC TGGAAAAGAA

6251 AAGAGGCGTA CTGCCTGAAC GAGAAGCTAT CACCGCCCAG CCTAAACGGA

6301 TGATCCCCCT ATGCAAGGGT TTATTGTTTT CTAAAATCTG ATTACCAATT

6351 AGAATGAATA TTTCCCAAAT ATTAAATAAT AAAACAAAAA AATTGAAAAA

6401 AGTGTTTCCA CCATTTTTTC AATTTTTTTA TAATTTTTTT AATCTGTTAT

6451 TTAAATAGTT TATAGTTAAA TTTACATTTT CATTAGTCCA TTCAATATTC

6501 TCTCCAAGAT AACTACGAAC TGCTAACAAA ATTCTCTCCC TATGTTCTAA

6551 TGGAGAAGAT TCAGCCACTG CATTTCCCGC AATATCTTTT GGTATGATTT

6601 TACCCGTGTC CATAGTTAAA ATCATACGGC ATAAAGTTAA TATAGAGTTG

6651 GTTTCATCAT CCTGATAATT ATCTATTAAT TCCTCTGACG AATCCATAAT

6701 GGCTCTTCTC ACATCAGAAA ATGGAATATC AGGTAGTAAT TCCTCTAAGT

6751 CATAATTTCC GTATATTCTT TTATTTTTTC GTTTTGCTTG GTAAAGCATT

6801 ATGGTTAAAT CTGAATTTAA TTCCTTCTGA GGAATGTATC CTTGTTCATA

6851 AAGCTCTTGT AACCATTCTC CATAAATAAA TTCTTGTTTG GGAGGATGAT

6901 TCCACGGTAC CATTTCTTGC TGAATAATAA TTGTTAATTC AATATATCGT

6951 AAGTTGCTTT TATCTCCTAT TTTTTTTGAA ATAGGTCTAA TTTTTTGTAT

7001 AAGTATTTCT TTACTTTGAT CTGTCAATGG TTCAGATACG ACGACTAAAA

7051 AGTCAAGATC ACTATTTGGT TTTAGTCCAC TCTCAACTCC TGATCCAAAC

7101 ATGTAAGTAC CAATAAGGTT ATTTTTTAAA TGTTTCCGAA GTATTTTTTT

7151 CACTTTATTA ATTTGTTCGT ATGTATTCAA ATATATCCTC CTCACTATTT

7201 TGATTAGTAC CTATTTTATA TCCATAGTTG TTAATTAAAT AAACTTAATT

7251 TAGTTTATTT ATAGATTTCA TTGGCTTCTA AATTTTTTAT CTAGATAATA

7301 ATTATTTTAG TTAATTTTAT TCTAGATTAT ATATGATATG ATCTTTCATT

7351 TCCATAAAAC TAAAGTAAGT GTAAACCTAT TCATTGTTTT AAAAATATCT

7401 CTTGCCAGTC ACGTTACGTT ATTAGTTATA GTTATTATAA CATGTATTCA

7451 CGAACGAAAA TCGCCATTCG CCAGGGCTGC AGGAATTCGA CTCTCTAGCT

7501 TGAGGCATCA AATAAAACGA AAGGCTCAGT CGAAAGACTG GGCCTTTCGT

7551 TTTATCTGTT GTTTGTCGGT GAACGCTCTC CTGAGTAGGA CAAATCCGCC

7601 GCTCTAGCTA AGCAGAAGGC CATCCTGACG GATGGCCTTT TTGCGTTTCT

7651 ACAAACTCTT GTTAACTCTA GAGCTGCCTG CCGCGTTTCG GTGATGAAGA

```
7701 TCTTCCCGAT GATTAATTAA TTCAGAACGC TCGGTTGCCG CCGGGCGTTT
7751 TTTATGCAGC AATGGCAAGA ACGTTGCTCG AGGGTAAATG TGAGCACTCA
7801 CAATTCATTT TGCAAAAGTT GTTGACTTTA TCTACAAGGT GTGGCATAAT
7851 GTGTGTAATT GTGAGCGGAT AACAATTAAG CTTAAGGAGG AAAGTCACAT
7901 TATGCC
```

ASAP1

ASAP1 sequence was obtained from Addgene (plasmid 52519).

```
   1 ATGGAGACGA CTGTGAGGTA TGAACAGGGG TCAGAGCTCA CTAAAACTTC
  51 GAGCTCTCCA ACAGCAGATG AGCCCACGAT AAAGATTGAT GATGGTCGTG
 101 ATGAGGGTAA TGAACAAGAC AGCTGTTCCA ATACCATTAG GAGAAAAATT
 151 TCCCCGTTTG TGATGTCATT TGGATTCAGA GTATTTGGAG TTGTGCTTAT
 201 CATTGTAGAC ATCATAGTGG TGATTGTGGA TCTGGCCATC AGTGAGAAGA
 251 AAAGAGGCAT TAGAGAGATT CTTGAAGGTG TTTCCCTGGC TATAGCACTC
 301 TTCTTCCTTG TTGATGTTCT CATGAGAGTG TTTGTTGAAG GCTTCAAGAA
 351 CTATTTCCGG TCCAAACTGA ATACTTTGGA TGCAGTCATA GTAGTGGGCA
 401 CTCTGCTAAT TAATATGACC TACTCCTTCT CTGACCTTGC TGCCTTTAAC
 451 AGCCATAACG TGTATATTAC CGCGGATAAA CAGAAAAACG GCATTAAAGC
 501 GAACTTTACC GTGCGCCATA ACGTGGAAGA TGGCAGCGTG CAGCTGGCGG
 551 ATCATTATCA GCAGAACACC CCGATTGGCG ATGGCCCGGT GCTGCTGCCG
 601 GATAACCATT ATCTGAGCAC CCAGACCGTG CTGAGCAAAG ATCCGAACGA
 651 AAAACGCGAT CACATGGTGC TGCTGGAATT TGTGACCGCA GCGGGCATTA
 701 CACACGGCAT GGATGAACTG TATGGCGGCA CCGGCGGCAG CGCGAGCCAG
 751 GGCGAAGAAC TGTTTACCGG CGTGGTGCCG ATTCTGGTGG AACTGGATGG
 801 CGATGTGAAC GGCCATAAAT TTAGCGTGCG CGGCGAAGGC GAAGGCGATG
 851 CGACCATTGG CAAACTGACC CTGAAATTTA TTTGCACCAC CGGCAAACTA
 901 CCGGTGCCGT GGCCGACCCT GGTGACCACC TTAACCTATG GCGTGCAGTG
 951 CTTTAGCCGC TATCCGGATC ATATGAAACG CCATGATTTT TTTAAAAGCG
1001 CGATGCCGGA AGGCTATGTG CAGGAACGCA CCATTAGCTT TAAAGATGAT
```

```
1051 GGCAAATATA AAACCCGCGC GGTGGTGAAA TTTGAAGGCG ATACCCTGGT
1101 GAACCGCATT GAACTGAAAG GCACCGATTT TAAAGAAGAT GGCAACATTC
1151 TGGGGCATAA ACTGGAATAT AACACAGATC AGATGCCGCA GATGGTTACT
1201 CTTCTTCGAG TTCTGAGAAT TGTTATCTTA ATAAGAATAT TTCGCCTGGC
1251 TTCACAGAAG AAACAACTTG AAGTGGTAAC CTAA
```

A.0.3 PAPS-Gt

```
   1 ATGTTAAAAC GTATCAAAAT TGTGACCAGC TTACTGCTGG TTTTGGCCGT
  51 TTTTGGCCTT TTACAACTGA CATCAGGCGG TCTGTTCTTT AATGCCTTAA
 101 AGAATGACAA AGAAAATTTC ACTGTTTTAC AAACCATTCG CCAGCAGCAA
 151 TCCACGCTGA ATGGCAGCTG GGTCGCGTTG TTGCAGACGC GTAACACCCT
 201 CAACCGCGCG GGTATCCGCT ACATGATGGA TCAGAATAAT ATTGGTAGCG
 251 GTTCAACCGT TGCTGAGCTG ATGGAGAGTG CCAGTATTTC GCTGAAACAG
 301 GCGGAAAAAA ACTGGGCGGA TTACGAAGCG TTGCCGCGTG ACCCGCGTCA
 351 GAGCACCGCC GCAGCGGCAG AGATCAAACG TAATTACGAT ATTTATCACA
 401 ATGCGCTGGC GGAGCTGATC CAACTGTTAG GTGCAGGCAA AATCAACGAG
 451 TTCTTTGATC AGCCGACCCA GGGATATCAG GACGGTTTCG AGAAGCAGTA
 501 TGTGGCTTAC ATGGAGCAAA ACGATCGGCT CCATGATATC GCCGTCAGCG
 551 ATAACAATGC CTCCTACAGC CAGGCGATGT GGATTCTGGT GGGCGTGATG
 601 ATCGTCGTAC TGGCGGTCAT CTTCGCCGTC TGGTTCGGTA TTAAAGCCAT
 651 GGAAACAACA GTCAGATATG AACAAGGCAG CGAACTGACA AAAACATCAT
 701 CATCACCGAC AGCAGATGAA CCGACAATCA AAATTGATGA TGGCAGAGAT
 751 GAAGGCAATG AACAAGATTC ATGCAGCAAT ACAATTCGCA GAAAAATTAG
 801 CCCGTTTGTC ATGAGCTTTG GCTTTAGAGT TTTTGGCGTT GTCCTGATTA
 851 TTGTCGATAT TATTGTGGTC ATTGTCGATC TGGCAATCAG CGAAAAAAAA
 901 CGCGGAATTA GAGAAATTCT GGAAGGCGTT TCACTGGCAA TTGCACTGTT
 951 TTTTCTGGTT GATGTTCTGA TGAGAGTCTT TGTCGAAGGC TTCAAAAACT
1001 ACTTTCGCAG CAAACTGAAT ACACTGGATG CAGTTATTGT TGTTGGCACA
```

```
1051 CTGCTGATCA ATATGACGTA TTCATTTTCA GATCTGGCTG CGTACAACTC
1101 CCACAACGTT TACATTACTG CTGACAAGCA GAAAAACGGC ATCAAAGCAA
1151 ACTTCAAGAT CCGTCACAAC ATTGAAGATG GTGGCGTACA GCTGGCAGAT
1201 CACTACCAGC AGAACACTCC AATCGGTGAT GGCCCAGTAC TGCTGCCAGA
1251 TAACCATTAC CTGTCCTACC AGAGCAAACT GTCTAAAGAC CCGAACGAAA
1301 AACGTGACCA CATGGTACTG CTGGAATTTG TTACCGCGGC AGGCATTACC
1351 CACGGTATGG ACGAACTGTA TAAAGGCGGC ACCGGCGGCA GCATGAGCAA
1401 AGGTGAAGAA CTGTTCACCG GCGTTGTGCC AATTCTGGTT GAGCTGGATG
1451 GTGACGTGAA TGGCCACAAA TTTTCCGTGT CTGGTGAAGG CGAGGGTGAT
1501 GCTACTTATG GCAAACTGAC TCTGAAACTG ATCTGTACCA CCGGCAAACT
1551 GCCTGTTCCG TGGCCAACTC TGGTCACTAC TCTGGGTTAC GGCCTGATGT
1601 GTTTTGCGCG TTACCCGGAT CACATGAAAC AGCATGACTT CTTCAAATCT
1651 GCCATGCCGG AAGGCTATGT CCAAGAACGT ACGATCTTTT TCAAGGACGA
1701 CGGCAACTAT AAAACCCGTG CCGAAGTTAA ATTCGAGGGT GACACCCTGG
1751 TTAACCGCAT CGAACTGAAA GGCATTGACT TCAAAGAGGA CGGCAACATT
1801 CTGGGTCACA AGCTGGAATA CAACACAGAT CAAATGCCGC AAATGGTTAC
1851 ACTGCTTAGA GTTCTGAGAA TTGTCATTCT GATTCGCATT TTTAGACTGG
1901 CGAGCCAAAA AAAACAACTG GAAGTTGTCA CGTAA
```

A.0.4 Primers

AP44 - ATGGCAAGAACGTTGCTCGAGG

AP45 - TCGGAAGGAAATGATGACCTCGT

AP586 - AGCCAAAAAAAACAACTGGAAGTTGTCA

AP590 - CGCAGCCAGATCTGAAAATGAATACG

AP592 - CAGTGTATTCAGTTTGCTGCGAAAGTA

B Appendix

FIGURE B.1: Insert site in pcDNA3.1 plasmid. Upper case and bold: CAG promoter; Kozak sequence; bGH polyalanine terminator. Lower case and bold: restriction sites for HindIII and NotI. Underlined: primers used for sequencing: CMVF_pcDNA3 and BGH_Reverse. Every inserted gene began with "ATG" start codon and ended with "TAG" stop codon.

B.0.1 DNA Templates

Here are listed the DNA sequences of the main constructs inserted in pcDNA3.1 plasmid. LOTEV1, LOTEV2 and TEVp were assembled together with P2A-YFP3xNuc (removing the TAA stop codon from the sequence here reported). All the DNA sequences are written from the 5'-end to the 3'-end.

pcDNA3.1 backbone

```
  1 GCGGCCGCTC GAGCATGCAT CTAGAGGGCC CTATTCTATA GTGTCACCTA
 51 AATGCTAGAG CTCGCTGATC AGCCTCGACT GTGCCTTCTA GTTGCCAGCC
101 ATCTGTTGTT TGCCCCTCCC CCGTGCCTTC CTTGACCCTG GAAGGTGCCA
151 CTCCCACTGT CCTTTCCTAA TAAAATGAGG AAATTGCATC GCATTGTCTG
201 AGTAGGTGTC ATTCTATTCT GGGGGGTGGG GTGGGGCAGG ACAGCAAGGG
251 GGAGGATTGG GAAGACAATA GCAGGCATGC TGGGGATGCG GTGGGCTCTA
301 TGGCTTCTGA GGCGGAAAGA ACCAGCTGGG GCTCTAGGGG GTATCCCCAC
```

```
 351 GCGCCCTGTA GCGGCGCATT AAGCGCGGCG GGTGTGGTGG TTACGCGCAG
 401 CGTGACCGCT ACACTTGCCA GCGCCCTAGC GCCCGCTCCT TTCGCTTTCT
 451 TCCCTTCCTT TCTCGCCACG TTCGCCGGCT TTCCCCGTCA AGCTCTAAAT
 501 CGGGGCATCC CTTTAGGGTT CCGATTTAGT GCTTTACGGC ACCTCGACCC
 551 CAAAAAACTT GATTAGGGTG ATGGTTCACG TAGTGGGCCA TCGCCCTGAT
 601 AGACGGTTTT TCGCCCTTTG ACGTTGGAGT CCACGTTCTT TAATAGTGGA
 651 CTCTTGTTCC AAACTGGAAC AACACTCAAC CCTATCTCGG TCTATTCTTT
 701 TGATTTATAA GGGATTTTGG GGATTTCGGC CTATTGGTTA AAAAATGAGC
 751 TGATTTAACA AAAATTTAAC GCGAATTAAT TCTGTGGAAT GTGTGTCAGT
 801 TAGGGTGTGG AAAGTCCCCA GGCTCCCCAG GCAGGCAGAA GTATGCAAAG
 851 CATGCATCTC AATTAGTCAG CAACCAGGTG TGGAAAGTCC CCAGGCTCCC
 901 CAGCAGGCAG AAGTATGCAA AGCATGCATC TCAATTAGTC AGCAACCATA
 951 GTCCCGCCCC TAACTCCGCC CATCCCGCCC CTAACTCCGC CCAGTTCCGC
1001 CCATTCTCCG CCCCATGGCT GACTAATTTT TTTTATTTAT GCAGAGGCCG
1051 AGGCCGCCTC TGCCTCTGAG CTATTCCAGA AGTAGTGAGG AGGCTTTTTT
1101 GGAGGCCTAG GCTTTTGCAA AAAGCTCCCG GGAGCTTGTA TATCCATTTT
1151 CGGATCTGAT CAAGAGACAG GATGAGGATC GTTTCGCATG ATTGAACAAG
1201 ATGGATTGCA CGCAGGTTCT CCGGCCGCTT GGGTGGAGAG GCTATTCGGC
1251 TATGACTGGG CACAACAGAC AATCGGCTGC TCTGATGCCG CCGTGTTCCG
1301 GCTGTCAGCG CAGGGGCGCC CGGTTCTTTT TGTCAAGACC GACCTGTCCG
1351 GTGCCCTGAA TGAACTGCAG GACGAGGCAG CGCGGCTATC GTGGCTGGCC
1401 ACGACGGGCG TTCCTTGCGC AGCTGTGCTC GACGTTGTCA CTGAAGCGGG
1451 AAGGGACTGG CTGCTATTGG GCGAAGTGCC GGGGCAGGAT CTCCTGTCAT
1501 CTCACCTTGC TCCTGCCGAG AAAGTATCCA TCATGGCTGA TGCAATGCGG
1551 CGGCTGCATA CGCTTGATCC GGCTACCTGC CCATTCGACC ACCAAGCGAA
1601 ACATCGCATC GAGCGAGCAC GTACTCGGAT GGAAGCCGGT CTTGTCGATC
1651 AGGATGATCT GGACGAAGAG CATCAGGGGC TCGCGCCAGC CGAACTGTTC
1701 GCCAGGCTCA AGGCGCGCAT GCCCGACGGC GAGGATCTCG TCGTGACCCA
1751 TGGCGATGCC TGCTTGCCGA ATATCATGGT GGAAAATGGC CGCTTTTCTG
```

1801 GATTCATCGA CTGTGGCCGG CTGGGTGTGG CGGACCGCTA TCAGGACATA

1851 GCGTTGGCTA CCCGTGATAT TGCTGAAGAG CTTGGCGGCG AATGGGCTGA

1901 CCGCTTCCTC GTGCTTTACG GTATCGCCGC TCCCGATTCG CAGCGCATCG

1951 CCTTCTATCG CCTTCTTGAC GAGTTCTTCT GAGCGGGACT CTGGGGTTCG

2001 AAATGACCGA CCAAGCGACG CCCAACCTGC CATCACGAGA TTTCGATTCC

2051 ACCGCCGCCT TCTATGAAAG GTTGGGCTTC GGAATCGTTT TCCGGGACGC

2101 CGGCTGGATG ATCCTCCAGC GCGGGGATCT CATGCTGGAG TTCTTCGCCC

2151 ACCCCAACTT GTTTATTGCA GCTTATAATG GTTACAAATA AAGCAATAGC

2201 ATCACAAATT TCACAAATAA AGCATTTTTT TCACTGCATT CTAGTTGTGG

2251 TTTGTCCAAA CTCATCAATG TATCTTATCA TGTCTGTATA CCGTCGACCT

2301 CTAGCTAGAG CTTGGCGTAA TCATGGTCAT AGCTGTTTCC TGTGTGAAAT

2351 TGTTATCCGC TCACAATTCC ACACAACATA CGAGCCGGAA GCATAAAGTG

2401 TAAAGCCTGG GGTGCCTAAT GAGTGAGCTA ACTCACATTA ATTGCGTTGC

2451 GCTCACTGCC CGCTTTCCAG TCGGGAAACC TGTCGTGCCA GCTGCATTAA

2501 TGAATCGGCC AACGCGCGGG GAGAGGCGGT TTGCGTATTG GGCGCTCTTC

2551 CGCTTCCTCG CTCACTGACT CGCTGCGCTC GGTCGTTCGG CTGCGGCGAG

2601 CGGTATCAGC TCACTCAAAG GCGGTAATAC GGTTATCCAC AGAATCAGGG

2651 GATAACGCAG GAAAGAACAT GTGAGCAAAA GGCCAGCAAA AGGCCAGGAA

2701 CCGTAAAAAG GCCGCGTTGC TGGCGTTTTT CCATAGGCTC CGCCCCCCTG

2751 ACGAGCATCA CAAAAATCGA CGCTCAAGTC AGAGGTGGCG AAACCCGACA

2801 GGACTATAAA GATACCAGGC GTTTCCCCCT GGAAGCTCCC TCGTGCGCTC

2851 TCCTGTTCCG ACCCTGCCGC TTACCGGATA CCTGTCCGCC TTTCTCCCTT

2901 CGGGAAGCGT GGCGCTTTCT CAATGCTCAC GCTGTAGGTA TCTCAGTTCG

2951 GTGTAGGTCG TTCGCTCCAA GCTGGGCTGT GTGCACGAAC CCCCCGTTCA

3001 GCCCGACCGC TGCGCCTTAT CCGGTAACTA TCGTCTTGAG TCCAACCCGG

3051 TAAGACACGA CTTATCGCCA CTGGCAGCAG CCACTGGTAA CAGGATTAGC

3101 AGAGCGAGGT ATGTAGGCGG TGCTACAGAG TTCTTGAAGT GGTGGCCTAA

3151 CTACGGCTAC ACTAGAAGGA CAGTATTTGG TATCTGCGCT CTGCTGAAGC

3201 CAGTTACCTT CGGAAAAAGA GTTGGTAGCT CTTGATCCGG CAAACAAACC

```
3251 ACCGCTGGTA GCGGTGGTTT TTTTGTTTGC AAGCAGCAGA TTACGCGCAG
3301 AAAAAAAGGA TCTCAAGAAG ATCCTTTGAT CTTTTCTACG GGGTCTGACG
3351 CTCAGTGGAA CGAAAACTCA CGTTAAGGGA TTTTGGTCAT GAGATTATCA
3401 AAAAGGATCT TCACCTAGAT CCTTTTAAAT TAAAAATGAA GTTTTAAATC
3451 AATCTAAAGT ATATATGAGT AAACTTGGTC TGACAGTTAC CAATGCTTAA
3501 TCAGTGAGGC ACCTATCTCA GCGATCTGTC TATTTCGTTC ATCCATAGTT
3551 GCCTGACTCC CCGTCGTGTA GATAACTACG ATACGGGAGG GCTTACCATC
3601 TGGCCCCAGT GCTGCAATGA TACCGCGAGA CCCACGCTCA CCGGCTCCAG
3651 ATTTATCAGC AATAAACCAG CCAGCCGGAA GGGCCGAGCG CAGAAGTGGT
3701 CCTGCAACTT TATCCGCCTC CATCCAGTCT ATTAATTGTT GCCGGGAAGC
3751 TAGAGTAAGT AGTTCGCCAG TTAATAGTTT GCGCAACGTT GTTGCCATTG
3801 CTACAGGCAT CGTGGTGTCA CGCTCGTCGT TTGGTATGGC TTCATTCAGC
3851 TCCGGTTCCC AACGATCAAG GCGAGTTACA TGATCCCCCA TGTTGTGCAA
3901 AAAAGCGGTT AGCTCCTTCG GTCCTCCGAT CGTTGTCAGA AGTAAGTTGG
3951 CCGCAGTGTT ATCACTCATG GTTATGGCAG CACTGCATAA TTCTCTTACT
4001 GTCATGCCAT CCGTAAGATG CTTTTCTGTG ACTGGTGAGT ACTCAACCAA
4051 GTCATTCTGA GAATAGTGTA TGCGGCGACC GAGTTGCTCT TGCCCGGCGT
4101 CAATACGGGA TAATACCGCG CCACATAGCA GAACTTTAAA AGTGCTCATC
4151 ATTGGAAAAC GTTCTTCGGG GCGAAAACTC TCAAGGATCT TACCGCTGTT
4201 GAGATCCAGT TCGATGTAAC CCACTCGTGC ACCCAACTGA TCTTCAGCAT
4251 CTTTTACTTT CACCAGCGTT TCTGGGTGAG CAAAAACAGG AAGGCAAAAT
4301 GCCGCAAAAA AGGGAATAAG GGCGACACGG AAATGTTGAA TACTCATACT
4351 CTTCCTTTTT CAATATTATT GAAGCATTTA TCAGGGTTAT TGTCTCATGA
4401 GCGGATACAT ATTTGAATGT ATTTAGAAAA ATAAACAAAT AGGGGTTCCG
4451 CGCACATTTC CCCGAAAAGT GCCACCTGAC GTCGACGGAT CGGGAGATCT
4501 CCCGATCCCC TATGGTCGAC TCTCAGTACA ATCTGCTCTG ATGCCGCATA
4551 GTTAAGCCAG TATCTGCTCC CTGCTTGTGT GTTGGAGGTC GCTGAGTAGT
4601 GCGCGAGCAA AATTTAAGCT ACAACAAGGC AAGGCTTGAC CGACAATTGC
4651 ATGAAGAATC TGCTTAGGGT TAGGCGTTTT GCGCTGCTTC GCGATGTACG
```

```
4701 GGCCAGATAT ACGCGTTGAC ATTGATTATT GACTAGTTAT TAATAGTAAT
4751 CAATTACGGG GTCATTAGTT CATAGCCCAT ATATGGAGTT CCGCGTTACA
4801 TAACTTACGG TAAATGGCCC GCCTGGCTGA CCGCCCAACG ACCCCCGCCC
4851 ATTGACGTCA ATAATGACGT ATGTTCCCAT AGTAACGCCA ATAGGGACTT
4901 TCCATTGACG TCAATGGGTG GACTATTTAC GGTAAACTGC CCACTTGGCA
4951 GTACATCAAG TGTATCATAT GCCAAGTACG CCCCCTATTG ACGTCAATGA
5001 CGGTAAATGG CCCGCCTGGC ATTATGCCCA GTACATGACC TTATGGGACT
5051 TTCCTACTTG GCAGTACATC TACGTATTAG TCATCGCTAT TACCATGGTG
5101 ATGCGGTTTT GGCAGTACAT CAATGGGCGT GGATAGCGGT TTGACTCACG
5151 GGGATTTCCA AGTCTCCACC CCATTGACGT CAATGGGAGT TTGTTTTGGC
5201 ACCAAAATCA ACGGGACTTT CCAAAATGTC GTAACAACTC CGCCCCATTG
5251 ACGCAAATGG GCGGTAGGCG TGTACGGTGG GAGGTCTATA TAAGCAGAGC
5301 TCTCTGGCTA ACTAGAGAAC CCACTGCTTA CTGGCTTATC GAAATTAATA
5351 CGACTCACTA TAGGGAGACC CAAGCTTGCC ACC
```

LOTUS-V

LOTUS-V sequence was obtained from www.addgene.org (plasmid 87127).

```
   1 ATGGAGGGAT TCGACGGTTC AGATTTTAGT CCTCCAGCTG ATTTAGTTGG
  51 CGTTGACGGT GCAGTCATGC GGAACGTCGT TGACGTCACG ATAAATGGTG
 101 ACGTCACTGC TCCGCCGAAA GCTGCGCCAA GAAAAAGTGA ATCGGTAAAG
 151 AAAGTTCATT GGAATGATGT AGACCAAGGA CCGAGTGAAA AACCAGAGAC
 201 AAGACAGGAG GAACGAATAG ATATACCCGA GATTTCAGGT CTATGGTGGG
 251 GCGAGAATGA ACATGGAGTG GACGATGGGA GAATGGAGAT ACCTACTACT
 301 GGTGTAGGGG ATCCGATGGT CTTCACACTC GAAGATTTCG TTGGGGACTG
 351 GCGACAGACA GCCGGCTACA ACCTGGACCA AGTCCTTGAA CAGGGAGGTG
 401 TGTCCAGTTT GTTTCAGAAT CTCGGGGTGT CCGTAACTCC GATCCAAAGG
 451 ATTGTCCTGA GCGGTGAAAA TGGGCTGAAG ATCGACATCC ATGTCATCAT
 501 CCCGTATGAA GGTCTGAGCG GCGACCAAAT GGGCCAGATC GAAAAAATTT
 551 TTAAGGTGGT GTACCCTGTG GATGATCATC ACTTTAAGGT GATCCTGCAC
```

```
 601 TATGGCACAC TGGTAATCGA CGGGGTTACG CCGAACATGA TCGACTATTT
 651 CGGACGGCCG TATGAAGGCA TCGCCGTGTT CGACGGCAAA AAGATCACTG
 701 TAACAGGGAC CCTGTGGAAC GGCAACAAAA TTATCGACGA GCGCCTGATC
 751 AACCCCGACG GCTCCCTGCT GTTCCGAGTA ACCATCAACG GAGTGACCGG
 801 CTGGCGGCTG TGCGAACGCA TTCTGGCGGA ATTCGGCGTG GGCCGCGTCC
 851 AGTTTCGTGT CCGAGCAGTG ATTGATCATC TAGGGATGCG AGTCTTTGGA
 901 GTCTTCCTAA TTTTCTTGGA CATCATCCTC ATGATCATTG ATCTCAGTCT
 951 TCCAGGAAAA AGTGAATCTT CACAATCCTT TTATGACGGG ATGGCTTTGG
1001 CTCTTTCTTG TTATTTCATG CTGGATTTAG GATTAAGGAT ATTTGCCTAC
1051 GGGCCCAAGA ATTTCTTCAC CAACCCCTGG GAGGTTGCTG ATGGTTTGAT
1101 TATCGTTGTC ACATTCGTCG TCACGATATT TTACACTGTG TTAGATGAAT
1151 ACGTGCAAGA AACAGGAGCC GATGGTTTGG GGCAGTTGGT TGTGTTGGCC
1201 CGTTTGCTGC GTGTGGTTCG ATTAGCAAGA ATATTTTATT CCCACCAACA
1251 AATGAAGGCT TCAAGCAGAA GAACAATATC ACTCGAGATG GTGAGCAAGG
1301 GCGAGGAGCT GTTCACCGGG GTGGTGCCCA TCCTGGTCGA GCTGGACGGC
1351 GACGTAAACG GCCACAAGTT CAGCGTGTCC GGCGAGGGCG AGGGCGATGC
1401 CACCTACGGC AAGCTGACCC TGAAGCTGAT CTGCACCACC GGCAAGCTGC
1451 CCGTGCCCTG GCCCACCCTC GTGACCACCC TGGGCTACGG CCTGCAGTGC
1501 TTCGCCCGCT ACCCCGACCA CATGAAGCAG CACGACTTCT TCAAGTCCGC
1551 CATGCCCGAA GGCTACGTCC AGGAGCGCAC CATCTTCTTC AAGGACGACG
1601 GCAACTACAA GACCCGCGCC GAGGTGAAGT TCGAGGGCGA CACCCTGGTG
1651 AACCGCATCG AGCTGAAGGG CATCGACTTC AAGGAGGACG GCAACATCCT
1701 GGGGCACAAG CTGGAGTACA ACTACAACAG CCACAACGTC TATATCACCG
1751 CCGACAAGCA GAAGAACGGC ATCAAGGCCA ACTTCAAGAT CCGCCACAAC
1801 ATCGAGGACG GCGGCGTGCA GCTCGCCGAC CACTACCAGC AGAACACCCC
1851 CATCGGCGAC GGCCCCGTGC TGCTGCCCGA CAACCACTAC CTGAGCTACC
1901 AGTCCGCCCT GAGCAAAGAC CCCAACGAGA AGCGCGATCA CATGGTCCTG
1951 CTGGAGTTCG TGACCGCCGC CGGGATCACT CTCGGCATGG ACGAGCTGTA
2001 CAAGTAG
```

B.0.2 LOTEV1

```
   1 ATGGAGGGAT TCGACGGTTC AGATTTTAGT CCTCCAGCTG ATTTAGTTGG
  51 CGTTGACGGT GCAGTCATGC GGAACGTCGT TGACGTCACG ATAAATGGTG
 101 ACGTCACTGC TCCGCCGAAA GCTGCGCCAA GAAAAAGTGA ATCGGTAAAG
 151 AAAGTTCATT GGAATGATGT AGACCAAGGA CCGAGTGAAA AACCAGAGAC
 201 AAGACAGGAG GAACGAATAG ATATACCCGA GATTTCAGGT CTATGGTGGG
 251 GCGAGAATGA ACATGGAGTG GACGATGGGA GAATGGAGAT ACCTACTACT
 301 GGTGTAGGGG ATCCCATGGG AGAAAGCTTG TTTAAGGGGC CGCGTGATTA
 351 CAACCCGATA TCGAGCACCA TTTGTCATTT GACGAATGAA TCTGATGGGC
 401 ACACAACATC GTTGTATGGT ATTGGATTTG GTCCCTTCAT CATTACAAAC
 451 AAGCACTTGT TTAGAAGAAA TAATGGAACA CTGTTGGTCC AATCACTACA
 501 TGGTGTATTC AAGGTCAAGA ACACCACGAC TTTGCAACAA CACCTCATTG
 551 ATGGGAGGGA CATGATAATT ATTCGCATGC CTAAGGATTT CCCACCATTT
 601 CCTCAAAAGC TGAAATTTAG AGAGCCACAA AGGGAAGAGC GCATATGTCT
 651 TGTGACAACC AACTTCCAAG AATTCGGCGT GGGCCGCGTC CAGTTTCGTG
 701 TCCGAGCAGT GATTGATCAT CTAGGGATGC GAGTCTTTGG AGTCTTCCTA
 751 ATTTTCTTGG ACATCATCCT CATGATCATT GATCTCAGTC TTCCAGGAAA
 801 AAGTGAATCT TCACAATCCT TTTATGACGG GATGGCTTTG GCTCTTTCTT
 851 GTTATTTCAT GCTGGATTTA GGATTAAGGA TATTTGCCTA CGGGCCCAAG
 901 AATTTCTTCA CCAACCCCTG GGAGGTTGCT GATGGTTTGA TTATCGTTGT
 951 CACATTCGTC GTCACGATAT TTTACACTGT GTTAGATGAA TACGTGCAAG
1001 AAACAGGAGC CGATGGTTTG GGGCAGTTGG TTGTGTTGGC CCGTTTGCTG
1051 CGTGTGGTTC GATTAGCAAG AATATTTTAT TCCCATCAAC AAATGAAGGC
1101 TTCAAGCAGA AGAACAATAT CACTCGAGAC TAAGAGCATG TCTAGCATGG
1151 TGTCAGACAC TAGTTGCACA TTCCCTTCAT CTGATGGCAT ATTCTGGAAG
1201 CATTGGATTC AAACCAAGGA TGGGCAGTGT GGCAGTCCAT TAGTATCAAC
1251 TAGAGATGGG TTCATTGTTG GTATACACTC AGCATCGAAT TTCACCAACA
1301 CAAACAATTA TTTCACAAGC GTGCCGAAAA ACTTCATGGA ATTGTTGACA
```

```
1351 AATCAGGAGG CGCAGCAGTG GGTTAGTGGT TGGCGATTAA ATGCTGACTC
1401 AGTATTGTGG GGGGGCCATA AAGTTTTCAT GGTGAAACCT GAAGAGCCTT
1451 TTCAGCCAGT TAAGGAAGCG ACTCAACTCA TGAATCGTCG TCGCCGTCGC
1501 TAA
```

B.0.3 LOTEV2

```
   1 ATGGAGGGAT TCGACGGTTC AGATTTTAGT CCTCCAGCTG ATTTAGTTGG
  51 CGTTGACGGT GCAGTCATGC GGAACGTCGT TGACGTCACG ATAAATGGTG
 101 ACGTCACTGC TCCGCCGAAA GCTGCGCCAA GAAAAAGTGA ATCGGTAAAG
 151 AAAGTTCATT GGAATGATGT AGACCAAGGA CCGAGTGAAA AACCAGAGAC
 201 AAGACAGGAG GAACGAATAG ATATACCCGA GATTTCAGGT CTATGGTGGG
 251 GCGAGAATGA ACATGGAGTG GACGATGGGA GAATGGAGAT ACCTACTACT
 301 GGTGTAGGGG ATCCCACTAA GAGCATGTCT AGCATGGTGT CAGACACTAG
 351 TTGCACATTC CCTTCATCTG ATGGCATATT CTGGAAGCAT TGGATTCAAA
 401 CCAAGGATGG GCAGTGTGGC AGTCCATTAG TATCAACTAG AGATGGGTTC
 451 ATTGTTGGTA TACACTCAGC ATCGAATTTC ACCAACACAA ACAATTATTT
 501 CACAAGCGTG CCGAAAAACT TCATGGAATT GTTGACAAAT CAGGAGGCGC
 551 AGCAGTGGGT TAGTGGTTGG CGATTAAATG CTGACTCAGT ATTGTGGGGG
 601 GGCCATAAAG TTTTCATGGT GAAACCTGAA GAGCCTTTTC AGCCAGTTAA
 651 GGAAGCGACT CAACTCATGA ATCGTCGTCG CCGTCGCGAA TTCGGCGTGG
 701 GCCGCGTCCA GTTTCGTGTC CGAGCAGTGA TTGATCATCT AGGGATGCGA
 751 GTCTTTGGAG TCTTCCTAAT TTTCTTGGAC ATCATCCTCA TGATCATTGA
 801 TCTCAGTCTT CCAGGAAAAA GTGAATCTTC ACAATCCTTT TATGACGGGA
 851 TGGCTTTGGC TCTTTCTTGT TATTTCATGC TGGATTTAGG ATTAAGGATA
 901 TTTGCCTACG GGCCCAAGAA TTTCTTCACC AACCCCTGGG AGGTTGCTGA
 951 TGGTTTGATT ATCGTTGTCA CATTCGTCGT CACGATATTT TACACTGTGT
1001 TAGATGAATA CGTGCAAGAA ACAGGAGCCG ATGGTTTGGG GCAGTTGGTT
1051 GTGTTGGCCC GTTTGCTGCG TGTGGTTCGA TTAGCAAGAA TATTTTATTC
```

```
1101 CCATCAACAA ATGAAGGCTT CAAGCAGAAG AACAATATCA CTCGAGATGG
1151 GAGAAAGCTT GTTTAAGGGG CCGCGTGATT ACAACCCGAT ATCGAGCACC
1201 ATTTGTCATT TGACGAATGA ATCTGATGGG CACACAACAT CGTTGTATGG
1251 TATTGGATTT GGTCCCTTCA TCATTACAAA CAAGCACTTG TTTAGAAGAA
1301 ATAATGGAAC ACTGTTGGTC CAATCACTAC ATGGTGTATT CAAGGTCAAG
1351 AACACCACGA CTTTGCAACA ACACCTCATT GATGGGAGGG ACATGATAAT
1401 TATTCGCATG CCTAAGGATT TCCCACCATT TCCTCAAAAG CTGAAATTTA
1451 GAGAGCCACA AAGGGAAGAG CGCATATGTC TTGTGACAAC CAACTTCCAA
1501 TAA
```

B.0.4 TEVp

```
   1 ATGGGAGAAA GCTTGTTTAA GGGGCCGCGT GATTACAACC CGATATCGAG
  51 CACCATTTGT CATTTGACGA ATGAATCTGA TGGGCACACA ACATCGTTGT
 101 ATGGTATTGG ATTTGGTCCC TTCATCATTA CAAACAAGCA CTTGTTTAGA
 151 AGAAATAATG GAACACTGTT GGTCCAATCA CTACATGGTG TATTCAAGGT
 201 CAAGAACACC ACGACTTTGC AACAACACCT CATTGATGGG AGGGACATGA
 251 TAATTATTCG CATGCCTAAG GATTTCCCAC CATTTCCTCA AAAGCTGAAA
 301 TTTAGAGAGC CACAAAGGGA AGAGCGCATA TGTCTTGTGA CAACCAACTT
 351 CCAAACTAAG AGCATGTCTA GCATGGTGTC AGACACTAGT TGCACATTCC
 401 CTTCATCTGA TGGCATATTC TGGAAGCATT GGATTCAAAC CAAGGATGGG
 451 CAGTGTGGCA GTCCATTAGT ATCAACTAGA GATGGGTTCA TTGTTGGTAT
 501 ACACTCAGCA TCGAATTTCA CCAACACAAA CAATTATTTC ACAAGCGTGC
 551 CGAAAAACTT CATGGAATTG TTGACAAATC AGGAGGCGCA GCAGTGGGTT
 601 AGTGGTTGGC GATTAAATGC TGACTCAGTA TTGTGGGGGG GCCATAAAGT
 651 TTTCATGGTG AAACCTGAAG AGCCTTTTCA GCCAGTTAAG GAAGCGACTC
 701 AACTCATGAA TCGTCGTCGC CGTCGCTAA
```

B.0.5 P2A-YFP3xNuc

```
   1 GCGCGCGAGA CGGGAAGCGG AGCTACTAAC TTCAGCCTGC TGAAGCAGGC
  51 TGGCGACGTG GAGGAGAACC CTGGACCTGG TCTCCGGCCG GCCACCATGG
 101 TGAGCAAGGG CGAGGAGCTG TTCACCGGGG TGGTGCCCAT CCTGGTCGAG
 151 CTGGACGGCG ACGTAAACGG CCACAAGTTC AGCGTGTCCG GCGAGGGCGA
 201 GGGCGATGCC ACCTACGGCA AGCTGACCCT GAAGCTGATC TGCACCACCG
 251 GCAAGCTGCC CGTGCCCTGG CCCACCCTCG TGACCACCCT GGGCTACGGC
 301 CTGCAGTGCT TCGCCCGCTA CCCCGACCAC ATGAAGCAGC ACGACTTCTT
 351 CAAGTCCGCC ATGCCCGAAG GCTACGTCCA GGAGCGCACC ATCTTCTTCA
 401 AGGACGACGG CAACTACAAG ACCCGCGCCG AGGTGAAGTT CGAGGGCGAC
 451 ACCCTGGTGA ACCGCATCGA GCTGAAGGGC ATCGACTTCA AGGAGGACGG
 501 CAACATCCTG GGGCACAAGC TGGAGTACAA CTACAACAGC CACAACGTCT
 551 ATATCACCGC CGACAAGCAG AAGAACGGCA TCAAGGCCAA CTTCAAGATC
 601 CGCCACAACA TCGAGGACGG CGGCGTGCAG CTCGCCGACC ACTACCAGCA
 651 GAACACCCCC ATCGGCGACG GCCCCGTGCT GCTGCCCGAC AACCACTACC
 701 TGAGCTACCA GTCCGCCCTG AGCAAAGACC CCAACGAGAA GCGCGATCAC
 751 ATGGTCCTGC TGGAGTTCGT GACCGCCGCC GGGATCACTC TCGGCATGGA
 801 CGAGCTGTAC AAGTCTCGAG CTGATCCAAA AAAGAAGAGA AAGGTAGATC
 851 CAAAAAAGAA GAGAAAGGTA GATCCAAAAA AGAAGAGAAA GGTAGGATCC
 901 ACCGGATCTA GATAG
```

LckCherry

LckCherry sequence was based on Lck-GFP from Addgene (plasmid 61099) and dsRed-3xNLS sequence (kindly provided by Dr Michael Wehr (Wehr et al., 2006)).

```
   1 ATGGGCTGTG GCTGCAGCTC AAACCCTGAA GATGACTGGA TGGAGAACAT
  51 TGACGTGTGT GAGAACTGCC ATTATCCCTC TAGCAGTGGC TCCGGTAGCG
 101 GATCAGGGTC TAGAGCTGCA GCTGCTAGCG GAGAGAACCT GTACTTTCAG
 151 TCTCCTAGTA GATCTGGCGT CGACGCCACC ATGGTGAGCA AGGGCGAGGA
```

```
201 GGATAACATG GCCATCATCA AGGAGTTCAT GCGCTTCAAG GTGCACATGG
251 AGGGCTCCGT GAACGGCCAC GAGTTCGAGA TCGAGGGCGA GGGCGAGGGC
301 CGCCCCTACG AGGGCACCCA GACCGCCAAG CTGAAGGTGA CCAAGGGTGG
351 CCCCCTGCCC TTCGCCTGGG ACATCCTGTC CCCTCAGTTC ATGTACGGCT
401 CCAAGGCCTA CGTGAAGCAC CCCGCCGACA TCCCCGACTA CTTGAAGCTG
451 TCCTTCCCCG AGGGCTTCAA GTGGGAGCGC GTGATGAACT TCGAGGACGG
501 CGGCGTGGTG ACCGTGACCC AGGACTCCTC CCTGCAGGAC GGCGAGTTCA
551 TCTACAAGGT GAAGCTGCGC GGCACCAACT TCCCCTCCGA CGGCCCCGTA
601 ATGCAGAAGA AGACCATGGG CTGGGAGGCC TCCTCCGAGC GGATGTACCC
651 CGAGGACGGC GCCCTGAAGG GCGAGATCAA GCAGAGGCTG AAGCTGAAGG
701 ACGGCGGCCA CTACGACGCT GAGGTCAAGA CCACCTACAA GGCCAAGAAG
751 CCCGTGCAGC TGCCCGGCGC CTACAACGTC AACATCAAGT TGGACATCAC
801 CTCCCACAAC GAGGACTACA CCATCGTGGA ACAGTACGAA CGCGCCGAGG
851 GCCGCCACTC CACCGGCGGC ATGGACGAAC TGTACAAGTG CTCTCGAGCT
901 GATCCAAAAA AGAAGAGAAA GGTAGATCCA AAAAAGAAGA GAAAGGTAGA
951 TCCAAAAAAG AAGAGAAAGG TAGGATCCAC CGGATCTAGA TAG
```

B.0.6 Cherry-Q

```
  1 ATGGTGAGCA AGGGCGAGGA GGATAACATG GCCATCATCA AGGAGTTCAT
 51 GCGCTTCAAG GTGCACATGG AGGGCTCCGT GAACGGCCAC GAGTTCGAGA
101 TCGAGGGCGA GGGCGAGGGC CGCCCCTACG AGGGCACCCA GACCGCCAAG
151 CTGAAGGTGA CCAAGGGTGG CCCCCTGCCC TTCGCCTGGG ACATCCTGTC
201 CCCTCAGTTC ATGTACGGCT CCAAGGCCTA CGTGAAGCAC CCCGCCGACA
251 TCCCCGACTA CTTGAAGCTG TCCTTCCCCG AGGGCTTCAA GTGGGAGCGC
301 GTGATGAACT TCGAGGACGG CGGCGTGGTG ACCGTGACCC AGGACTCCTC
351 CCTGCAGGAC GGCGAGTTCA TCTACAAGGT GAAGCTGCGC GGCACCAACT
401 TCCCCTCCGA CGGCCCCGTA ATGCAGAAGA AGACCATGGG CTGGGAGGCC
451 TCCTCCGAGC GGATGTACCC CGAGGACGGC GCCCTGAAGG GCGAGATCAA
```

```
501 GCAGAGGCTG AAGCTGAAGG ACGGCGGCCA CTACGACGCT GAGGTCAAGA
551 CCACCTACAA GGCCAAGAAG CCCGTGCAGC TGCCCGGCGC CTACAACGTC
601 AACATCAAGT TGGACATCAC CTCCCACAAC GAGGACTACA CCATCGTGGA
651 ACAGTACGAA CGCGCCGAGG GCCGCCACTC CACCGGCGGC ATGGACGAAC
701 TGTACAAGTG CGAGAACCTG TACTTCCAGA GCTGCAACGA CAGCAGCGAC
751 CCTCTGGTGG TGGCCGCCTC TATCATCGGA ATCCTGCACC TGATCCTGTG
801 GATCCTGGAC AGACTGTAG
```

B.0.7 Primers

AP568 - ATGCATGCTCGAGCGGC

AP634 - GCTTATCGAAATTAATACGACTCACTATAGGG

B.1 Mammalian Physiological Solution

The three versions of MPS were obtained following the recipe from (Huckstepp et al., 2010):

- 100% Na saline: 140 mM NaCl, 1.25 mM NaH_2PO_4, 3 mM KCl, 10 mM D-glucose, 1 mM $MgSO_4$, 2 mM $CaCl_2$.
- 50% Na, 50% K saline: 70 mM NaCl, 1.25 mM NaH_2PO_4, 70 mM KCl, 10 mM D-glucose, 1 mM $MgSO_4$, 2 mM $CaCl_2$.
- 100% K saline: 3 mM NaCl, 1.25 mM NaH_2PO_4, 140 mM KCl, 10 mM D-glucose, 1 mM $MgSO_4$, 2 mM $CaCl_2$.

Every solution was adjust to a final pH of 7.4.